DUST IN SUPERNOVAE AND SUPERNOVA REMNANTS

by

James Richard Graham

Astrophysics Group
Blackett Laboratory
Imperial College of Science and Technology
LONDON SW7

A thesis submitted for the degree of
Doctor of Philosophy of the University of London
and for the
Diploma of Membership of the Imperial College

March 1985

ABSTRACT

DUST IN SUPERNOVAE AND SUPERNOVA REMNANTS

New infrared observations of supernovae and supernova remnants from 1-100μm are presented and discussed.

The supernova observations significantly increase the available data base. This sample includes three supernovae which exhibit infrared (1-3μm) emission which is brighter than extrapolation from optical wavelengths would predict, bringing the number of "infrared excess" supernovae to five. This excess is attributed to supernova heated dust. It is established, for the first time, that this dust was part of a shell which formed prior to the supernova explosion. The infrared light curves of SN1982e are analysed in terms of radiative transfer in a circum-supernova dust shell, and the inferred dust cloud used to reconstruct the pre-explosion evolution of the supernova.

Dust grains in hot (~10^6K) gas may be heated by gas-grain collisions, reaching temperatures ~ 30K. If dust survives these severe conditions then grains will radiate copiously at far-infrared wavelengths, cooling the gas an order of magnitude more efficiently than atomic processes.

Supernova remnants are ideal natural laboratories in which to study grain cooling. Lacking sensitive far-infrared observations of supernova remnants, a theoretical study of the fate of dust grains in a supernova remnant was undertaken to discover whether or not the efficiency of dust cooling could be inferred from observations at other wavelengths. X-ray emission is found to be particularly sensitive to dust cooling, and has been used to show that dust could contribute significantly to the cooling of hot gas. IRAS (12-100μm) additional observation data is presented, showing that luminous ($10^5 L_\odot$) infrared sources are associated with supernova remnants. Comparison of the infrared and x-ray data show that the sources are probably due to collisionally heated dust.

In summary, this work demonstrates the important role which dust plays in supernovae and supernova remnants.

ACKNOWLEDGEMENTS

I would like to thank Peter Meikle, under whose careful supervision this work was undertaken, for the essential help, advice and encouragement which he has provided.

Special thanks, for their enthusiasm, are due to David Allen, Andy Longmore and Perry Williams, whose observing skills contributed immensely to obtaining the supernova photometry. Nye Evans and Mike Bode were also collaborators and deserve special mention. Terry J. Jones was responsible for educating me at an A.A.S. meeting about asymptotic giant branch evolution, and pointing out how a low mass star can go through a phase of intense mass loss.

I would also like to thank many friends and colleagues for providing such a stimulating, if at some times distracting, environment in which to write this thesis. The principal perpetrators were Bob Joseph, Jim Ring, Norna Robertson, Simon Chase, Steve Hart, and Gillian Wright, who also bravely attempted the Herculean task of banishing, from the text, my innumerable typographical errors.

CONTENTS

LIST OF TABLES

LIST OF FIGURES

CHAPTER I

AN INTRODUCTION TO SUPERNOVAE AND SUPERNOVA REMNANTS

1.1 INTRODUCTION

Supernovae were first observed as "guest stars", objects which suddenly appeared in the night sky as new stars which rivalled Jupiter, Venus, or even the cresent Moon in brightness. After this remarkable appearance they faded away after a number of months. The Renaissance supernovae observed by Tycho (SN1572 A.D.), and by Galileo and Kepler (SN1604 A.D.) were the first supernovae observed in a recognizably systematic manner. However, no supernova has been discovered within our Galaxy since Galileo turned the telescope to astronomical use. But several hundred extra-galactic supernovae have been discovered and studied in the past century. Many supernova remnants, including those of SN1572 and SN1604, have been identified in the Galaxy, and supernova remnants have been discovered in the Magellanic Clouds and in members of the Local Group of galaxies.

Supernovae are one of the most important and complex phenomena known to astrophysics. Observations of supernovae and their remnants test the most advanced techniques of astronomy to their limits, and the theoretical investigation of supernovae requires virtually every branch of physics. Supernovae are extremely energetic events. For a brief period a supernova rivals the brightest galaxies in luminosity, and supernova remnants are among the most conspicuous radio and x-ray sources in the Galaxy.

Supernovae however, constitute much more than just an exciting problem in physics, because supernovae are central to many branches of astrophysics. Supernovae represent the final stages of stellar evolution. They are the birth places of neutron stars and pulsars. They are involved in the production and dispersal of most of the heavy elements. They control the structure of the interstellar medium; inhibiting or triggering star formation, and thereby shape the evolution of galaxies . (A supernova might even have triggered the formation of the solar system). Supernovae are also important as they are observed to accelerate electrons to relativistic energies and are

therefore thought to be the major source of the Galactic cosmic rays.

The following sections consitute a brief description of the present state of knowledge of supernovae. The observable properties of supernovae, their spectra and light curves, are described, followed by a discussion of the nature of supernovae based upon these assembled facts. Current theories of explosion mechanisms are then reviewed. The aftermath of a supernova explosion is described. The evolution of a supernova remnant is followed, and the contribution of supernovae to the Galactic cosmic ray population and the heavy element abundance is outlined.

1.2 THE SPECTRA OF SUPERNOVAE

1.2.1 TYPE I SPECTRA

Most supernovae (SN) fall into one of two spectroscopic classes. The spectra of type I supernovae (SNI), which constitute approximately one half of all SN discovered, show broad overlapping emission and absorption bands. Type I supernovae are characterised by the almost complete lack of hydrogen lines (Kirshner & Oke 1975, but see Branch et al. 1983 for a possible detection), and the strength of all emission and absorption features, indicating a high ratio of line to continuum opacity. The emergent spectrum of a SNI obviously is not Planckian; the spectrum from 0.4μm to 2.2μm can be approximated by a black body ($T \sim 10^4$K at maximum), but shortward of 0.4μm the spectrum falls far beneath the extrapolated Planck function (Branch et al. 1983)

Attempts to identify lines in the complex early-time spectra of SNI are usually made on the basis that the observed features are P-Cygni type profiles due to the permitted lines of neutral and singly ionized metals superimposed on a thermal continuum. Because of the large Doppler broadening and blending, the identifications, based on wavelength coincidence, are subject to ambiguity. However, the recent development of synthetic spectra, which allows for the effects of blending to be included, has helped to establish more reliable line identifications. Figure 1.1 shows the spectrum of SN1981b at maximum light compared with a synthetic spectrum from Branch et al. (1983). A few tenths of a solar mass of He, O, Mg, Si, S, and, Ca, (but no H)

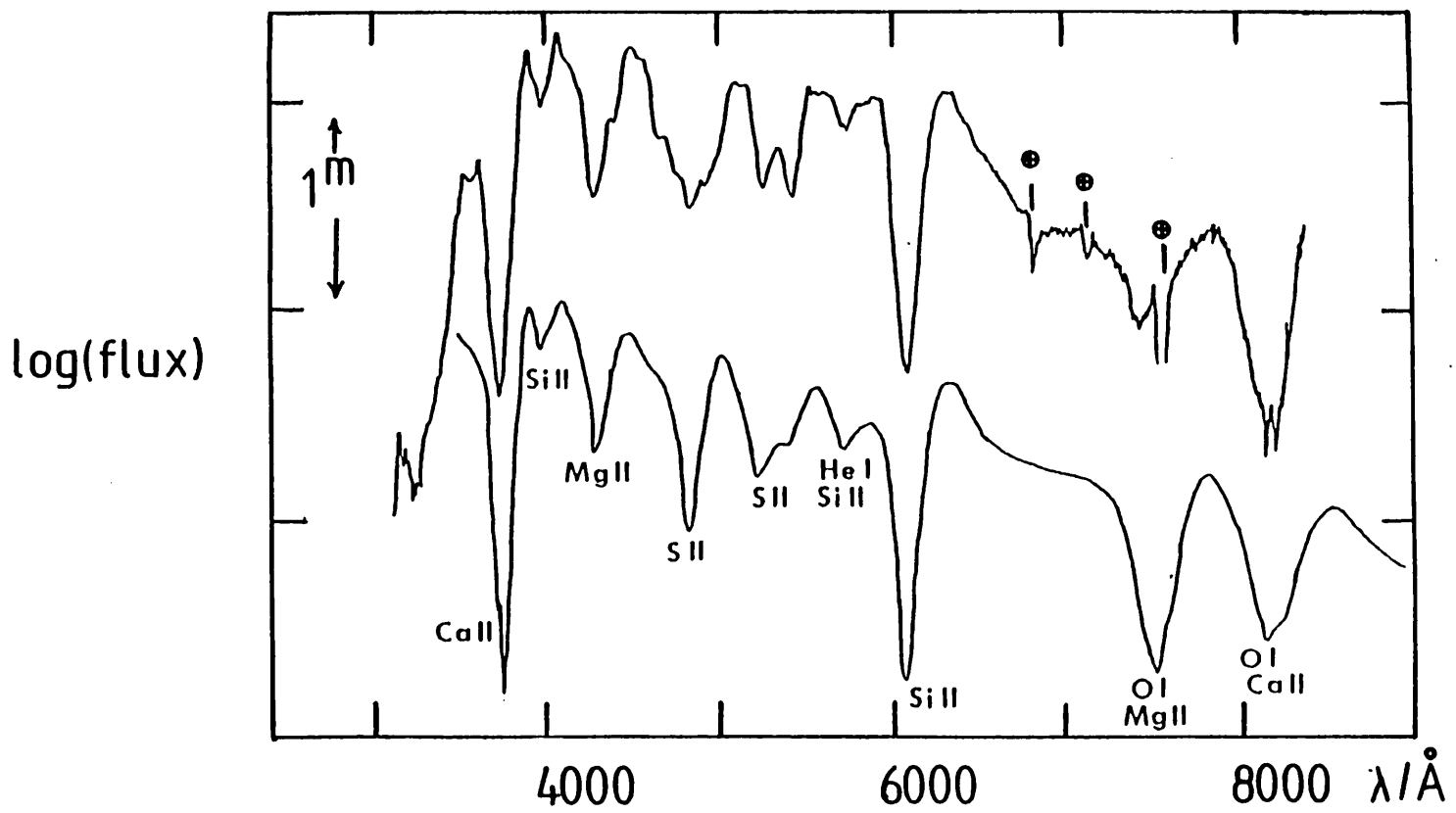

Figure 1.1

The spectrum of the type I supernova SN1981b at maximum light (upper tracing), compared with a synthetic spectrum.

above the photosphere account for all the major observed features. The relative abundances of Ca, Si, Mg, S, and O, appear to be consistent with solar, and hydrogen is found to be deficient (Branch et al. 1983). About 20 days after maximum iron must be added to the list of elements present in the spectra. As the SN ages iron becomes more and more dominant in the spectrum, until by day 100 only Fe and Na are seen. The changes in the spectra cannot be attributed to changes in temperature alone. As the SN expands it appears that the ejecta become optically thin and the interior of the SN can be observed. So that by about a year after maximum light the spectrum of the SN can be attributed almost entirely to forbidden lines of FeII and FeIII (Kirshner and Oke 1975).

Velocities derived from Doppler shifts of absorption lines indicate that the velocity just above the photosphere drops from ~11,000 km/s at maximum to ~8,000 km/s about a month later. The fall in velocity is interpreted as the photosphere penetrating deeper into the slower moving material as the expansion continues.

1.2.2 TYPE II SPECTRA

Type II supernovae are recognised by the presence of hydrogen lines in their spectra and their smooth continua (see figure 1.2). Abundances cannot yet be derived unambiguously, but no obvious inconsistency arises if normal solar abundances are assumed (Kirshner and Kwan 1975). The continuum carries most of the radiated energy for up to a year, (unlike SNI where this is true for only the first month), and can be described by a black body which gradually declines in temperature from 10,000K at maximum light to 6,000K a few weeks later. The characteristic velocities derived from SNII spectra are ~ 5,000 km/s. While, as for SNI, only ~0.1M$_\odot$ are required in the line forming region above the photosphere of a SNII, ~5M$_\odot$ in addition to this are required to maintain the optically thick continuum for over a year, given the rapid expansion of the envelope (Panagia et al. 1980).

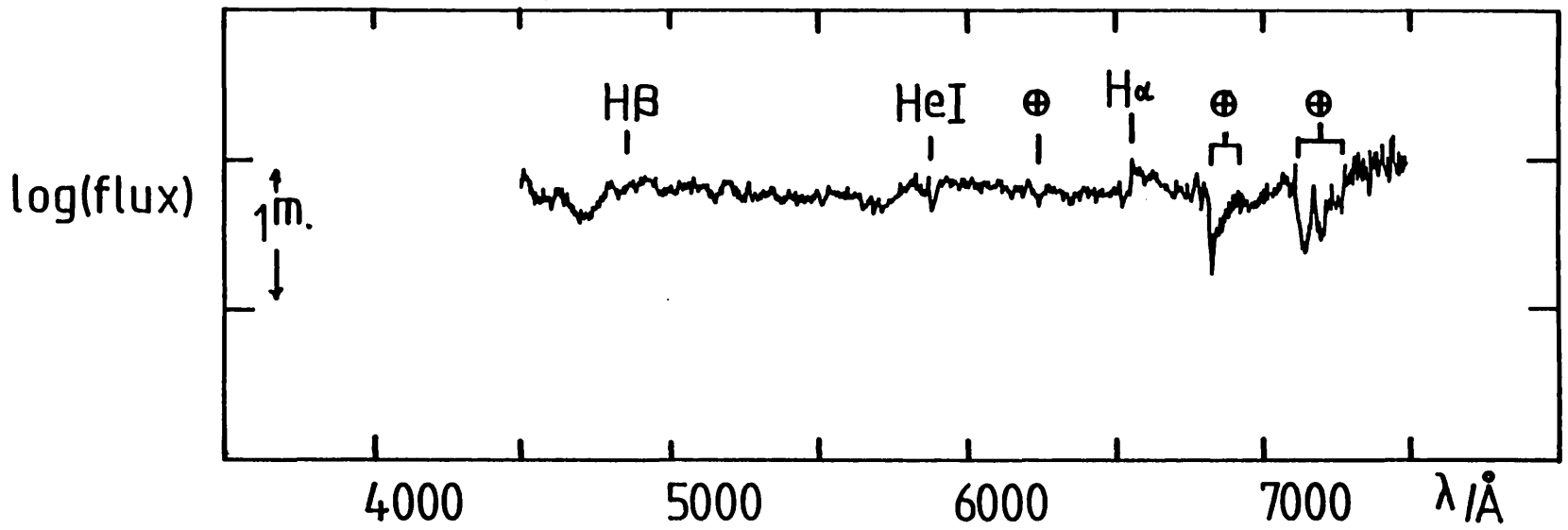

Figure 1.2

The spectrum of the type II supernova SN1979c at maximum light.

1.3 SUPERNOVA LIGHT CURVES

1.3.1 TYPE I LIGHT CURVES

Type I supernovae are intrinsically brighter than type II supernovae and show smaller scatter in peak magnitude. At maximum light $M_B=-19.7+5\log$ (Ho/50km/s/Mpc), with a dispersion of $0.^m4$ (Tammann 1982). The light curve of a type I supernova shows a rapid rise to maximum. Those few which have been discovered before maximum have rates ~ $-0.^m4$/day. A SNI then decays by about 3^m in the first 30 days or so, then the decline slows and maintains a remarkable long term exponential decay ($\tau_{1/2}\approx60$ days) which in some supernovae has been followed for 10 half-lives. Figure 1.3 shows the light curve of the well observed supernova SN1972e.

1.3.2 TYPE II LIGHT CURVES

Despite the spectroscopic differences between the two classes of supernovae, SNI and SNII light curves are remarkably similar. SNII get bright quickly, reaching a peak brightness $M_B=-19.0+5\log$(Ho/50km/s/Mpc), with a dispersion about this mean value of ~ 1^m (Tammann 1982). They then fade away slowly at a mean rate of $0.^m02$/day. Most (2/3) SNII have their decline interrupted after about a month by a plateau phase which lasts for some 30 to 60 days, after which the decline continues. Some SNII then show a late time (t>200 days), low luminosity, exponential tail, which persists for at least another 150 days. Figure 1.4 shows the light curve of SN19691.

1.4 THE OCCURRENCE OF SUPERNOVAE

1.4.1 TYPE I SUPERNOVAE

Type I supernovae have been discovered in all morphological classes of galaxy. In particular the occurrence of SNI in elliptical galaxies suggests that SNI come from an old, low mass, stellar population. Tammann (1978) finds that SNI discovered in spiral galaxies suffer more extinction in highly inclined galaxies, and hence do not belong to the

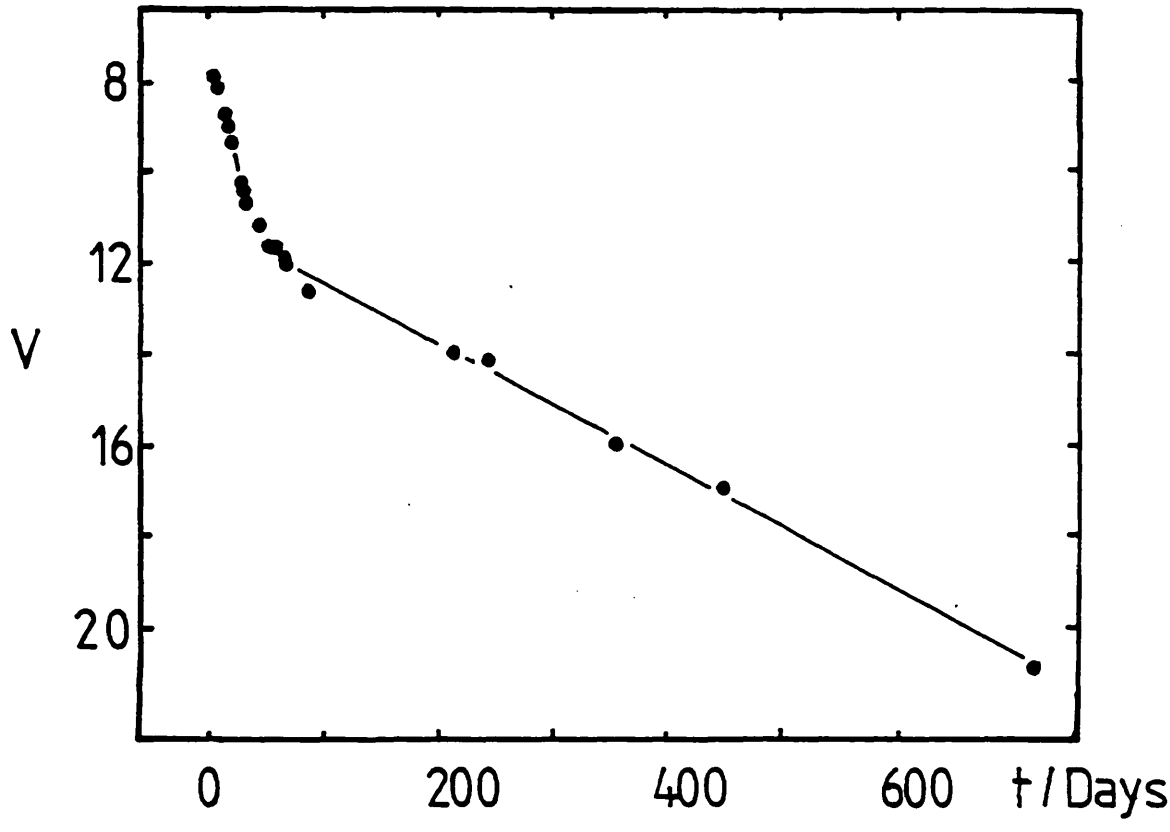

Figure 1.3

The V magnitude light curve of the type I supernova SN1972e.

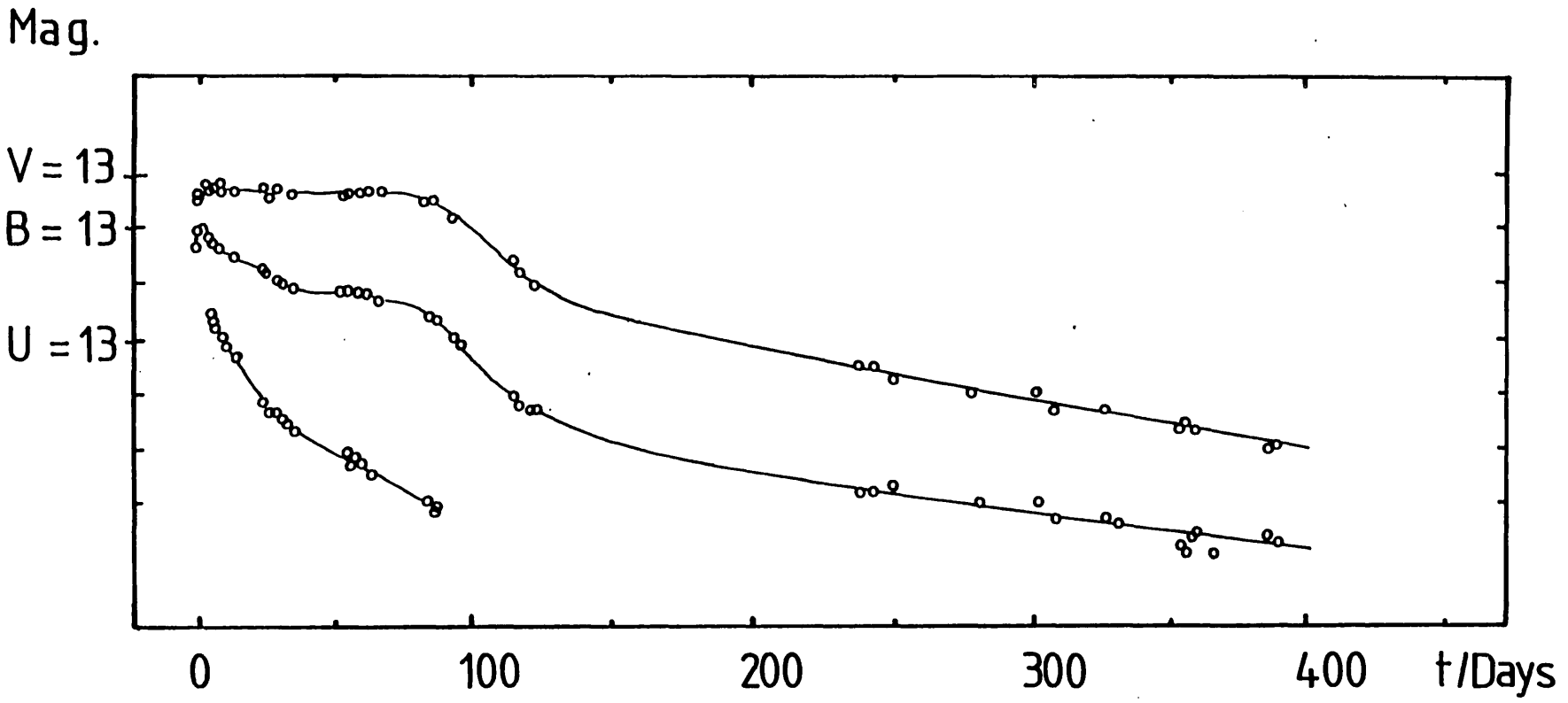

Figure 1.4

The U,B, and V magnitude light curves of the type II supernova SN19691,

halo but the disc. Their lack of confinement to spiral arms (Maza and van den Berg 1976) also points to low mass stars. There is, however, some dissent. Oemler and Tinsley (1979) have proposed that some SNI come from a young stellar population. Their argument is based chiefly upon the observation that the rate of SNI production in IO(IrrII) galaxies is anomalously high. Since IO galaxies consist of an old stellar population interlaced with regions of intense starformation they argue that the high SNI rate implies that SNI are associated with recently formed stars. Their SNI rate for IO galaxies is based upon 4 supernovae in 29 galaxies out of a sample of 173 SN in a total of 2955 galaxies.

1.4.2 TYPE II SUPERNOVAE

Type II supernovae have not been observed in elliptical galaxies, but are restricted to galaxies showing strong spiral structure; type Sab - Sd (Tammann 1982). Indeed, SNII are confined to the spiral arms in these galaxies (Maza and van den Berg 1976). It would therefore seem that SNII arise from a population of young massive stars.

1.5 THE NATURE OF SUPERNOVAE

Let us assemble some of the above observations to obtain an "order of magnitude" physical picture of a supernova. In summary, supernovae reach a peak absolute blue magnitude of ~-19. The effective temperature at maximum is ~10^4K. Therefore, taking the bolometric correction into account, the peak luminosity is ~2×10^{43} erg/s. The corresponding photospheric radius is R~2×10^{15}cm. This luminosity decays with an e-folding time ~2×10^6s, so the total electromagnetic radiation emitted comes to a total of E~4×10^{49}erg. The decay timescale is determined roughly by the rate of radiative diffusion through the SN, so we can estimate the density ρ from the e-folding time by equating it to the diffusion timescale τ

$$\tau \sim \frac{\rho R^2 \kappa}{c}$$

if we know the opacity κ. c is the speed of light, and R is the SN radius. The material will be highly ionised, because T~10^4K, therefore the opacity will be close to the value for Thomson scattering

so we deduce that $\rho \sim 7 \times 10^{-14}$ g/cm^3, or alternatively that a total mass ~1M$\odot$ is indicated. The observed expansion velocity can be used to show that the kinetic energy associated with the expansion is $\sim 1 \times 10^{51}$erg. The energy released by the SN explosion is distributed through the star by a shock which both heats and accelerates the stellar material. A shock establishes approximate equipartition between internal and kinetic energy, therefore the initial internal energy, E_0, of the SN must also be $\sim 10^{51}$erg. The difference between this figure and the amount of energy radiated must be due to adiabatic losses as the SN expands from its initial radius R_0.

The temperature of the SN is lowest at the surface because of radiative diffusion, so material temperatures within the SN must be greater than the observed effective temperatures ~(5-10)x10^{3}K. Under these conditions of temperature and density, radiation pressure, $aT^4/3$ (a is the radiation density constant) exceeds the thermal gas pressure $\rho kT/m$ (k is the Boltzmann constant and m is the mean particle mass). The equation of state is that of a photon gas, the internal energy $E = aT^4V$ where V is the volume. Adiabatic expansion yields that

$$\frac{E}{E_0} = \frac{R_0}{R}$$

Thus if the optical display of a SN is due to the diffusive release of the stored thermal energy (in the form of photons) deposited in the star by an explosion then the initial radius of the star must be ~1000R$\odot$ (3×10^{13}cm). The only stars which fulfil this criterion are the K and M super-giants (M~10-20M$\odot$). The corollary of this deduction is that compact stars (ordinary giants, main sequence dwarfs and white dwarfs) cannot produce a spectacular outburst unless some of the explosion energy is stored by other than thermal means.

By this simple chain of argument we have identified the physical reasons for the traditional assumption that the progenitors of type II supernovae are massive late-type super-giant stars. Historically this belief was founded upon the observation that SNII come from regions of formation of massive stars, and that the abundances in their envelopes

are not significantly different from solar. The light curves of SNII are indeed well modelled by a point explosion in a red super-giant star (Falk & Arnett 1977). The original shock gives a burst of UV and soft x-ray emission when it breaks the surface (Klein & Chevalier 1978), and the subsequent diffusion of thermal energy provides the peak in the optical light. The shock drives the envelope into homologous free expansion, with the outer layers travelling fastest. The photosphere expands but the density drops as the expansion continues so that the photosphere recedes in a Lagrangian sense causing the photospheric velocity to decline.

1.6 THE NATURE OF THE EXPLOSION

1.6.1 TYPE II SUPERNOVAE

Stars as massive as the proposed progenitors of SNII burn all the elements up to the iron peak non-degenerately. Therefore, evolution continues peacefully until the iron core approaches the Chandrasekhar limit. Nuclear binding is at a maximum near iron; thus these cores are not capable of further burning and so collapse is inevitable. The core looses energy and contracts until $\rho \sim 10^9 g/cm^3$ and $T \sim 10^9 K$ when nuclear photo-disintegration becomes important in removing photons from the radiation field as Fe is broken up to He and subsequently He is reduced to its constituent nucleons (Burbidge et al. 1957). Neutrino pair production increases, further depleting the radiation field, and removes energy from the core. As the supporting pressure is lost the core must contract, heating up as it does. The Fermi level of the degenerate electrons rises as the density increases initiating inverse beta decay. As electrons are lost the electron pressure drops still further. The core then begins collapsing on a dynamical timescale to nuclear densities or beyond, releasing $\geq 10\%$ of the rest mass energy. The collapse releases $\geq 10^{53}$ erg of gravitational energy, of which a few percent must be coupled to the envelope of the star to produce a SN like event. Unless some of this energy can be converted into an outward propagating shock of sufficient strength to blow off the outer layers of the star, collapse to a black hole will ensue. The key question is how this is accomplished. In recent years attention has been centred on two mechanisms; neutrino interaction, and core bounce.

In the neutrino interaction model it is proposed that neutrinos stream out of the core and deposit sufficient energy and momentum in the infalling envelope to halt its collapse and cause ejection. However, recent calculations of the physical state in the core including detailed numerical simulations (e.g. Tubbs et al. 1980) show that the collapsing core of a massive star is optically thick to neutrinos, so that they do not escape. However, as mentioned above photo-disintegration and inverse beta decay increases as the collapse proceeds. The core evolves towards a non-relativistic neutron gas. If nucleon pressure can halt the infalling core before the neutrons become relativistic then a hydrodynamic core bounce will occur. If the core rebounds, the overlying layers, which are still falling in, are compressed, setting up a shock wave which ejects the stellar mantle. The results of core bounce depend critically upon the equation of state of nuclear matter, requiring for a successful outcome that it be particularly "soft" ($\gamma \leq 4/3$) during the early stages of collapse, and then "stiffening" ($\gamma \geq 5/3$) rather suddenly (Arnett 1980). Although it is possible to engineer a successful core bounce by adjusting the equation of state, our present understanding of matter under such extreme conditions is poor so that the outcome of core collapse is at best uncertain.

1.6.2 TYPE I SUPERNOVAE

There is a general consensus that type I supernovae are the explosions of relatively low mass stars, at least compared to type II, and that the stars involved are devoid of any substantial hydrogenic envelopes, and as shown in section 1.5, some energy input is required that is not degraded by adiabatic expansion. The most readily accepted solution as to how 2×10^{16} erg/g can be stored in the ejecta is suggested by the exponential form of the light curve - the light curve is a result of the delayed energy input by the radioactive decay of nuclei produced in the explosion (Burbidge et al. 1957), principally the nucleus ^{56}Ni ($\tau 1/2 = 6.1$days), and its daughter ^{56}Co($\tau 1/2 = 78.5$days) (Colgate and McKee 1967). From an evolutionary point of view the most favoured models are white dwarfs accreting material in a binary system (Iben & Tutukov 1984). The accretion rate and mass of the dwarf determine the fate of the system. At the fastest accretion rates (i.e. just less than the Eddington limited accretion rate

$\sim 10^{-5}$ M⊙/year), the energy released cannot be radiated away quickly enough, and a giant-type envelope will suround the white dwarf (Fujimoto 1980). For lower mass transfer rates cataclysmic variable systems, powered by strong hydrogen shell flashes, can be produced (McDonald 1983). These flashes are violent enough so that the mass of the dwarf shrinks rather than grows. For intermediate accretion rates ($10^{-9} < \dot{M}$ (M⊙/year) $< 10^{-7}$) the hydrogen burns to helium which accumulates in a thick shell (Fujimoto 1980). Eventually the helium will ignite at the interface with the carbon/oxygen core, and drive detonation waves both inwards and outwards. For the slowest accretion rates ($\dot{M} < 10^{-9}$ M⊙/year), carbon will ignite centrally. Both models lead to complete or almost complete disruption of the white dwarf. The temperatures and densities in the explosion are such that nuclear statistical equilibrium is achieved. Explosive burning therefore proceeds to the most tightly bound nucleus ^{56}Ni, and so the SN ejecta contains a large fraction of this radioactive isotope to power the light curve.

1.7 SUPERNOVA REMNANTS

The conspicuous debris discovered at the position of the supernovae of 1054, 1572, and 1604 constitute the spectacular aftermath of a supernova explosion. The Crab Nebula, the remnant of SN1054, is a copious source of electromagnetic radiation over a range of frequency which spans 19 decades from radio to γ rays. The Crab Nebula is perhaps most famous for its pulsar, which demonstrates that some supernovae suffer core bounce and produce neutron stars. The remnants of Tycho's (SN1572) and Kepler's (SN1604) supernovae are much less spectacular than the Crab. Some faint filamentary wisps of optical nebulosity have been observed, but it is at radio, and x-ray wavelengths that these remnants are most outstanding. Although these are comparatively young remnants they are much more representative of the majority of supernova remnants (SNR) in that they exhibit the traditional signatures of a supernova remnant; extended nonthermal radio emission, and extended thermal x-ray emission. The remnants of many other older and more distant supernovae, which were either never discovered optically , or are now forgotten, are still observable. Nearby SNR are conspicuous on account of nebular emission from an intricate network of filaments which accompanies the x-ray and radio emission. Most remnants are more distant than these and are identified

only by their radio emission.

1.7.1 THE INITIAL EVOLUTION OF SUPERNOVA REMNANTS

Once the SN has faded the remaining energy is mainly in the form of kinetic energy of expansion. In the hundreds to thousands of years following the explosion this energy is transferred to the surrounding interstellar medium. As the ejected shell expands it sweeps up the surrounding material driving a shock, as a supersonic piston would, into this material. When the mass of material swept up becomes comparable to the ejected mass the ejecta are decelerated by a reverse shock. Thus the interior of SNR's are heated to x-ray emitting temperatures. X-ray images of the young SNR Cas A show a clumpy shell of radius 102" and 17" thick, which accounts for most of the x-ray emission, but a second fainter shell of 150" radius surrounds the first (Fabian et al. 1980). The natural interpretation of the remnant structure is that the outer shell is the shock in the interstellar medium, while the inner shell is the ejecta passing through the reverse shock. This deceleration leaves the material at the interface between the ejecta and the ambient medium Rayleigh-Taylor unstable. Gull (1973a) suggests that this instability generates turbulent motions which are important for the acceleration of relativistic particles. Gull has shown that ~1% of the supernova energy is converted into turbulent energy so that in the presence of a magnetic field equipartition produces a population of relativistic electrons which can account for the radio synchrotron emission from young SNR's (Gull 1973b)

This picture is obviously simplistic. It is possible that much of the ejecta is initially clumpy, as the x-ray image of Cas A suggests. The optical emission of Cas A is dominated by emission line knots which fall into two classes. The fast moving knots have large proper motions and Doppler shifts corresponding to velocities ~ 6000km/s (Kamper and van den Berg 1978). The so called "quasi stationary flocculi" move at about 150 km/s. The fast moving knots show very peculiar composition (Kirshner & Chevalier 1977), including some knots which are composed of pure oxygen, and some with oxygen and the products of oxygen burning; S, Ar, and Ca, indicating that these knots are undiluted SN ejecta.

1.7.2 ADIABATIC AND RADIATIVE PHASES

Once the supernova ejecta, whether in clumps or smoothly distributed, have interacted with approximately equal mass of interstellar gas, and the SN energy has been transferred to the interstellar gas, the subsequent evolution of the SNR can be described by an adiabatic blast wave in a uniform medium. Sedov theory for such an idealized explosion provides the basis for understanding the x-ray structure of supernova remnants (Heiles 1964). However, it is the departures from this idealization which lead to the diversity exhibited by SNR's. As the SNR shock weakens radiative cooling (bremsstrahlung and recombination lines) causes the gas to cool rapidly behind the shock so that the adiabatic approximation is no longer valid. Eventually gas temperatures reach ~10^4K and optical lines make an important contribution to the cooling. The Cygnus Loop is probably the best known example of a SNR where the shock is radiative, and the SNR is delineated by an optical filamentary shell. There is a general correlation between the brightness of different regions at x-ray, optical, and radio wavelengths. But optical and x-ray observations indicate very different physical conditions. Cox (1972a) found that models of radiative shocks having velocities ~100km/s matched optical emission spectra. X-ray observations (Ku et al. 1983) indicate substantial quantities of gas T~10^6K requiring shock velocities ~ 400km/s. It is generally supposed that the x-ray emission arises from a 400km/s shock in the inter-cloud gas of density ~0.2/cm^3, which drives slower (100km/s) radiative shocks into clouds which are engulfed.

1.7.3 FINAL STAGES OF EVOLUTION

When the SNR shock becomes radiative the remnant starts to form a dense neutral shell because of the high degree of post-shock compression (Cox 1972b). The dynamics of this non-adiabatic expansion are determined by considering the conservation of momentum of the dense shell as it sweeps up interstellar material. Such shells have been detected. Neutral hydrogen radio observations of old SNR's show a supersonic expanding shell (e.g. Assousa et al. 1973). Galactic 21cm surveys also show very large (>>1°) neutral shells - "super bubbles" . The momentum associated with of some of these shells is compatible with SN origin, and so these may represent the very last stages of SNR evolution (Heiles 1976). The SNR will finally disappear when the

ordered motion of its expansion becomes comparable to the random motion of clouds (~20km/s; Spitzer 1978)

1.7.4 NON-THERMAL ASPECTS

The explanation for the shell-like radio morphology of SNR's such as the Cygnus Loop is due to van der Laan (1962) who argued that radiative cooling of shocked gas will lead to high post-shock compression. This in turn would amplify the magnetic field and accelerate the relativistic electrons within the remnant leading to enhanced synchrotron emissivity. The direct association of optical emission line filaments and radio features in remnants like the Cygnus Loop and IC443 (Duin & van der Laan 1975) provides impressive support for this idea. A natural modification of the van der Laan mechanism compatible with a multiphase model of the interstellar medium is to localize all the gas that is dense enough to cool in clouds. When these clouds are engulfed by the main blast wave, slower secondary shocks propagate into them. These clouds may then be crushed and the magnetic field amplified.

Radio observations of Galactic remnants were thought for some time to show a correlation between surface brightness and diameter; the Σ-D relation which implied that the radio luminosity of a SNR was proportional to its diameter (Clark and Caswell 1976). It is now evident that such an apparent correlation arose partly from measurement errors due to resolution effects, partly because low luminosity small diameter SNR's had not been detected, and partly because of a distance scale derived from a set of calibrators of uncertain distance (Mills 1983). This conclusion is further strengthened by recent radio observations of Large Magellanic Cloud SNR's (which are all at a known distance), which show that remnants of the same diameter show a spread in luminosity of the same magnitude as the range of observed luminosities (Mills 1983)

1.8 SUPERNOVAE AND THE GALAXY

Although the SNR will no longer be recognizable as an ordered expansion once the velocity has become comparable with the random motions of clouds, the collective effect of many SN can be identified in the Galaxy, either directly (e.g. cosmic rays and newly synthesised elements) or by the way SN shape the evolution of the interstellar

medium (e.g. the SN energy).

1.8.1 SUPERNOVA ENERGY

Supernovae are one of the major energy sources of the interstellar medium (ISM). The heating and stirring up of the ISM by supernova remnants therefore affects its structure, and ultimately the star formation process, which in turn leads to more supernovae.

When considering the large scale structure of the ISM one must take into account the large quantities of tenuous ($n \sim 0.01$ cm^{-3}) hot gas ($T \sim 10^6$K) generated by supernova remnants. Evidence for the existence of this hot gas comes from observations of the soft x-ray background (Sanders et al. 1984) and interstellar O VI (χ=138eV) absorption lines (Jenkins and Meloy 1974). It has even been suggested that our local ISM is actually the interior of a SNR, because the local soft x-ray (1keV) and E-UV (0.1keV) background is higher than expected if the solar system were located in between SNR's (Sanders et al. 1977). This proposal is consistent with the very low neutral hydrogen densities within 100pc of the Sun (Frisch and York 1983), and the detection of the x-ray lines of O and C by Inoue et al. (1980) and Schnopper et al. (1982).

Cox and Smith (1974) suggested that similar gas might occupy a substantial fractional volume of the ISM. The energy lost to radiative cooling by a SNR is small if the ambient density is small. If the fractional volume of the hot gas in the ISM is above a critical level radiative losses will be negligible, and supernova remnants will expand until they overlap. If the fractional volume is less than this critical level SNR's do not intersect, but remain distinct. At least 30% of the ISM can be maintained in this hot phase once the critical filling factor is achieved (Smith 1977).

The soft x-ray emitting gas and the O VI absorbing gas are at somewhat different temperatures (Shapiro and Field 1976). Consequently it is thought that the OVI absorption occurs in the interface between the hot x-ray emitting gas, and cool clouds. Heating of the cool clouds would occur at this interface (McKee and Ostriker 1977). McKee and Ostriker (1977) propose a three phase model of the ISM where evaporation of clouds by conduction in SNR heated gas plays an important role. It is

supposed that most of the ISM is pervaded by hot gas from SNR's, but there are also cool clouds and a warm component (T~10^4K). A steady state is achieved by the balance between cloud formation by SNR induced compression and cloud evaporation within SNR's. Rough agreement with the soft x-ray flux is obtained. However, according to McKee and Ostriker (1977) SNR's only enter the dense shell phase at R≈200pc, as they expand into a very low density medium. If the occurrence of dense shells in young remnants, e.g. the neutral shell in S147, d~40pc, (Assousa et al. 1973) is widespread, then this would constitute strong evidence against this model.

Supernovae are also important contributors to the kinetic energy of interstellar clouds. A few percent of the initial energy is converted into cloud motions (Spitzer 1978). This energy is subsequently dissipated in cloud-cloud collisions.

1.8.2 NUCLEOSYNTHESIS

Burbidge et al. (1957) established the network of nuclear reactions, and their siting in stars, which allows us to understand the synthesis of the heavy elements from primordial hydrogen and helium. The heavy elements are produced mainly by massive stars, and returned to the interstellar medium by supernova explosions.

The main group of elements from carbon to iron (C, O, Ne, Mg, Si, Fe) can be produced in essentially their observed cosmic abundances by stars of masses from 12-70M⊙ (Arnett 1975). Stars below 22M⊙ contribute about one half of the total contribution. The lighter elements (C, O, Ne) are produced and expelled in larger proportions in the lower mass stars, whereas Si to Fe are produced in larger proportions by the high mass stars. Elemental and isotopic abundances are fine tuned by explosive nucleosynthesis as the supernova shock propagates through the star to give detailed agreement (Woosley, Arnett, and Clayton 1973).

Explosive carbon/oxygen burning, which is thought to power SNI produces large quantities of iron peak elements, particularly ^{56}Ni, which decays to ^{56}Fe. Most models disrupt the exploding star, and so ~0.5M⊙ of Fe is contributed by every SNI event. At this rate SNI could easily have produced all the iron in the Galaxy (Tinsley

1980). This is consistent with the contribution from massive stars which could be small. The amount of iron ejected by a massive star depends upon the mass of the core which collapses - this as indicated earlier is somewhat uncertain. Woosley et al. (1984) have studied the synthesis of other elements in SNI. Those models which yield Cr, Mn, Fe, Co, and Ni in the correct ratios produce optical spectra which are quite unlike observations, whereas explosions which produce good synthetic spectra give unacceptable nucleosynthesis. So the contribution of SNI to Galactic abundances are still uncertain.

1.8.3 COSMIC RAYS

The same acceleration processes which produce the relativistic electrons which give rise to the synchrotron radiation observed in SNR's are also expected to produce relativistic protons and heavy nuclei - i.e. cosmic rays. Supernova remnants are therefore candidates for the acceleration sites of the cosmic rays observed at Earth. Evidence for this proposal comes from the isotopic and elemental composition which indicates that about 50% interstellar material and 50% supernova ejecta are required to reproduce the observations (Hainebach et al. 1976). Such a composition results naturally from the turbulent acceleration mechanism proposed by Gull (1973a). Most acceleration occurs when the mass of swept-up gas equals the mass of ejected gas, because the turbulent energy is greatest at this time. The correct cosmic ray composition is achieved if the ejecta become well mixed with the swept up mass at the same time.

The energy budget of cosmic rays is less certain than the composition because they suffer losses which could reduce their energy by more than an order of magnitude (Kulsrud et al. 1975). However, on the basis of the synchrotron emission from Cas A the efficiency of cosmic ray acceleration is sufficiently high to account for the observed cosmic ray energy density, given the Galactic supernova rate (Lingenfelter 1973).

1.9 THE INFRARED STUDY OF SUPERNOVAE AND THEIR REMNANTS

Our present knowledge of supernovae and supernova remnants relies upon both the traditional tools of optical astronomy, and the more contemporary sciences of radio and x-ray astronomy. However, to date

the study of supernovae has remained principally the occupation of optical astronomers. A few supernovae have been detected at radio wavelengths, and one at x-ray wavelengths. While it has been suggested that SN could be targets for the more exotic "new astronomies"; γ-ray, neutrino, and gravitational wave, the potential benefits which the fairly well established techniques of infrared astronomy could bring to the subject seem to have been virtually overlooked. The rationale for a programme of infrared photometry of SN is presented next, and the results and analysis of such a study is reported in Chapters 2 and 3.

By comparison with supernovae, supernova remnants fall in the domain of x-ray and radio telescopes. However, the launch of the infrared satellite observatory IRAS provided a unique opportunity to change this monopoly and study supernova remnants at infrared wavelengths. Consequently Chapters 4 and 5 are devoted to theoretical considerations and observational results relating to infrared emission from supernova remnants.

CHAPTER II

THE INFRARED STUDY OF SUPERNOVAE

2.1 INTRODUCTION

The reasons for proposing an infrared (IR) study of supernovae (SN) are reviewed. Previous observations are described, and new observations presented. The diversity of the IR behaviour of SN is noted, and three more SN with IR excesses, in addition to the two already known, are reported. The available data for IR excess SN are examined, and thermal emission from dust grains is proposed as the emission mechanism. The new observations of SN1982e and SN1982r are the first for which it is possible to draw firm conclusions about the origin of this dust. It is demonstrated that the dust grains in these SN must have formed prior to the SN explosion. Dust condensation in novae and in supernovae are compared and contrasted, and observations which might reveal the presence of freshly condensed dust in a SN are described.

2.2 RATIONALE

This study of supernovae arose from a program of infrared observations of recent extragalactic supernovae which was originally embarked upon with the following aims.

i) To determine the origin of the recently discovered excess IR emission from supernovae (Merrill 1980; Telesco et al. 1981). Compare the IR temporal development of TypeI and TypeII supernovae, and from this data infer possible differences in grain origin and heating processes in the supernova environment, and differences in progenitor types.

ii) Carry out rapid follow-up IR observations of supernovae discovered by the Berkeley supernova search; a project which uses a dedicated 36" telescope coupled to a CCD array and a computer controlled guidance system to search automatically for new supernovae. The search is revolutionary because, with a planned detection threshold of m_v=18.8, 100 supernovae per year should be discovered pre-maximum (Kare et al. 1982)

iii) Investigate the possibility of exploiting IR emission from supernovae to give extragalactic distance measurements superior to those obtained through optical methods. Distances determined from IR observations should be less affected by uncertainties in extinction and in effective photospheric temperatures.

While the above goals are general aims of a long term programme, it was clear that the basic need at the time of inception was to add to the one or two serendipitious IR observations. In the following two sections (2.3 and 2.4), some more specific details are outlined.

2.3 INFRARED EMISSION MECHANISMS

Two radically different ideas, both invoking dust in SN, have been proposed to account for the IR excess emission observed several months after optical maximum.

2.3.1 A PRE-EXISTING DUST SHELL

The progenitors of TypeII supernovae are thought to be red supergiants (Trimble 1982), stars which are often observed to have circumstellar dust shells (Zuckermann 1980). If any of this dust survives the explosion of the star then it will be revealed by the presence of a cool thermal IR component. Study of such a dust shell, and understanding its origin would undoubtedly provide a powerful tool for understanding pre-SN evolution.

2.3.2 DUST FORMED IN THE SUPERNOVA

An alternative model for the IR development, investigated by Clayton (1979) among others, is that grains form in the supernova ejecta. This condensation might explain the isotopic anomalies found in meteorites (Clayton 1982), and, indeed, Dwek and Scalo (1980) have suggested that a significant fraction of interstellar grains might originate in SN explosions. Dinerstein et al. (1981) have claimed the detection of hot dust within the fast moving knots in the Cas.A supernova remnant, however she has recently determined that some of this flux is due to IR emission lines (private communication 1983).

2.4 INFRARED OBSERVATIONS AROUND MAXIMUM LIGHT

An overwhelming reason for observing at infrared wavelengths is that interstellar extinction falls as wavelength increases. Therefore uncertainties which are present in optical observations due to uncertain extinction are reduced at IR wavelengths by an order of magnitude. Sections 2.4.1 and 2 discuss observations which would capitalize upon these advantages.

2.4.1 THE PEAK BRIGHTNESS OF TYPE I SUPERNOVAE

Type I supernovae (SNI) show a small scatter in Mv (0.4 magnitudes) at maximum (Colgate 1979). It is of key importance to the understanding of SNI energetics whether or not this scatter is intrinsic or due to variable interstellar absorption. If this variation in brightness from SN to SN is in fact due to extinction, then IR observations would reduce the scatter to a few percent.

2.4.2 SUPERNOVAE AND THE EXTRAGALACTIC DISTANCE SCALE

Supernovae are among the brightest events known to astronomy. Their peak luminosity is an appreciable fraction of that of the brightest galaxies. Therefore, they can be observed at large distances. SN are events rather than objects. The variation with time of observable parameters constitutes an additional information channel which is unavailable for steady sources. One way which this information can be used is to derive the distance to the SN. One of the simplest ways in which SN can be used as distance indicators is to use the Baade method for variable stars (Branch et al. 1981). This technique relies soley on knowing the effective temperature of the expanding photosphere around the time of optical maximum, and its velocity, having adopted some specific atmospheric model.

The use of IR rather than optical data with this method would increase the reliability of distances thus determined. The derived distances are of course sensitive to the measured temperature. Blackwell and Shallis (1977) have pointed out the relative insensitivity of derived angular diameters to the estimated effective photospheric temperature when IR rather than optical monochromatic fluxes are used. Furthermore, IR derived temperatures are more accurate because of the reduced effects

of interstellar extinction and line blanketing (Blackwell et al, 1979). So by observing supernovae in the IR around the time of maximum light, we should obtain better estimates of photosphere angular diameters, which when combined with the photospheric velocity, should give an improved distance measurement.

The part of this part of the work related to distance studies relies on being able to observe supernovae near maximum light. Such supernovae could be provided by the Berkeley search because they will discover supernovae at less than 10% of maximum light. Reasonably accurate IR photometry of supernovae at cosmologically interesting distances is feasible. IR magnitudes for all Type I supernovae which have been observed at or near maximum (Elias et al. 1981) imply that 10% photometry at JHK could be typically achieved on a 4m class telescope for supernovae at distances in excess of 100Mpc.

2.5 RESULTS

The ensuing research could have progressed in many different possible directions. So far our work has concentrated on the development of IR excesses, and as a result of this program the nature and to some extent the occurrence of IR excesses in supernovae can be discussed. Unfortunately, the Berkeley search is still not operational. Even so the supernova 1983n in M83 was discovered almost two weeks before optical maximum and an early IR light curve was obtained. Further work on this supernova, this time infrared spectroscopy at a much later epoch, yielded the discovery of [FeII] 1.644μm emission line. This discovery has been used to provide a critical test of the radioactive decay model by demonstrating directly, for the first time, the presence of ~1M⊙ of Fe in the ejecta of a Type I supernova (see Appendix). The rest of this chapter reviews previous IR observations, presents our new data, and examines the nature of the IR emission from supernovae.

2.6 OBSERVATIONS

2.6.1 PREVIOUS INFRARED SUPERNOVA OBSERVATIONS

Before this programme of IR SN observations was started 6 SN had been observed at IR wavelengths. A summary of these observations is presented below.

2.6.1.1 1972e

SN1972e in NGC5253 was the first SN observed in the IR at 1.25 and 2.2μm (Lee et al. 1972). The flux at these wavelengths remained constant, while the SN declined, suggesting that a long wavelength excess was present on day 47, when the second measurement was made. The SN was also observed between 3 and 79 days at optical and infrared wavelengths by Kirshner (1973). The spectra from 0.4 to 2.2μm was found to be Planckian with a temperature decreasing from 10,000-7000K over the observation period, and therefore there was no detectable IR excess.

2.6.1.2 1979c

SN1979c is the prototype SN with an IR excess. J (1.25μm), H(1.65μm), K(2.2μm), and L(3.4μm) observations are available for this bright type II SN from 5 to 440 days after maximum (Merrill private communication 1981). The observations can be divided into two distinct phases. For the first 60 days the optical-IR continuum can be described simply in terms of photospheric emission. However, when the SN was recovered on day 259 an additional long wavelength component was present. This component continued to be present until the final observation on day 440. The late time observations dereddened with E(B-V)=0.1 (Panagia et al. 1980) are presented in fig. 2.1 showing the flux rising towards long wavelengths.

2.6.1.3 1980n, 1981n, and 1981d

IR observations of these three Type I SN were reported by Elias et al. (1981). These supernovae were observed extensively for the first 100 days, and then, only occasionally until one year after maximum. The IR light curves are quite remarkable. They show a secondary maximum, not

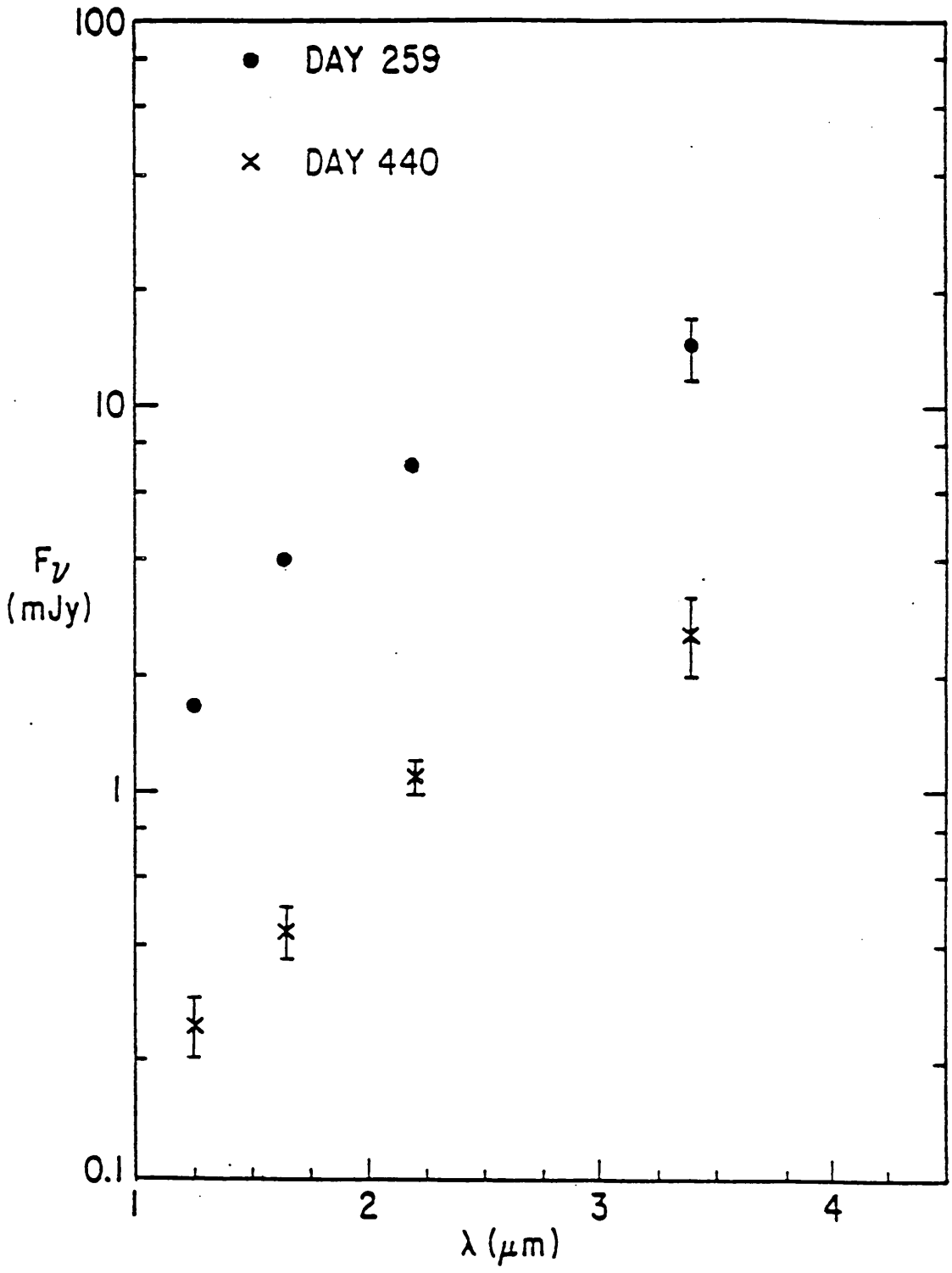

Figure 2.1

The near infared spectrum of SN1979c, showing the flux rising toward long wavelengths.

seen at optical wavelengths, about 20 days after discovery, and the three SN light curves overlie each other within the observational uncertainties, suggesting that the IR properties of Type I SN are extremely uniform. However, at no time did the IR colours show any evidence for an additional component at long wavelengths.

2.6.1.4 1980k

SN1980k was discovered on 1980 October 21 (Wild 1980). This bright SNII was observed at various epochs at all wavelengths from x-rays to radio, including 1-4μm (Dwek et al. 1983). For the first two months of observation the JHKL colours corresponded to those of a black-body with an average temperature of ~5000K. Renewed observation in May the following year showed that the SN had developed an infared excess after December 1980. This excess persisted through October 1981, and was consistent with thermal emission with a characteristic temperature falling from 900K to 700K on top of a hotter photosphere.

2.6.2 NEW OBSERVATIONS

An observing log complete up to the end of 1982 is given in table 2.1. The SN parent galaxy and Kowal's SN scheme are used to identify the SN (Kowal private communication 1984). The discovery date, and optical magnitude on that date are also given. Subsequent IR observations are tabulated, and the telescope which was used is indicated. Most of the observations were carried out by collaborating resident astronomers (D.A. Allen, A.J. Longmore and P.M. Williams) - whose help and enthusiasm made this programme feasible. Object selection, preparation; including measurement strategy, and final data reduction and analysis was done at Imperial College.

Advance telescope scheduling is much better suited to observing long term behaviour $\gtrsim$ 6 months after explosion, at intervals of months, than it is for providing the continous coverage required to follow the rapid evolution (~days) of a SN at maximum. For this reason our observations relate chiefly to the development of the IR excess.

The IR data are presented graphically in two forms. The absolute K magnitude, M_K (fig. 2.2), and H-K colour (fig. 2.3) are shown plotted against time since discovery. The distance modulus has

Table 2.1

New Observations

SN Information						Observation Information					
Parent Galaxy/ SN designation	SN Discovered	m_v or m_{pg} at max.	Type	V_o (km/s)	m-M	Date	J	H	K	L	Telescope
NGC1532 81a	03-03-82	13.5	I	1019	31.55	03-05-82			K>17.2(3σ)*		AAT
MCG-5-28-17 82a	19-01-82	16.5			36.1	03-05-82	17.48(6)	16.88(9)	16.48(11)		AAT
NGC4716 81f	30-06-81	15	I		34.6	30-07-82			K>16.0(3σ)		AAT
NGC5090 81c	02-03-81	14.5		2982	33.88	03-06-82	16.53(4)	15.80(5)	15.55(4)		AAT
NGC4490 82f	29-03-82	16		629	30.50	25-04-82	15.0(11)	13.96(4)	13.63(5)	>12.2(3σ)	UKIRT
NGC5597 81e	25-05-82	17	II	2579	33.56	08-07-82		See notes			
MCG-7-6-13 81i	10-08-81	15			34.6	03-08-82			K>18.0		
NGC1332 82e	29-03-82	14		1471	32.34	08-07-82	17.39(10)	15.47(5)	13.81(3)		AAT
						25-07-82		16.0(40)	14.3(15)		UKIRT
						03-08-82	18.28(9)	15.96(4)	14.19(3)		AAT
						13-09-82			14.91(6)	>12.5(3σ)	UKIRT
						06-10-82		17.78(11)	15.60(5)		AAT
						01-12-82			17.1(30)		AAT
						26-12-82			>17.2(3σ)		AAT
NGC7713 821	21-07-82	16.0	II	662	30.61	13-09-82		14.4(10)	13.92(6)		UKIRT
						07-10-82	15.74(4)	15.24(4)	14.66(4)		AAT

NGC0521 82o	19-08-82	15.0		5099	35.04						
NGC1255 80o	30-10-80	13.0	II	1738	32.71	13-09-82			K>17.0		UKIRT
NGC1187 82r	24-10-82	14.4	I	1413	32.26	27-10-82	14.0(10)	14.2(10)	13.9(10)		IAUC 3740
						01-12-82	15.29(4)	15.06(4)	14.71(6)		AAT
						26-12-82	16.04(5)†	15.92(7)	15.31(6)	13.0(30)	UKIRT
						27-12-82	15.87(5)	16.06(7)	15.34(6)		UKIRT

*The figure in brackets indicates the percentage error, or the significance of the upper limit.

†The airmass correction is poorly known, and consequently there is a large systematic error ≈10%

Notes:

NGC1532 — This supernova was classified spectroscopically with maximum probably on 1-3-82. (IAUC 3578, 3580, and 3585).

MCG-5-28-17 — A magnitude of J = 18.0 was measured at an equal offset distance from the nucleus at a point diametrically opposite the SN.

NGC5090 — SN position was mapped, and no point source brighter than K = 16 (3σ) was seen.

NGC4490 = Arp 269 — SN was visible on T.V. guider V ≈ 16.

NGC5597 — Mapped no point object.

NGC7713 — Optical data of 2-8-82 gives B = 16.4 and V = 16.2 (IAUC 3720).

NGC1187 — The spectrum of 24-10-82 was used to estimate that maximum occurred around 1-10-82. Optical data is available on the following date: 24-10-82; V = 14.4, B = 14.8, U = 15.05, 25-10-82 V = 14.37, B = 14.95 (IAUC 3739, 3740).

MCG-7-6-13 — On 13-08-81 V = 16.20, B = 16.62, and U = 16.80 (IAUC 3627).

been derived from the redshift assuming Ho=50km/s/Mpc. The exceptions are those SN for which no redshift is available, in which case an absolute visual magnitute of -19.6 has been adopted to derive the distance modulus. This diagram also shows the IR light curves of 1979c (Merrill private communication 1981), 1980k (Dwek et al. 1983) and the mean of three SNI's observed by Elias et al. (1981). The distances to the nearby galaxies NGC6946 and M100 have been chosen to be consistent with the long distance scale, and so the distance to 1979c in NGC6946 is 16Mpc and 5.5Mpc to 1980k in M100.

Although the initial K magnitudes are roughly similar, they begin to diverge rapidly after about 100 days, with a difference of 5 magnitues apparent between 1979c and the Elias et al. (1981) SNI's after 250 days. The colour curves also show similar disparity. The H-K colour of the three Elias' SNI's remain close to the origin with a gradual increase in redness after 100 days. All the other SN show a much redder colour at all times, with SN1979c, 80k, 82l, and 82r showing roughly similar behaviour. In particular, SN1982r which was a SNI, is markedly different from the SNI's observed by Elias et al. (1981), and demonstrates that the IR properties of SNI are not highly uniform as they anticipate.

Among these new observations are light curves for SN1982e which cover the almost unexplored interval between 100 and 200 days. Consequently these are worthy of description here.

SN1982e in NGC1332 was discovered on 1982 March 28 at m_{pg}=14.0, (Maza 1982) some 30kpc (Ho=50km/s/Mpc) from the nucleus of the parent SO galaxy (de Vaucouleurs et al. 1976). No other optical data have been reported so the SN type is uncertain, although it is probable that this was a type I supernova because no type II SN has ever been identified in a galaxy earlier than SA. IR observations were carried out at the AAT and UKIRT in the J,H, and K bands, and a single upper limit at L was also obtained. The IR colours J-H and H-K indicate that the IR flux is due to a thermal continuum with a colour temperature which falls gradually from 1170K on day 100 to 970K on day 200, and any contribution to the flux at wavelengths $\lambda>1\mu m$ from the photosphere is less than a few percent.

The overall picture which emerges from figures 2.2 and 2.3 is one in

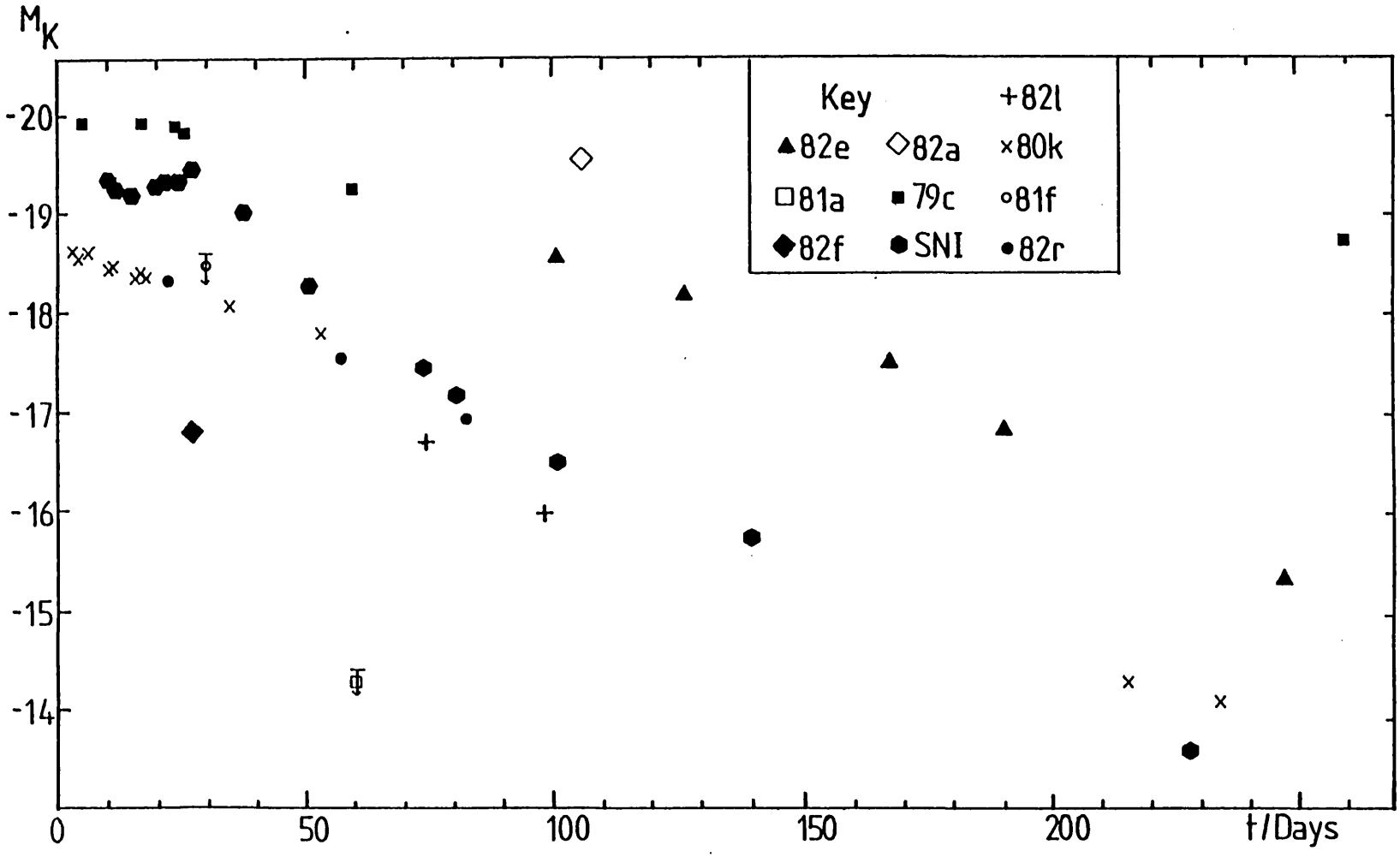

Figure 2.2

Absolute K magnitude light curve. SNI represents the composite behaviour of the three SNI's observed by Elias et al. (1981).

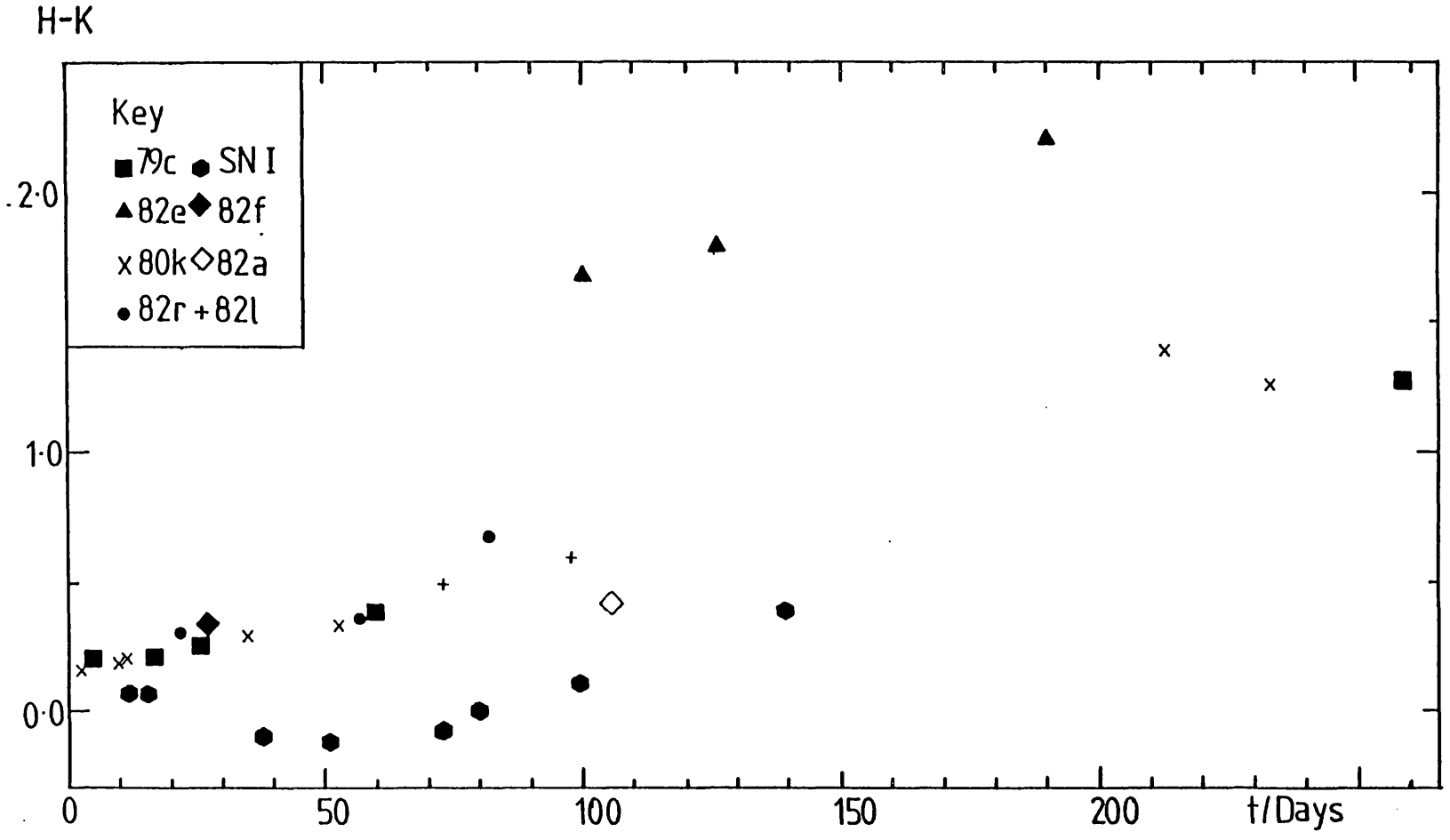

Figure 2.3

The H-K colour curve. SNI represents the composite behaviour of the three SNI's observed by Elias et al. (1981).

which there is great diversity of IR behaviour from event to event, and one in which IR excesses are common in both type I and type II SN. Let us focus our attention on determining the nature of this IR excess.

2.7 THE INFRARED EXCESS

The emergence of an IR excess is most clearly demonstrated by the simultaneous UBVJHKLL' observations of SN1980k (Dwek et al. 1983). Figure 2.4 illustrates two distinct phases in the development of the IR spectrum; and initial phase when the infrared emission is the long-wavelength extension of the photospheric emission seen at optical wavelengths, and then a second phase during which the longer wavelength infrared emission is dominated by thermal radiation from a distinct cool component. Figs 2.5 to 2.8 illustrate the same qualitative behaviour for other SN (SN1979c, SN1982e, SN1982l, and SN1982r) with the IR flux rising towards longer wavelengths.

The IR emssion from SN1980k is considered by Dwek et al. (1983). They suggest that the emssion is due to freshly condensed dust because novae, in which dust condensation is generally accepted, also show excess IR emission which only develops some time after optical maximum. One of the major pieces of observational evidence cited to support the condensation model for novae is the simultaneous rapid optical decline and IR rise . It is supposed that dust formed above the photosphere absorbs optical light and re-radiates it at longer wavelengths. No such behaviour is seen in SN light curves and so this comparison is unwarranted. In a separate paper Dwek (1983) interprets the IR light curves of 1979c and 1980k within the framework of the echo model where pre-existing dust is responsible for the IR behaviour. Although he demonstrates that his model can reproduce the observed spectra he does not show that freshly condensed dust is not a viable alternative and so there is no compelling reason for favouring either model. A critical examination of the previous observations and our new data is therefore required if we are to establish the origin of this dust.

2.7.1 ORIGIN OF THE EXCESS INFRARED EMISSION

Thermal emission from dust grains seems to provide the most plausible explanation for the excess IR emission. The absence of an excess shortward of 1μm is understood because dust grains will evaporate

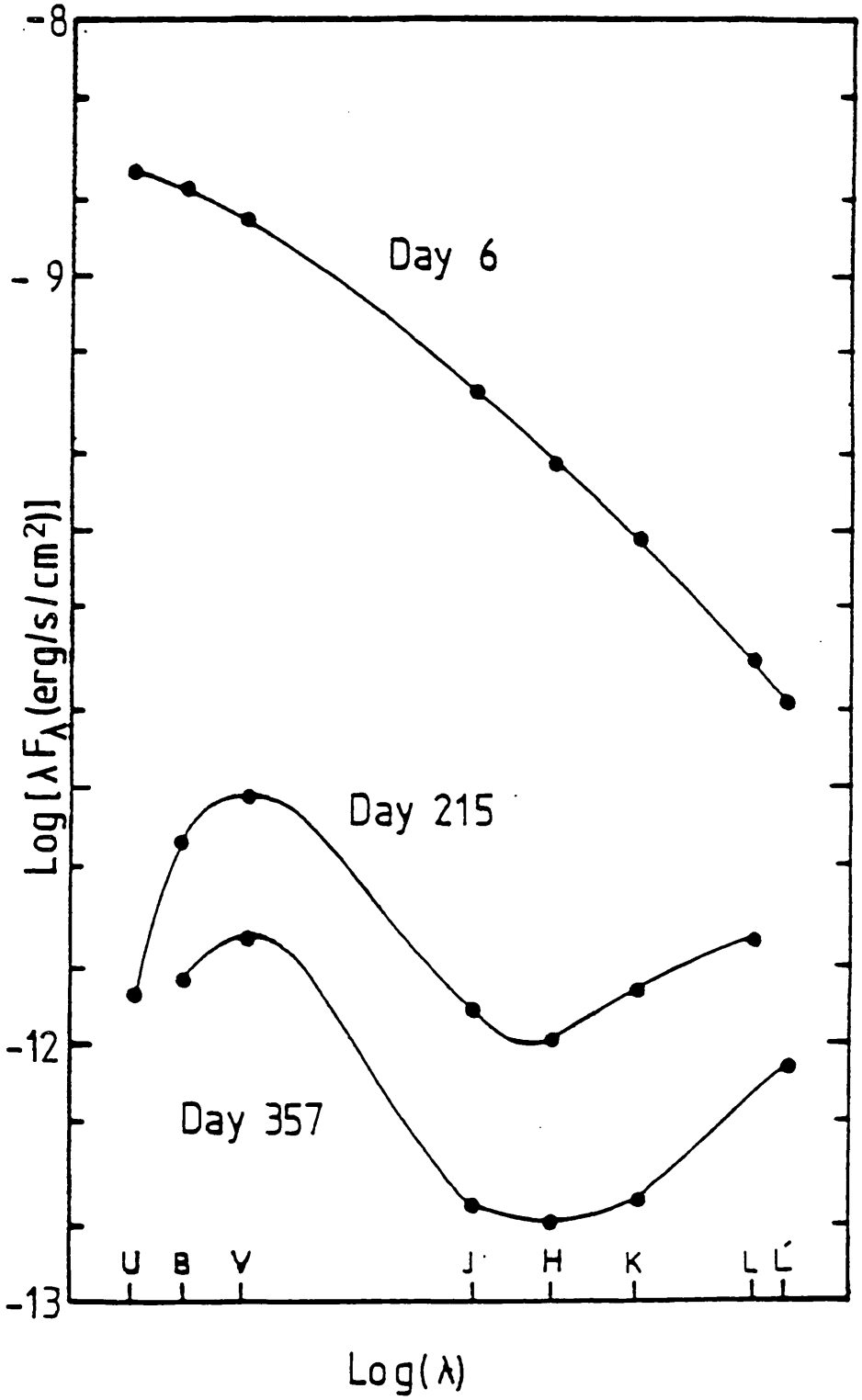

Figure 2.4

The near infrared spectrum of SN1980k. The IR emission displays two distinct phases; an initial phase where the IR is the long wavelength extension of the photospheric emission seen at optical wavelengths (upper spectrum), and then a second phase during which the IR emission is dominated by thermal radiation from a distinct cool component (lower two spectra).

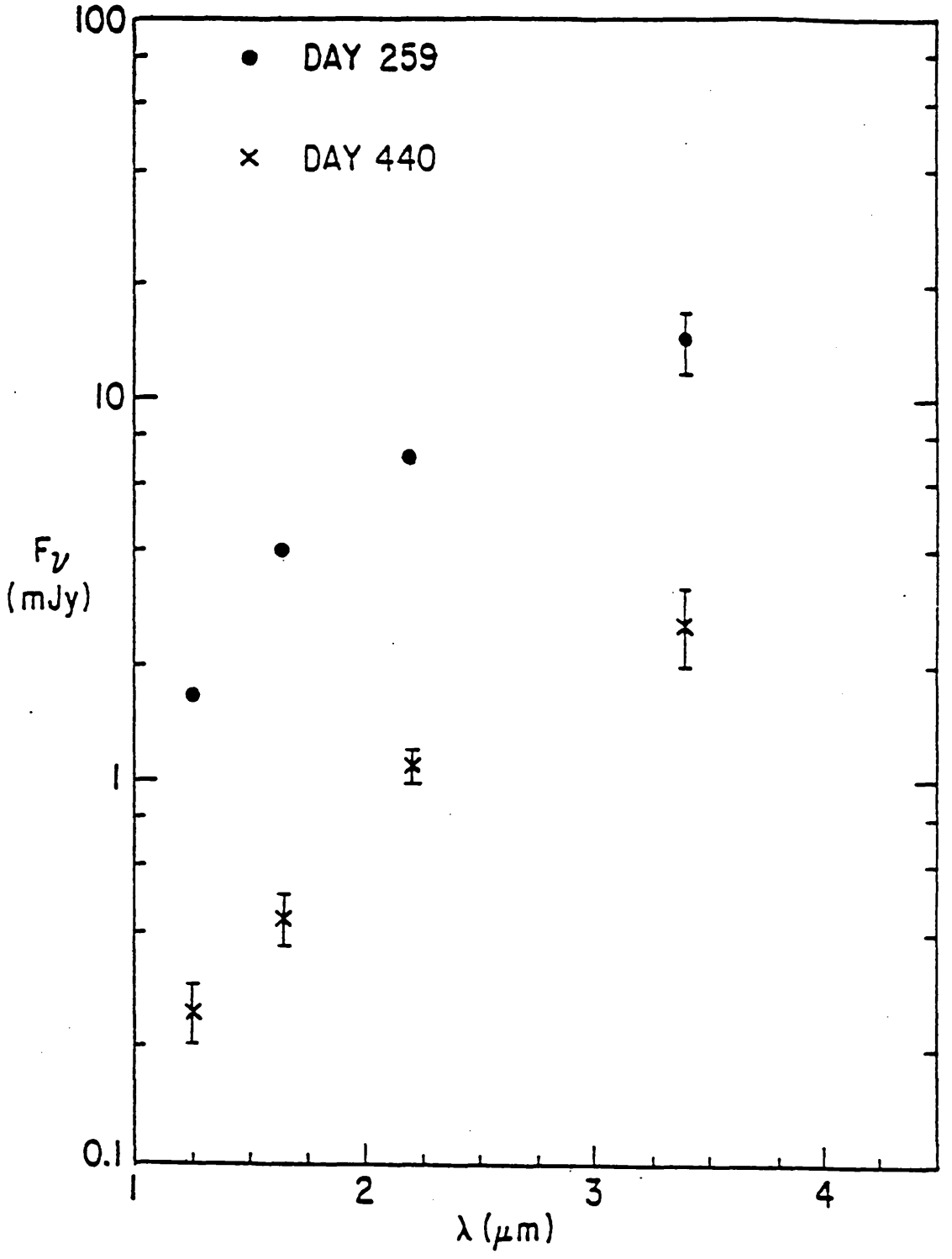

Figure 2.5

The near infrared spectrum of SN1979c.

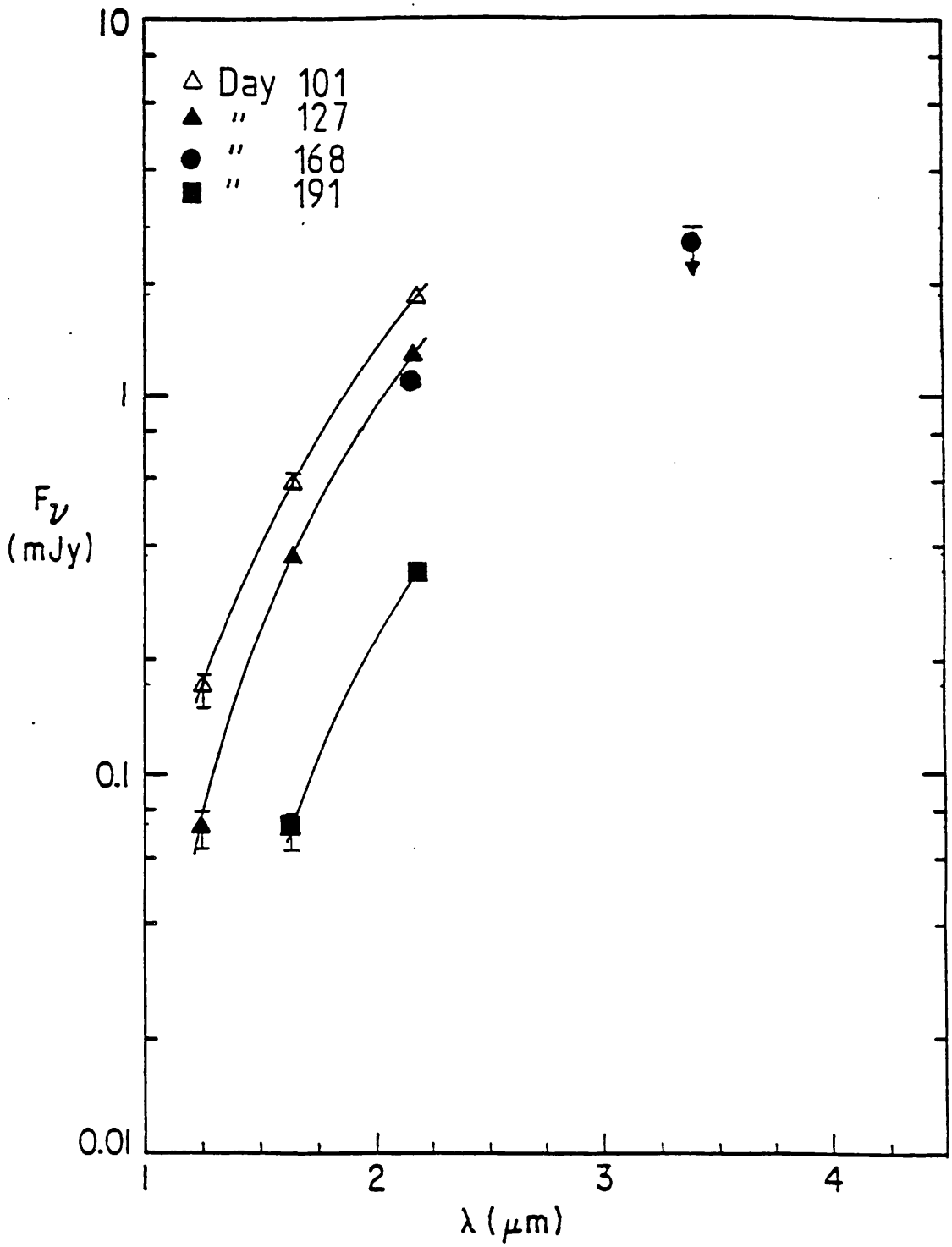

Figure 2.6

The near infrared spectrum of SN1982e.

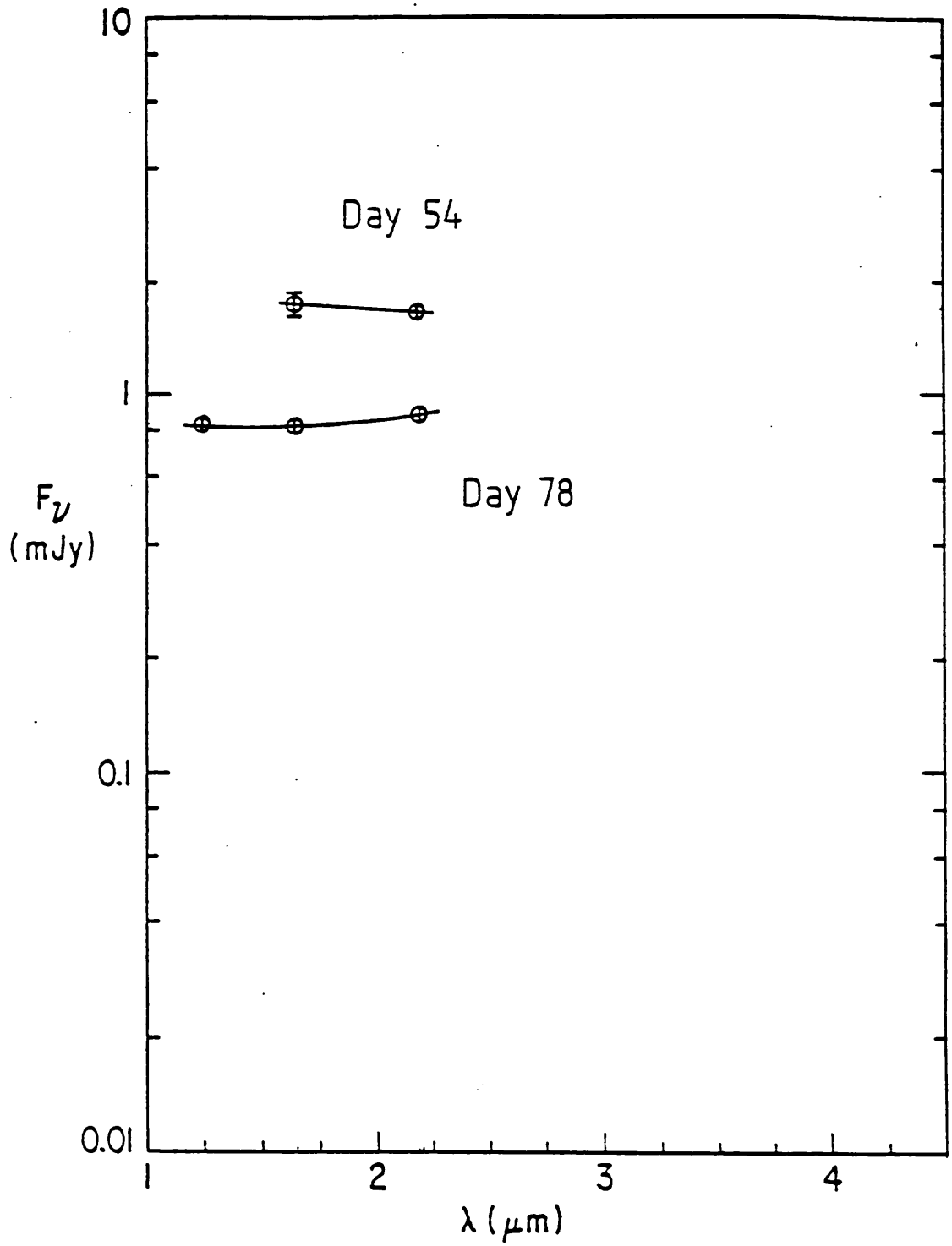

Figure 2.7

The near infrared spectrum of SN19821.

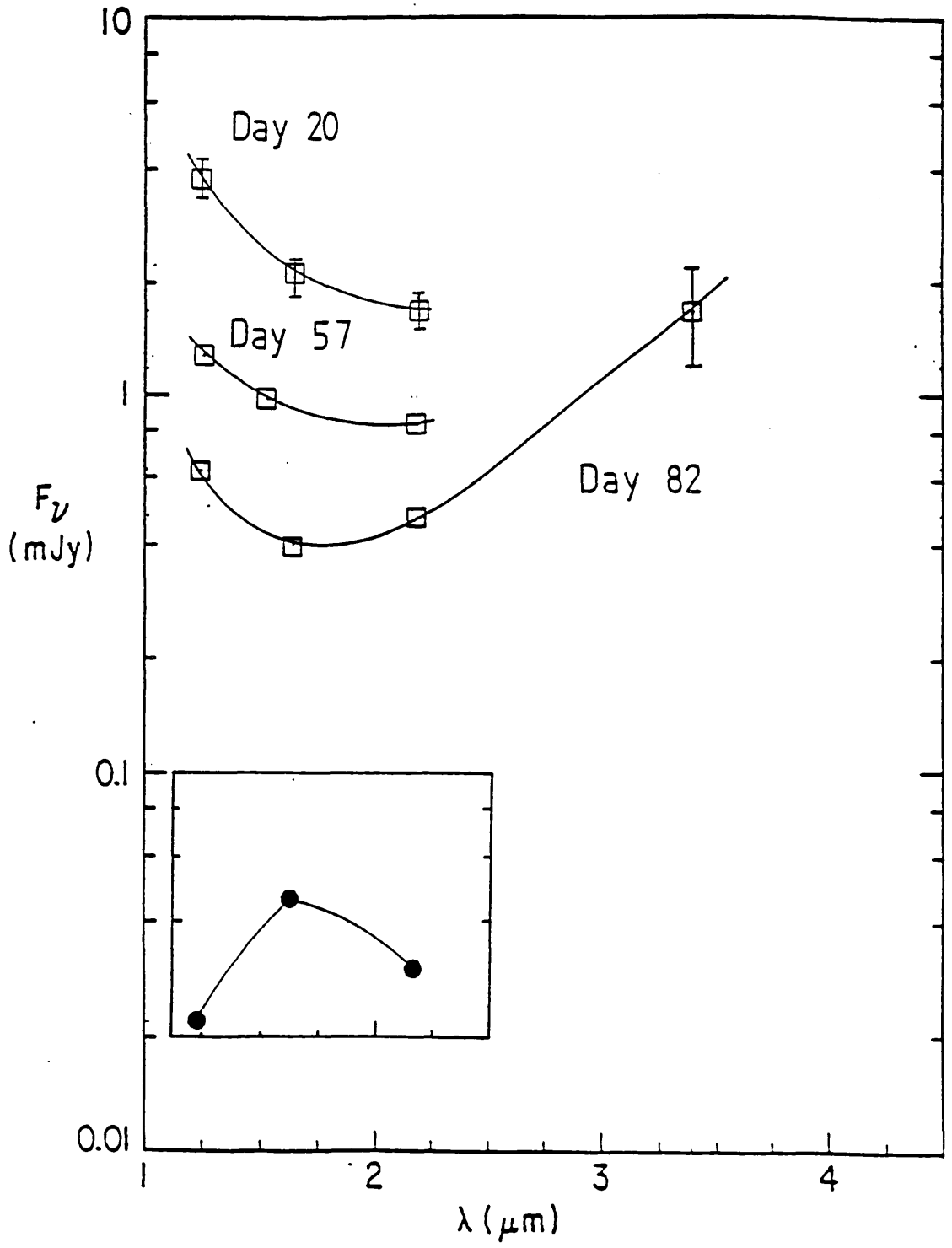

Figure 2.8

The near infrared spectrum of SN1982r. The inset spectrum is that of SN1981d on day 20. Both these SN were type I, therefore this comparison illustrates that not all SNI show similar IR spectra.

at high temperatures in excess of ~1500K. The turnover in the spectrum between 3μm and 6cm indicated by radio observation of 1980k and 1979c (Weiler et al. 1982) is accounted for by the approximately Planckian spectrum emergent from an assemblage of dust grains.

These radio data can be used to place a limit on the contribution to the measured IR flux from free-free emission which might arise from tenuous shocked circumstellar gas (Chevalier 1981). The free-free emissivity of a thermal plasma is $\propto g(\nu,T)e^{-h\nu/kT}$, where $g(\nu,T)$ is the gaunt factor (tabulated by Karzas and Latter, 1961). For a plasma temperature $T=10^4$K, the emissivity ratio $\varepsilon(3.4\mu m)/\varepsilon(20cm)=0.096$. Almost simultaneous radio and IR observations are avaiable, thus we can see from table 2.2, which displays the IR to radio flux ratios, that only a small fraction of the IR can arise from hot circumstellar gas.

TABLE 2.2

Radio to IR flux ratios

Epoch	SN	F(3.4μm)/F(20cm)
440	79c	>26
215	80k	2.1

Just as the IR properties vary greatly from SN to SN the radio behaviour shows little uniformity (Weiler et al. 1981), so generalising the above conclusion to SN without radio observations is probably unjustified. However, the IR appears to be qualititatively similar in different events, suggesting a common origin. Though it may not be proved, we may take as a plausible working hypothesis that the excess IR emission is due to thermal emission from dust grains, and establish as a particular goal the determination of the origin of these putative dust grains.

2.7.2 PRELIMINARY ANALYSIS FOR SN1980k

It is instructive to compare the optical and IR emitting region on the assumption of black-body emission. This is a reasonable description of the photospheric emission, but the apparent lack of dimming or

reddening of the photosphere at the onset of dust emission means that the dust layer cannot be optically thick, so in the following analysis the size of the IR emitting region will be underestimated. Table 2.3 shows the two component best fit black bodies, described by temperature T and solid angle Ω fitting the optical and IR data. IR temperatures were derived assuming a grain absorption coefficient which varies as $1/\lambda$ in the near IR (see section 3.4.1).

Table 2.3

SN1980k: Best fit black-bodies

Epoch	Optical T (K)	Optical Ω (Str)	IR T (K)	IR Ω (Str)	ΩIR/Ωopt	V(Ho/50km/s/Mpc)$^{-1}$ (km/s)
215	4500	2.5(-21)*	920±70	$3\pm\frac{1}{2}$(-19)	120	$3000\pm^{500}_{1000}$
357	5200	3.3(-22)	720±50	4±2(-19)	1100	2000±600

* e.g. 2.5(-21) = 2.5×10^{-21}

Thus we can see that the IR emitting region is considerably larger than the corresponding optical emission region. If we assume that the dust is distributed with spherical symmetry then the radius of that region can also be calculated and expressed as an "ejection velocity", V; the velocity which which dust formed at t=0 would have to be ejected from the SN to project the observed solid angle (see Table 2.3). As black-body emission and spherical geometry has been assumed then this velocity is an absolute lower limit. The derived "ejection velocities" are in fact comparable to the expansion velocities deduced from the widths of lines in the optical spectra at maximum light (5000km/s for a typeII,and 10,000km/s for a type I, Wheeler 1981). Dust could quite conceivably have condensed in the ejecta and reached such large distances in such a short time. Note, that if the dust cloud is optically thin, then the "ejection velocity" would be ~ $\sqrt{1/\tau}$ times greater.

2.7.3 IS DUST CONDENSATION PLAUSIBLE FOR SN1980k?

For the moment we suppose that the dust is indeed freshly condensed,

and therefore heated directly by radiation from the photosphere. We can deduce, by comparing the IR and optical luminosity, that the optical depth of the dust shell is ~ 0.4, and therefore this model is not unreasonable energetically. The required "ejection velocity" must be increased to 5000km/s, which is comparable with the highest velocities observed in a SNII. This configuration implies an upper limit on the dust temperature because we have set a lower limit on the size of the IR region. On the assumption of radiative equilibrium, considering two concentric emitting surfaces, the highest possible dust temperature is

$$T_{IR}^{4} = \frac{\Omega_{opt}}{4\ \Omega_{IR}}\ T_{opt}^{4} \qquad (2.1$$

and so $T_{IR} \leq 960K$ on day 215 , and $T_{IR} \leq 620K$ on day 357. These values are sufficiently close to the observed values that we can conclude that not only can direct photospheric heating power the IR, but it can also maintain the observed grain temperature. Thus it is not possible to exclude the possibility that the IR excess emission from SN1980k is due to freshly condensed dust grains. However, these grains would have to have formed in the fastest moving ejecta; the very outermost layers of the SN.

2.7.4 INFRARED PROPERTIES OF OTHER SUPERNOVAE

Let us apply similar analyses to the IR observations of other SN with spectra which indicate a bright IR component. (SN1982l is not considered here. It is difficult to study the IR excess of this SN because at the time of observation (80 days) photospheric and dust emission made approximately equal contributions to the flux measured at infrared wavelengths.)

We see from Table 2.4, which shows the results of the analysis used for SN1980k applied to three more SN, that the dust seen by virtue of its IR emission in SN1982e, SN1982r, and possibly in SN1979c on day 259 cannot have originated from within the SN ejecta, because the "ejection velocities" ,V, exceed by factors of 2-3 the velocities observed in the respective SN types! How is this dust heated? We have just shown for SN1980k that dust near the photosphere can be heated to temperatures which are representative of the observations. Yet this dust is clearly far beyond the photosphere and consequently should be much cooler.

Table 2.4

Best fit black-bodies

SN	t (Days)	T_{IR} (K)	Ω_{IR} (10^{-19}Str)	V(Ho/50km/s/Mpc)$^{-1}$ (km/s)
79c	259	1120±90	$6\pm^{2}_{4}$	$9400\pm^{1000}_{3000}$
	440	$1060\pm^{150}_{115}$	$1.3\pm^{0.7}_{1.2}$	$2600\pm^{700}_{1800}$
82e	101	1040±30	2.7±0.5	30000±3000
	127	950±20	3.9±0.6	29000±4500
	168	>780(3σ)	<9.6	<3500
	191	811±35	3±1	17000±3000
82r	82	900±100	2±1	30000±10000

2.8 HEATING OF PRE-EXISTING DUST GRAINS

Let us first note two important facts. SN typically reach a maximum luminosity ~10^{43} erg/s (Colgate 1979), and refractory dust grains will have, depending upon composition, an evaporation temperature somewhere in the range 1000-2000K (Salpeter 1974). Therefore grains within a radius of ~100 light days of a SN will be heated above their evaporation temperature and so destroyed. Given the necessarily extended nature of any dust cloud which survives the SN outburst (i.e. >100 light days) light travel times across the cloud must be considered, and so one might expect that the emission might resemble the UV-echo fluorescence SN model of Morrison & Sartori (1969).

2.8.1 THERMAL BALANCE OF PRE-EXISTING GRAINS

The SN flash of radiation is sharply peaked (Colgate 1979) so that we can approximate the time dependence of the luminosity to a top hat function

$$L_o = \begin{cases} 10^{43}\,\text{erg/s} & 0<t<10\,\text{days} \\ 0 & t\geq 10\,\text{days} \end{cases} \qquad (2.2$$

where t is the time since the outburst, which will be assumed to be close to the discovery date. A consequence of this narrow pulse is that only the thin shell of dust (10 light days thick) coincident with this pulse of energy is hot at any given instant.

The temperature of the dust within this shell is determined by the radiation balance

$$\frac{L_o}{4\pi r^2}\,\pi a^2 \bar{Q}(a,T_{SN}) = 4\pi a^2 \bar{Q}(a,T_g)\,\sigma T_g^4 \qquad (2.3$$

where r is the SN-hot grain distance, $\bar{Q}(a,T)$ the Planck average emissivity, a the grain radius, T_{SN} the colour temperature of the SN photosphere, T_g the grain temperature, and σ Stephan's constant. This equation predicts that dust temperature will fall in a well defined way as the pulse of radiation propagates further out into the dust cloud.

The near-IR optical properties of amorphous carbon are representative of many different possible grain types, and are therefore adopted (See Sec. 3.4.1). Using $\bar{Q}$ from Draine (1981) Eqn. 2.3 can be written to give the grain temperature as a function of the distance, in light days (l.d.), which the pulse has propagated into the cloud,

$$T_g = 950(r/100\ \text{l.d.})^{-2/5}\ \text{K} \qquad (2.4$$

if a=0.1μm and $L_o=10^{43}$ erg/s. Clearly the SN pulse can raise dust temperatures to the observed temperatures. Furthermore, only a tiny optical depth of ~0.01 across the 10 light day shell would be required to provide the observed luminosity.

The observed grain temperature indicates the distance r, at which the heated grains lie from the SN. By rearranging eqn 2.3 once again we find

$$r = 7.2\times10^{24}\ Tg^{-5/2}(a/0.1\mu m)^{-1/2}(Lo/10^{43}\text{erg/s})^{1/2}\ \text{cm}. \qquad (2.5$$

The distances thus inferred from the IR spectra are shown in Table 2.5.

Table 2.5

SN to hot grain distances

SN	t (Days)	T (K)	Lo (10^{43}erg/s)	r (10^{17}cm)	v (10^{10}cm/s)
80k	215	920±70	0.6	2.17±0.4	1.17±0.2
	357	720±50		4.01±0.7	1.30±0.1
79c	259	1120±90	2.5	2.7±0.5	1.22±0.2
	440	$1060\pm^{150}_{115}$		$3.1\pm^{1.1}_{0.85}$	$0.82\pm^{0.3}_{0.2}$
82e	101	1040±30	1†	2.06±0.2	2.37±0.2
	127	950±20		2.59±0.1	2.36±0.1
	191	811±35		3.84±0.4	2.33±0.3
82r	82	900±100	1†	3±1	4±1

† assumed luminosity

The case of SN1982e is particularly interesting. On a plot of SN hot grain distance versus time the data lie on a straight line which passes through the origin (fig. 2.9). The best fit straight line has a gradient

$$v = (2.4\pm0.1) \times 10^{10} \, (a/0.1\mu m)^{-1/2} \, (Lo/10^{43}erg/s)^{1/2} \quad cm/s \qquad (2.6.1$$

and an intercept

$$r_o = (0.0\pm0.1)\times10^{17} \quad cm \qquad (2.6.2$$

The echo model predicts this linear behaviour with zero intercept, and that the gradient of this line should be ~ of the speed of light, as shown below.

When a source switches on in a dust cloud, light travel time arguments show that the grains from which a distant observer receives IR emission lie within a paraboloid of revolution $r=ct/(1-\cos\theta)$. For a pulse like light curve heated dust is confined within a thin shell such as is illustrated in fig. 2.10. For a given paraboloid the temperature distribution is such that the hottest dust is situated at the vertex ($r=ct/2, \theta=\pi$), the point closest to the SN. Integrating the flux from the paraboloidal shell one can show that nearly all the flux comes

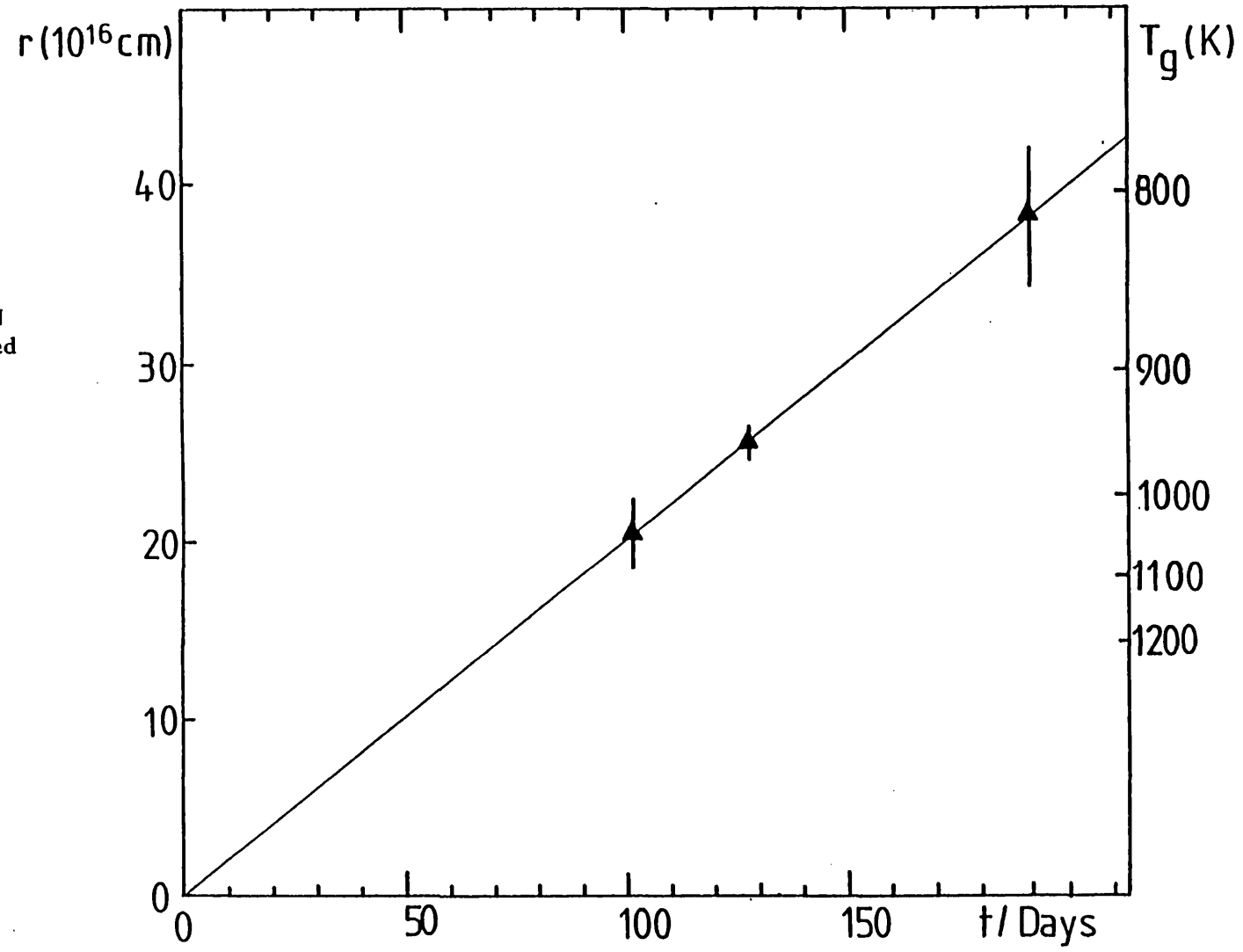

Figure 2.9

The hot grain to SN distance, r, plotted against time. The solid line is the best fit straight line.

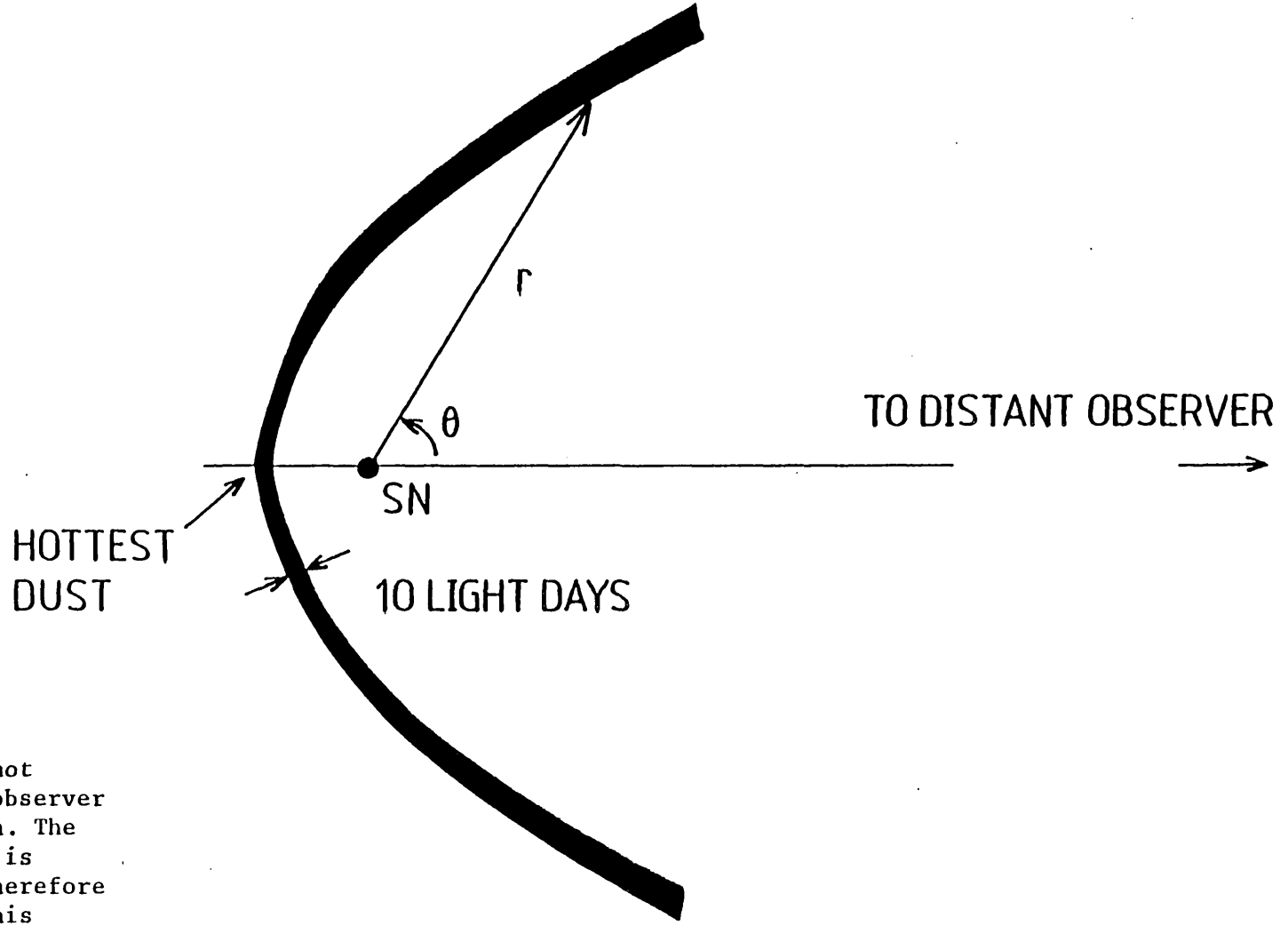

Figure 2.10

The paraboloidal shell of hot dust from which a distant observer receives infrared radiation. The hottest dust is that which is closest to the SN and is therefore located at the vertex of this paraboloid.

from the hot region around the vertex, provided that the observations are made on the Wien slope of the thermal emission. For example, if the dust at the vertex has a temperature of 1000K, and the observations are made at 2.2μm, then 90% of the flux comes from within 30° of the vertex. Thus the temperature derived from near-IR photometry is that of dust around the vertex. The apparent recession velocity derived from the cooling rate of the dust is

$$\frac{\partial}{\partial t}\left(\frac{ct}{1-\cos\theta}\right)\Big|_{\pi} = c/2 \qquad (2.7$$

which is consistent with the determined velocity, given uncertainties in grain size and SN luminosity. Furthermore, the linearity and zero intercept of the r,t graph of SN1982e all add extra weight to the echo hypothesis. Additionally, a straight line through the origin with a gradient ~ c/2 fits both the data points of SN1979c and 1980k (fig. 2.11), indicating that the temporal evolution of the temperature is that expected from an echo. It is interesting that, for these two SN for which the peak luminosity has been measured, a single r,t line, i.e. a single cooling law, can, within the errors, describe both data sets, and the gradient of this line (1.2×10^{10}cm/s) is remarkably close to the predicted value of c/2.

2.9 SUMMARY

The undoubted conclusion of the preceding section must be that the IR emission from SN1982e was due to dust grains which formed long before the explosion. These dust grains are found at distances > 100 light days from the SN, and are heated by radiation which left the SN during its most luminous phase. SN1982r no doubt exhibited similar behaviour to 1982e. Unfortunately, no further observations of this SN are available. The origin of the dust in SN1979c and SN1980k is uncertain. Firm conclusions are made impossible by the poor temporal coverage and inadequate photometric accuracy. However, the quantitative similarity of these SN to SN1982e, especially in regard to the time evolution of the temperature, could be interpreted as indicating that these SN also had pre-existing dust shells.

IR excesses have been observed in both type I and type II SN. Some SNI show excesses (2) where observations at the same epoch of other SNI's

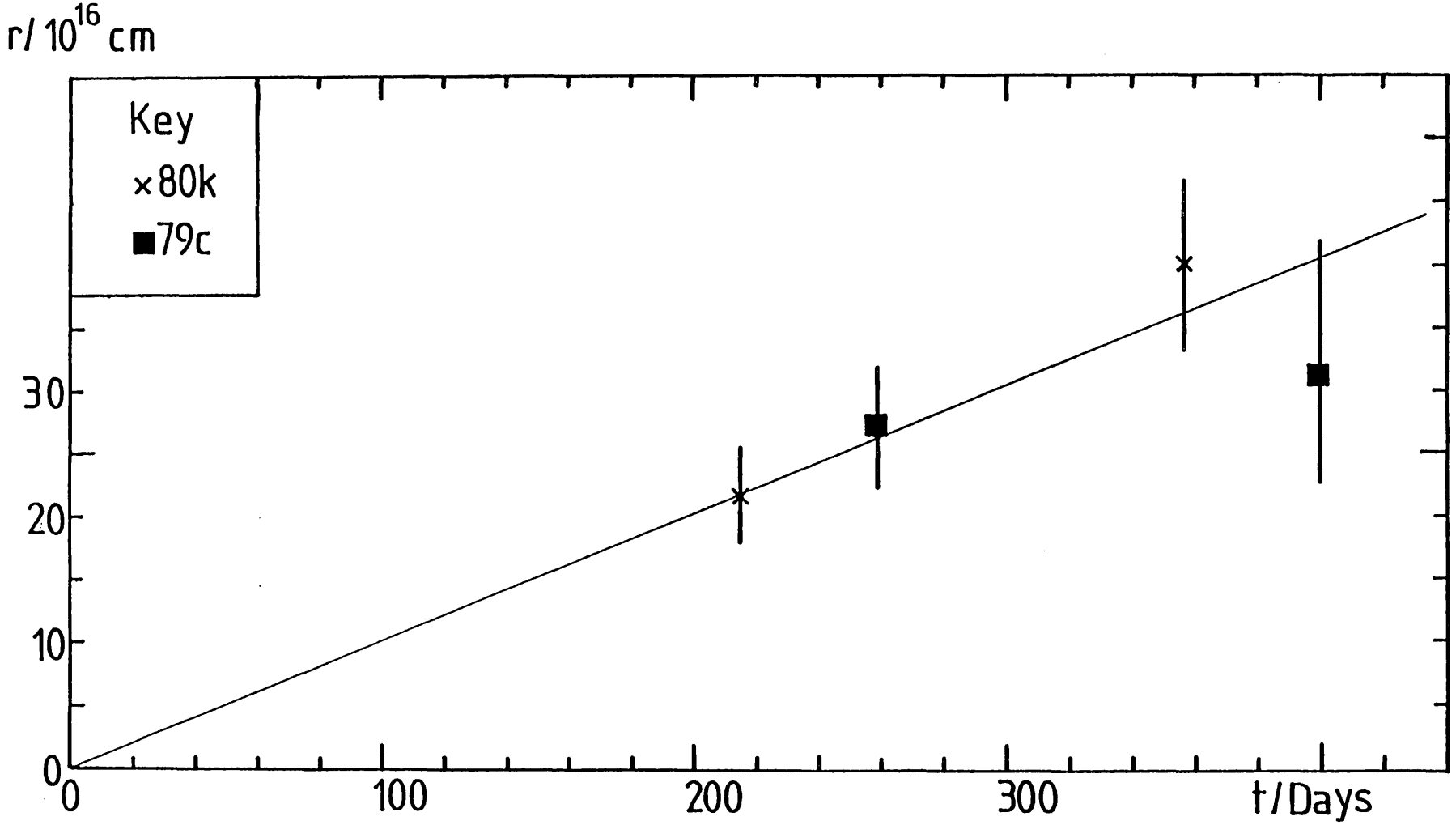

Figure 2.11

The SN-hot grain distance, r, for SN1979c and SN1980k.
The solid line is the best straight line through the origin.

(4) demonstrate that others do not. All type II SN (3) observed a few months after maximum have shown evidence for an additional long wavelength component. The present data set is subject to uncertain selection effects and much too small to draw any further conclusions regarding the occurrence of excesses.

2.10 DISCUSSION: CONDENSATION IN NOVAE AND SUPERNOVAE

One of the principal pieces of evidence adduced to support the hypothesis that dust condenses in nova ejecta is the observation of the simultaneous rapid rise and fall of the IR and optical fluxes respectively (e.g. Ney and Hatfield 1978). It is this behaviour which is interpreted as being due to dust condensing in the ejecta above the photosphere absorbing optical radiation and re-radiating it in the IR. A gradual optical recovery period follows this transition phase during which it is supposed that the absorbing dust is diluted by the expansion.

Should similar behaviour be seen in a SN? Novae and SN are quite different systems. While expansion velocities are comparable, the luminosity of a nova is only $\sim 10^{-4}$ of that of a SN at maximum (Bath and Shaviv 1976). As peak temperatures in novae and SN are similar the nova photosphere is some 100 times smaller. Nova ejecta also suffer severe adiabatic losses because the material must expand from an originally compact configuration, whereas a SNII is thought to originate from an explosion within a red supergiant, with an initial radius $\sim 10^{14}$cm, and a SNI ejecta contains decaying radioactive nuclides (Colgate and McKee 1969) which supply a continuing source of energy and thus in either case high temperatures ($>10^3$K) are maintained for $\sim 10^3$ days. All these factors will conspire so that dust condensation in SN will lag behind condensation in novae.

The presence of non-thermal particles (gamma rays and relativistic positrons) in a SNI complicate any consideration of condensation so the following discussion will be confined to SNII. A SNII is thought to occur when a red supergiant star suffers core collapse. When numerical models of SNII based on this premise are calculated they are found to be in good agreement with the observations (Falk and Arnett 1979). In particular the resultant temperature evolution for the period for which relevant data are available (~100 days) is in excellent agreement

with observations. Therefore these models can probably be used to predict the conditions in the ejecta somewhat beyond this time. According to Falk and Arnett (1979) only a small fraction of the hydrogen rich envelope cools below 2000K before 200 days. Therefore condensation can only occur before this date, if, as in novae, the expansion can carry material sufficiently far above the photosphere so that radiative heating does not destroy any grains which do form, by raising their temperatures above their evaporation limit. In a nova ($L \approx 5 \times 10^{38}$ erg/s) after only 30 days the expansion has carried the ejecta far enough away so that dust grains can survive, i.e $T_g < 2000$K. Similar consideration for a SNII (based on the extensive bolometric light curve of SN19691, Weaver and Woosley; 1980) indicates that dust cannot condense until after 200 days.

Perhaps it is not surprising that the dust seen before ~200 days has been attributed to a pre-existing shell. However, it is not implausible that dust seen after this date could be dust which condensed within the SN ejecta. The problem of identifying this dust would seem to be that of distinguishing it against a background of IR emission from pre-existing grains. Freshly condensed dust will presumably be most readily detectable when it has just condensed and consequently hottest. So the way to discover this dust is to search for an additional hot component in the IR spectrum which emerges after ~200 days. Thus we must observe the onset of IR emission due to pre-existing dust, follow the IR light curves, and determine the echo cooling law. It will then be possible to determine whether or not subsequent observations made after ~200 days include an extra hot component in addition to pre-existing grains. Dust producing such a component can only be hotter than pre-existing dust if it lies within the volume where the pre-existing grains were destroyed by the SN at maximum, and therefore a hot dust component constitutes evidence for condensation within the ejecta.

CHAPTER III

THE INFRARED ECHO MODEL

3.1 INTRODUCTION

The infrared light curves of SN1982e in NGC1332 described in the previous chapter represent the most complete and accurate set of data relating to the development of thermal dust emission from a supernova. In Chapter II it was demonstrated that the emitting dust pre-existed the supernova explosion, and lies within a dust shell of a radius of at least a few hundred light days. This discovery warrants further investigation. In this chapter the details of time varying dust temperatures in a circum-supernova dust shell, and the resultant infrared radiation are worked out, so that the structure of the dust cloud around SN1982e can be studied.

The consequences of the presence of this dust cloud for the understanding of pre-supernova evolution are discussed, and a novel insight into the triggering of a supernova explosion is presented.

3.2 RADIATIVE TRANSFER IN A DUST SHELL

The problem of calculating the radiative transfer in a circumstellar dust cloud and the subsequent infrared radiation has been treated many times (e.g. Jones & Merrill 1976, Rowan-Robinson 1980) The additional difficulties which arise when the source of short wave radiation is variable have also been considered in some depth (Bode & Evans 1979), and a special variant of the theory has been developed to explain the infrared emission from novae (Bode & Evans 1980). But to date discussions have been fairly abstract. The supernova in NGC1332 is the first infrared source which has been shown conclusively to be due to an echo; the infrared emission of novae is usually understood in terms of dust condensation (e.g. Ney and Hatfield 1978). So for the first time there is the opportunity of using observations coupled with echo theory to yield information about the source of primary radiation and the dust cloud and its constituent grains. Here we incorporate the basic property of any echo model i.e. we take account of the finite light travel time across the dust cloud, but our approach is to tailor the

model to describe the conditions in supernova dust clouds, whilst retaining as much simplicity as possible without prejudicing accuracy. We hope to maximise the information which we can extract during the analysis by minimising our assumptions.

We consider a spherically symmetric dust cloud centred on the supernova composed of spherical dust grains of a unique size and composition. We assume that the cloud is optically thin to its own infrared ($\lambda > 1\mu m$) radiation, and is static on timescales ~ few hundred days.

3.2.1 DUST GRAIN TEMPERATURE

If the supernova is surrounded by a dust cloud of sufficiently great extent, there will be a significant time delay t', due to the finite velocity of light, between observation of the optical photons which set out from the supernova directly towards the earth, and those photons which were absorbed and re-radiated into the infrared by a dust grain at (r,θ). This delay is given by

$$t' = (r/c)(1 - \cos\theta). \qquad (3.1$$

See figure 3.1 for an illustration of the co-ordinates used.

If a distant observer sets his clock, which reads t_0, to 0, when he sees the leading edge of the UV-optical light pulse, then grains at (r,θ) whose IR emission is due to absorption of radiation from the leading edge of the pulse is not observed until $t_0 = t'$. So the grains heated by the leading edge of the pulse lie on a paraboloidal surface of revolution

$$r = ct_0/(1 - \cos\theta), \qquad (3.2$$

where the supernova is located at the focus of the paraboloid. The time t' at which the observer first receives IR radiation from a particular paraboloidal surface, i.e. when it is first heated by the leading edge of the pulse, is a useful co-ordinate which we will use later to identify any paraboloid within the cloud.

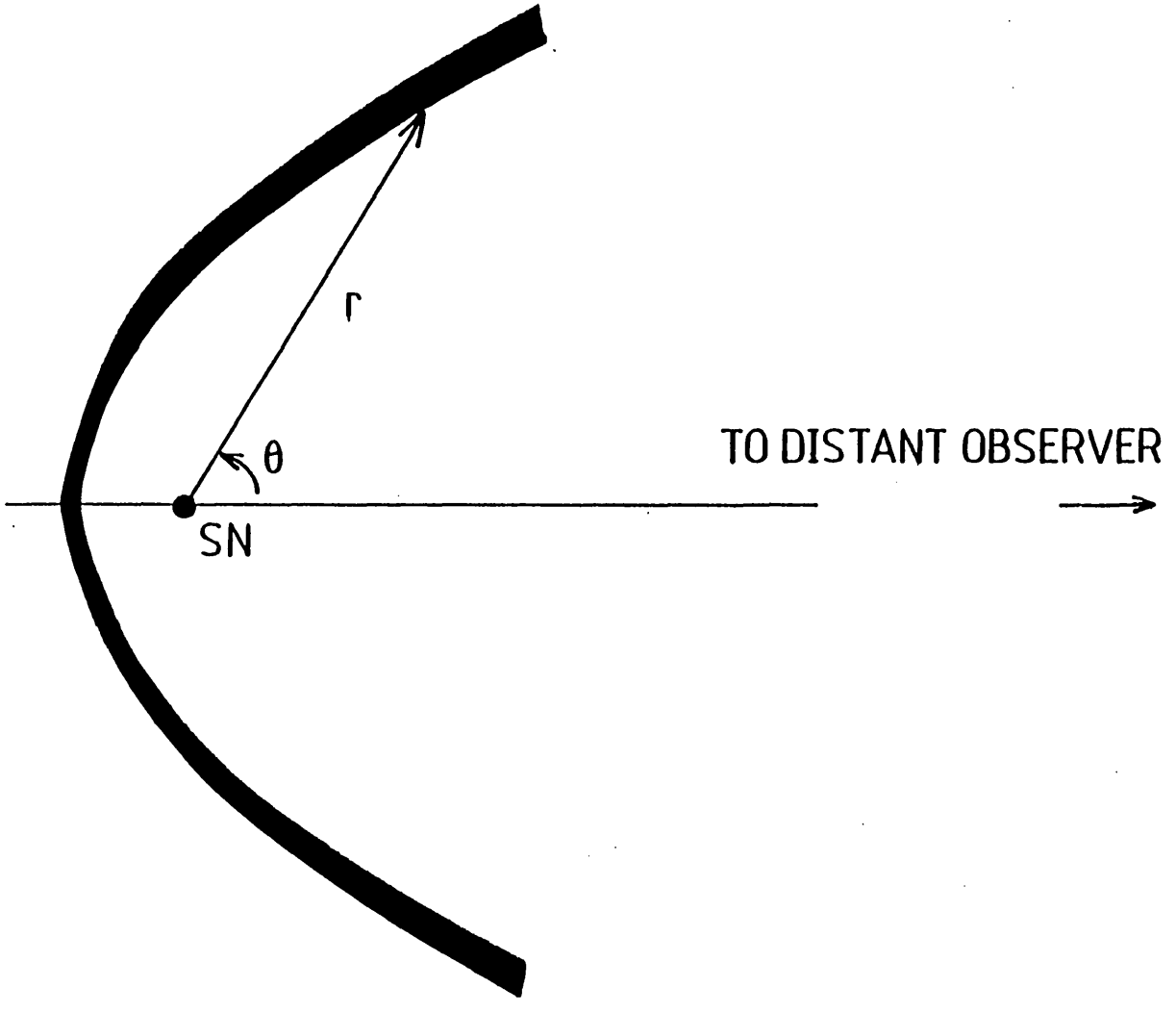

Figure 3.1

Dust cloud geometry; a paraboloidal shell of dust surrounding the SN is shown, and the cloud co-ordinate system is illustrated.

The consequence of the time delay is that according to a distant observer the temperature of a dust grain within the cloud is not only a function of its distance from the supernova and the time since the supernova explosion was observed, but also a function of the angle which the radius vector from the supernova to the dust grain makes with the line of sight.

If the UV-optical luminosity observed at time t_o is $L(t_o)$, then the simultaneously observed IR emission from paraboloid t' is caused by absorption and re-radiation of the UV-optical energy corresponding to the earlier epoch $t_o - t'$ when the observed UV-optical luminosity was $L(t_o - t')$. The temperature of dust grains, T_g, on the paraboloidal surface t' is given by the radiation balance equation

$$\frac{L(t_o - t')\ e^{-\tau^*}}{4\pi r^2}\ \pi a^2\ \bar{Q}(a, T_{SN}) = 4\pi a^2\ \bar{Q}(a, T_g)\ \sigma T^4 \qquad (3.3$$

τ^* is the optical depth from the supernova to a grain located at paraboloid t' at optical-ultraviolet wavelengths. a is the grain radius, $\bar{Q}(a,T)$ is the Planck average emissivity, T_{SN} is the colour temperature of the supernova, and σ is Stephan's constant.

3.3 THE EMERGENT FLUX

In order to work out the IR flux at the earth resulting from a particular temperature structure in the cloud, we divide it into infinitessimal paraboloidal shells and calculate the contribution to the flux from each shell. Assuming the cloud to be optically thin to its own IR radiation and neglecting scattered supernova light, we then integrate over all the shells and so obtain the total IR flux from the cloud at any time t_o. The IR flux dF_ν from one paraboloidal shell at distance d is

$$dF_\nu = \int_{ct'/2}^{R_2} nQ_a \pi B_\nu(T_g) \frac{4\pi a^2}{4\pi d^2} \, dV, \qquad (3.4$$

where the integral extends over the spatial extent of the paraboloid, i.e. from the vertex ($r' = ct'/2$) to the outer radius ($r' = R_2$) of the dust shell. n is the grain number density, Q_a is the absorption efficiency, $B_\nu(T_g)$ is the Planck function and dV is an infinitessimal volume element of the shell. In polar co-ordinates the above integral can be re-written as

$$dF_\nu = \frac{cdt'}{d^2} \int_{ct'/2}^{R_2} n\pi a^2 \, Q_a \, B_\nu(T_g) \, 2\pi r dr \qquad (3.5$$

by using equation 3.1 The total flux $F_\nu(t_0)$ from the cloud at time t_0 is therefore obtained by integrating over all the paraboloidal shells, i.e. by integrating over the co-ordinate t'.

$$F_\nu(t_0) = \int_0^{t_0} dt' \int_{ct'/2}^{R_2} \frac{c}{d^2} \, n\pi a^2 \, Q_a \, B(T_g) 2\pi r \, dr \qquad (3.6$$

The limit $t' = 0$ corresponds to dust along the line of sight to the supernova, and $t' = t_{obs}$ corresponds to the outermost heated paraboloid from which IR radiation is received at time t_{obs}.

With our limited knowledge about the nature, size and distribution of the grains in the cloud, it is not possible to uniquely determine the temperature within the cloud or the total flux. In order to make a start we have to make reasonable assumptions about the nature of the dust cloud and the supernova. For the dust grains we will have to assume their optical properties and restrict the nature of their distribution. As we do not have bolometric measurements for the supernova in NGC 1332 we depend upon the fact that supernovae form a fairly homogeneous class and assume a typical bolometric light curve. But by assuming only the functional dependence of supernova luminosity on time, of grain absorbtion efficiency on wavelength, and a power law grain number density distribution, we will show that the model is able

to reproduce the observed IR light curves in a self-consistent manner together with providing information about the ratio of peak supernova luminosity to grain absorption efficiency, the grain evaporation temperature, the optical depth due to dust and also the index of the dust cloud power law density distribution. Finally by assuming the optical absorption efficiency per grain we can find the grain radius, and, if the density of the solid material which composes the grains is known, the total mass of dust in the cloud.

3.4 BOUNDARY CONDITIONS

3.4.1 DUST GRAIN OPTICAL PROPERTIES

For the first stage of the echo analysis it is only neccessary to decide upon the wavelength dependence of the absorption efficiency because at first we only want to reproduce the IR colours and the shape of the IR light curves. The absolute value of the efficiency per grain is only required when we need to calculate the mass of dust in the cloud. The infrared colours are equally well fitted by a black-body, or typical grain emissivity laws which vary as $1/\lambda$, or $1/\lambda^2$. Consequently it is not possible to determine the emission law directly. Indeed this approach could well be misleading because we are not observing dust at a single temperature. We must choose a form of efficiency which will be appropriate for either carbon or oxygen rich grain compositions. An absorption efficiency which varies as $1/\lambda$ in the near infrared ($1<\lambda<3\mu m$) seems reasonable for both cases and corresponds to the small particle limit of Mie scattering for particles with a constant complex refractive index (Aannestad 1975). The most likely grain type in a carbon rich environment, amorphous carbon, exhibits this behaviour (Koike et al. 1980). Crystalline carbon, graphite, although a favoured grain type for some time, seems unlikely to form in astrophysical environments (Donn et al, 1981.). The amorphous allotrope is also favoured by long wavelenghth IRAS observations of dusty carbon stars (Rowan-Robinson 1984). If the grain composition was oxygen rich and consequently of a "silicate" type then our choice of the near infrared wavelength dependence of Q_a would be the same. Silicate material which is though to be found in astrophysical environments - "dirty silicates" (Jones and Merril, 1976) - also have an absorption efficiency which varies as $1/\lambda$ in

the wavelength interval 1-7μm. The efficiency of these grains is high and comparable to that measured for amorphous carbon (Koike et al. 1980). In the range of temperatures of interest 800-1000K; the temperature range which characterises our observations, most of the grain radiation is emitted in the interval where $Q_a \propto 1/\lambda$ and so we expect that $\bar{Q} \propto T$ will be a good approximation. We have calculated Planck averaged emissivities for the "dirty silicates" of Jones and Merrill (1976), and the emissivity is proportional to T in the range $700<T<1000$ K, and the corresponding Planck average emissivity for amorphous carbon is given by $\bar{Q} \propto T$ so long as $T<1000$K (Draine,1981).

When it comes to evaluating the efficiency of an individual grain so that we can calculate the mass of dust we will use the optical properties of amorphous carbon, which have been measured by Koike et al. (1980), to typify all grain materials. We approximate their results for $1<\lambda<100\mu$m for grains formed by burning xylene in air by $Q_a/a=2.5/\lambda$ For the sake of simplicity we will assume that grains will absorb the radiation from the supernova efficiently, so that in the UV and optical $Q_a=1$, and $\bar{Q}(T_{SN})=1$.

3.4.2 THE DUST GRAIN DISTRIBUTION

Only power-law grain distributions of the form $n \propto r^{\beta}$ will be considered. This choice covers most of the plausible possibilities, e.g. $\beta=0$, represents a constant grain distribution as might be expected if the supernova were embedded in a dusty ambient medium, or $\beta=-2$ if the grain distribution results from grain condensation in a stellar wind of constant $\dot{M}/V_{wind}$. The cloud is also chosen to have sharp inner and outer edges.

3.4.3 THE INNER CLOUD LIMIT

A grain with a sublimation temperature ~1000K will be destroyed out to about 50 light days. As grain condensation is expected to occur within a few tens of stellar radii then the closest distance at which we will find dust depends upon whether or not pre-existing dust there has been destroyed. Grain survival depends almost exclusively upon the maximum grain temperature reached due to the supernova radiation field

(Falk & Scalo 1975) which, in turn, depends only upon its distance from the supernova. As the supernova radiation propagates outward into the dust cloud it will continue to evaporate dust for some time until the radiation becomes so dilute that it can no longer raise grains above their evaporation temperature. Thus, ignoring partially evaporated grains, we can define an evaporation temperature T_{evap}. Grains heated above T_{evap} are completely destroyed, but grains which do not exceed this temperature survive intact. From equation 3.3 we can see that T_{evap} corresponds to a radius R_{evap} within which grains are heated to destruction. For some time $t_{obs}<2R_{evap}/c$ an "evaporation wave" propagates outward into the dust cloud creating a dust free cavity, leaving the radiating dust observed at the Earth contained between the outermost paraboloid ($t' = t_0$) and the cavity - see figure 3.2

Grain destruction is almost instantaneous. The heating timescale $U/\dot{U}\sim 0.01$s so the evaporation wave is very thin and contains only a very small mass of dust at any instant. The resultant infrared radiation from evaporating grains is therefore negligible.

3.4.4 THE OUTER CLOUD LIMIT

The outer limit to the dust cloud can not be determined so easily. Initially assume that R_2 is practically infinite, i.e. $R_2>>ct_0/2$ so that the dust at the outer edge of the cloud is cold, and makes no significant contribution to the flux. As observations extend to ~ 250 days it will be possible to test whether or not there is still dust at the corresponding distance from the SN.

3.4.5 THE BOLOMETRIC LIGHT CURVE

The infrared radiation from a SN dust cloud must depend strongly on the input light curve, but the bolometric light curves of SNI's and SNII's are remarkably similar in spite of the very different mechanisms supposedly responsible for the explosion. The most apparent difference is the greater luminosity at maximum of SNI's. The bolometric light curve can be characterised by a very rapid rise to maximum. The initial

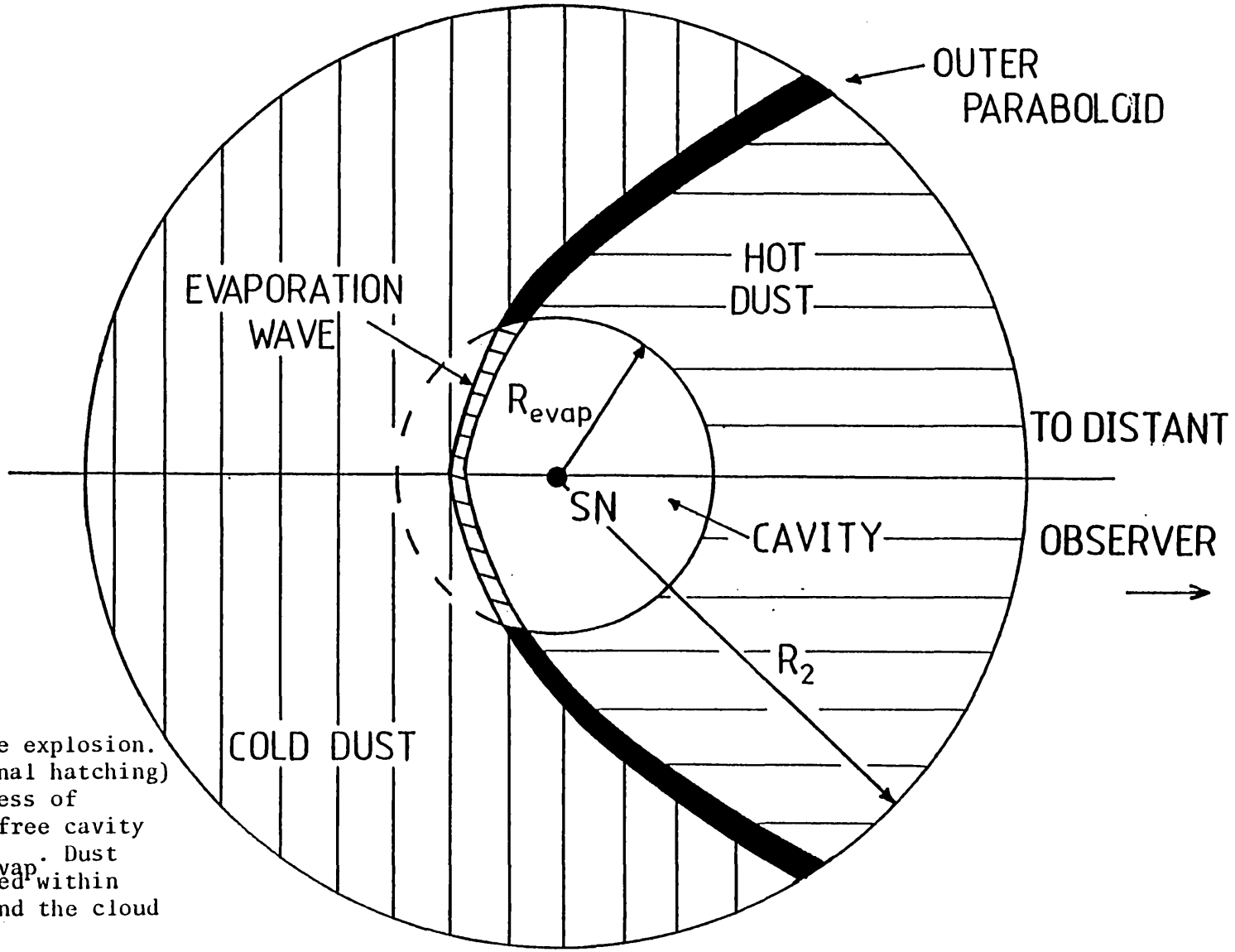

Figure 3.2

The SN dust cloud after the explosion. An evaporation wave (diagonal hatching) is illustrated in the process of creating a spherical dust free cavity around the SN of radius R_{evap}. Dust heated by the SN is confined within the outermost paraboloid and the cloud limit R_2.

decline of a type I event has an e-folding time of ~ 20 days, and lasts about 50 days. This is followed by a final decline with an e-folding time of about 70 days (Barbon et al. 1973). A type II's initial luminosity is more impulsive, falling by a factor of 10 in the first 30 days, after which it goes through a plateau phase, which lasts another 50 days (Barbon et al. 1979). In either case most of the energy is radiated in the first 20-30 days. It is this highly peaked outburst combined with the echo geometry and the grain density distribution that primarily determines the development of the emergent infrared radiation.

It is very likely that SN 1982e was a type I event. This follows from: a) The early parent galaxy type (SO) - no type II has ever been observed in a galaxy of type SA or earlier (Kowal 1984). b) The large distance (~30 kpc, Ho = 50 km/s/Mpc) of the supernova from the nucleus - well away from any region of recent starformation where the massive progenitors of type II SN are thought to be born (Maza and van den Berg 1976). Lacking any optical observations, apart from the discovery plate, we can only assume that SN 1982e was typical of other SNI's. SNI optical light curves show a remarkably small scatter in peak brightness and evolution (Barbon et al. 1973). We can therefore represent the SN 1982e bolometric light curve with those of other, better observed SNI's. We shall therefore use the bolometric light curve of SN 1972e as reconstructed by Axelrod (1980). This supernova was observed between 1400 - 22000Å around maximum light, and 3500 - 10000Å at later times. Taking the distance to the parent galaxy NGC5253 to be 4Mpc (Sersic et al. 1972), a least squares double exponential fit to the bolometric light curve gives

$$L = L_0 \quad x \quad \begin{cases} e^{-t/22.8} & 0<t<54 \\ 0.181\, e^{-t/73.5} & t>54 \end{cases} \qquad (3.7$$

$L_0 = 2.0 \times 10^{43}$ erg/s, with t in days.

3.5 COMPARISON OF THE MODEL WITH THE DATA

Equations 3.3 and 3.6 are now combined to enable the evaluation of the

flux and colour evolution. To do this we adopt the emissivity wavelength dependance, the grain distribution, and the bolometric light curve described above. In order that the most important parameters in the problem can be identified, a few approximations will be made, and the integral will be recast using substitutions. First, our observations are made on the Wien slope. The hottest dust is at about 1200K, and the longest wavelength is 2.2μm so hν/kT=5.5, so an error of only a few percent is introduced if the Wein approximation to the Planck function is used. The temporal dependence of T demonstrated in Chapter II requires that the dust cloud be opticaly thin. We will assume that this is in fact true, but will show that this can be justified in a self-consistent manner.

If we parameterize the optical properties in the following dimensionless form

$$Q_a = Q_0(\nu/\nu_0)^{\alpha}, \qquad (3.8$$

so that the Planck average emissivity is

$$\overline{Q} = \frac{15}{\pi^4}\,\Gamma(4+\alpha)\zeta(4+\alpha)Q_0(kT/h\nu_0)^{\alpha}, \qquad (3.9$$

where Γ and ζ are the gamma and Riemann zeta functions respectively, and the dust grain number density is

$$n = n_0(r/r_0)^{\beta}, \qquad (3.10$$

then the flux at Earth is given by

$$F_\nu(t_0) = \frac{c}{d^2}\int_0^{t_0} dt' \int_{R_1}^{R_2} \pi a^2 Q_0(\nu/\nu_0)^{\alpha}\,\frac{2h\nu^3}{c^2}\,e^{-\frac{h\nu}{kT}}\,n_0(r'/r_0)^{\beta}\,2\pi r'dr'. \qquad (3.11$$

With $R_1 = ct'/2$ or R_{evap}, whichever is the greater.

Where

$$T(t_0,t,r)^{4+\alpha} = \frac{\pi^3 L(t_0-t)\,(h\nu_0/k)^{\alpha}}{240\Gamma(4+\alpha)\zeta(4+\alpha)Q_0\sigma r^2}. \qquad (3.12$$

If we set r'=ct'/2 then $T(t_0,t',r')$ is the vertex temperature of the parabola t' at t_0. This suggests a substitution which will

combine all the unknowns which determine the temperature in the dust cloud into one function. If $q_\nu=(h\nu/kT_v)$ where T_v is the vertex temperature of parabola t', and $x'=r'/r'_v$, where r'_v is the vertex distance ct'/2 of parabola t', then

$$F_\nu(t_o) = \frac{2\pi^2 a^2 n_o Q_o}{d^2}\frac{2h\nu^{3+\alpha}}{2^{\beta+2} r_o^\beta \nu_o^\alpha c^2}\int_0^{t_o} t'^{\beta+2}dt' \int_{x_1}^{x_2} e^{-q_\nu(t_o,t')}\, x'^{2/(4+\alpha)}\, x'^{\beta+1}dx'. \qquad (3.13$$

An inspection of equation 3.13 reveals that for known α,β, and cloud limits the temporal evolution of an echo from an optically thin dust cloud depends only upon $q_\nu(t_o,t')$. This function determines the dust temperature at every vertex point in the dust cloud, and is the key to untangling the IR light curves, and deducing the nature of the dust cloud. $q_\nu(t_o,t')$ must contain information about the SN luminosity, its time dependence, and the absorption efficiency of the dust. We note that the time dependence, if not the absolute value, of L is rather well known. Therefore, if we are prepared to assume cloud limits, and values of α and β, then, using observations at different wavelengths, we can solve for the combination of unknowns $L_o\nu_o^\alpha/Q_o$. If the flux at two different frequencies ν_i and ν_j are F_i, and F_j respectively, then the flux ratio can written as

$$\frac{F_i}{F_j} = (\nu_i/\nu_j)^{3+\alpha}\, \frac{\int_0^{t_o} t'^{\beta+2}dt' \int_{x_1}^{x_2} e^{-q_i(t_o,t')}\, x'^{2/(4+\alpha)}\, x'^{\beta+1}dx'}{\int_0^{t_o} t'^{\beta+2}dt' \int_{x_1}^{x_2} e^{-q_j(t_o,t')}\, x'^{2/(4+\alpha)}\, x'^{\beta+1}dx'}, \qquad (3.14$$

where $q_i=(\nu_i/\nu_j)q_j$, and

$$q_\nu(t_o,t') = \frac{h\nu}{k}\left[\frac{\pi^3 L(t_o,t')(h\nu_o/k)^\alpha(2/ct')^2}{240\Gamma(4+\alpha)\zeta(4+\alpha)Q_o\sigma}\right]^{-1/(4+\alpha)} \qquad (3.15$$

As we know the explicit time dependence of q_ν we can solve Equ. 3.14 for $L_o\nu_o^\alpha/Q_o$, and hence T_v^o, the vertex temperature of the outermost parabola, can be found from our observations. Equ. 3.14 was solved iteratively by evaluating the double integral using the trapezoidal rule on Romberg's principle.

3.5.1 DETERMINING VERTEX TEMPERATURES AND CLOUD STRUCTURE

If it can be demonstrated that $L_o\nu_o^\alpha/Q_o$ can be determined indepenently of the initial assumptions, i.e. the dust grain distribution, then we can present a rigorous form of the "speed of light " argument of Chapter II. Once T_v^o has been found in this self-consistent manner then we can show whether or not the fall in dust temperature is due only to geometric dilution as the radiation from the supernova propagates outward into the cloud. Any deviation from this behaviour could be due to the break down of any one of the assumptions. The most probable causes of failure of the assumptions are either that the optical depth to the SN radiation is not small so that the radiation is attenuated, or that the optical properties of the dust are not uniform throughout the cloud.

We should recall at this stage why the simple arguments were successful in demonstrating the presence of a light echo. In Chapter II it was shown that the IR colour temperature $\propto t^{-2/5}$; the behaviour expected of T_v^o. This is because most of the radiation actually comes from the region around the vertex of the outermost parabaloid. This is where the combination of the pulse like light curve and the echo geometry conspires to locate the hottest dust. We are observing at short wavelengths on the Wien slope, so that the contribution from dust which is anywhere else, and consequently cooler, is insignificant. The corollary of this is that we expect that the emergent near IR spectrum depends only upon the SN luminosity, the grain efficiency, and the time since the explosion. As far as the IR colours,

and their time evolution are concerned, the global distribution of dust is unimportant because the IR emission arises only from a localised patch within the cloud. Thus for the first stage of this analysis we compare the shape of the light curves predicted by the optically thin model with the data.

Figures 3.3 and 3.4 show the light curves calculated for models with different density distributions and cloud limits, so that the effect on the shape of the light curve of changing these parameters can be illustrated.

When equation 3.14 is solved for T_v^o these expectations are confirmed. If we take the time dependance of the SN bolometric light curve discussed above, the grain absorption efficiency given by $\alpha=1$, and $x_{evap}<<1$, and $x_2>>1$, then the outer vertex temperatures determined on the basis of the value of $L_o\nu_o^{\alpha}/Q_o$ for $\beta=-1$ and -2 differ by less than 1%. The assumption that the cloud is very large compared to $ct_o/2$ is a fairly reasonable assumption, but postulating that the inner radius is small is questionable. As noted before, dust grains can be destroyed out to ~ 50 light days from the SN. However, if $L_o\nu_o^{\alpha}/Q_o$ is known even approximately then R_{evap} can be found because the echo reaches maximum luminosity at $t_o \approx 2R_{evap}/c$, which is about 100 days after the explosion; a part of the IR light curves which are well covered. By adjusting R_{evap} it should be possible to fit the early part of the IR light curves. Minimising residuals by eye yields $R_{evap} = 1.30\pm0.07\times10^{17}$ cm for $\beta=-2$, and 1.23×10^{17}cm with a similar uncertainty when $\beta=-1$. With a value for R_{evap} established $L_o\nu_o^{\alpha}/Q_o$ was re-evaluated, and the temperatures thus derived changed by < 0.5%, demonstrating, once again, the insensitivty of $L_o\nu_o^{\alpha}/Q_o$ to the cloud structure and hence the correctness of our approach.

We note one very important fact. The time evolution of the JHK data for $t_o>127$days is well fitted by the model in its simplest form; i.e. assuming $R_{evap}<<ct_o/2<<R_2$, $Q\propto1/\lambda$, and the exponential light curve if the grain density distribution is given by $\beta=-2$. In contrast, a flatter or steeper density law does not fit the late points at all well. Given that $\beta=-2$ would have been a plausible a priori choice it would seem most reasonable to deduce that

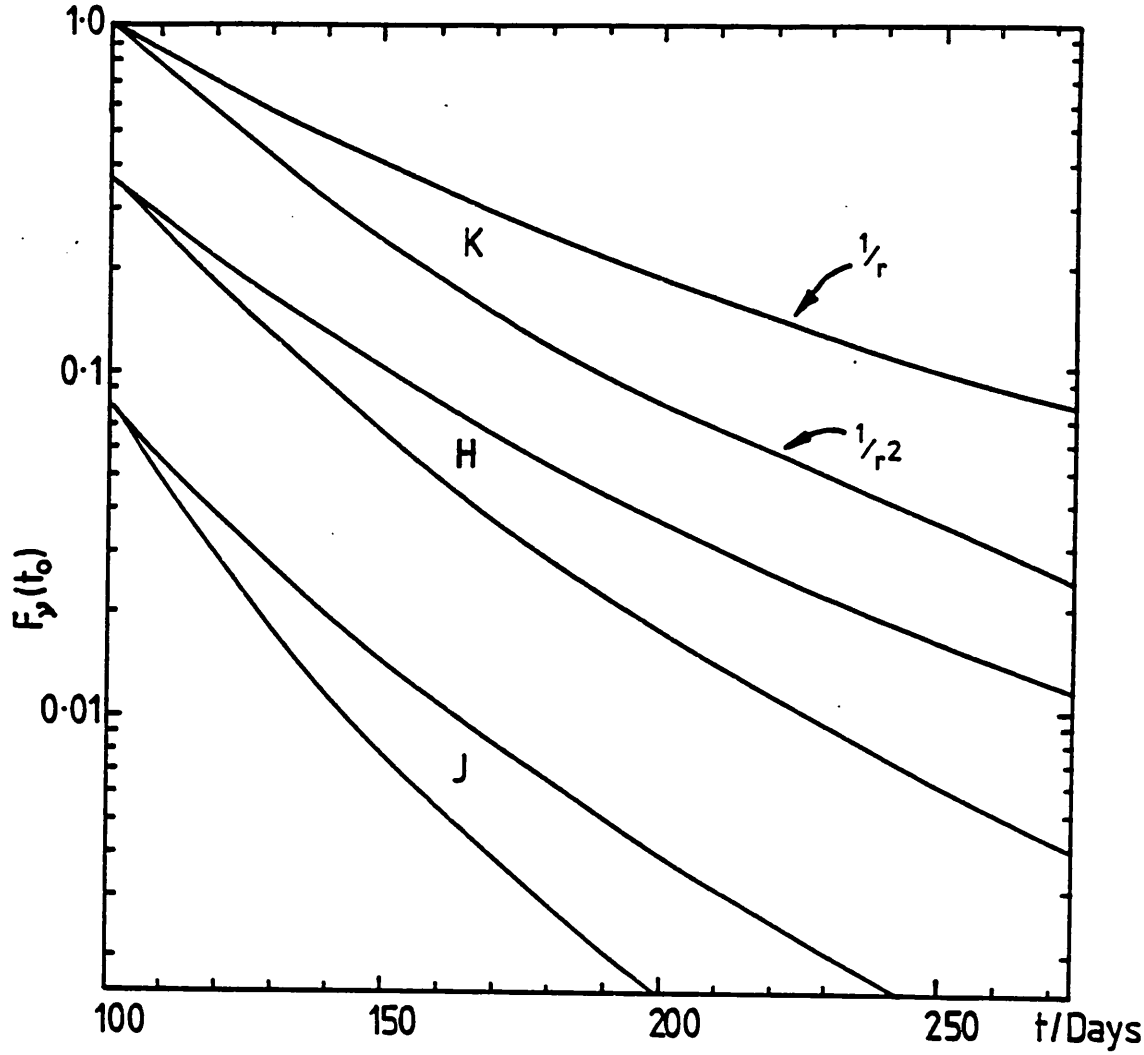

Figure 3.3

An illustration of the development of the IR echo from dust clouds with different density distributions. The light curves for the three IR filters, J,H, and K are shown with flux normalised to unity on day 100 at K. The upper light curve of the pair is the echo due to a $^1/r$ distribution, and the lower curve is the echo from a $^1/r^2$ law. The cloud limits are such that $R_{evap} << {}^{2t_o}/_c << R_2$ at all times. The bolometric light curve described in the text is used with $L_o = 2 \times 10^{43}$ erg s^{-1} and the grains are amorphous carbon of radius 0.16 μm.

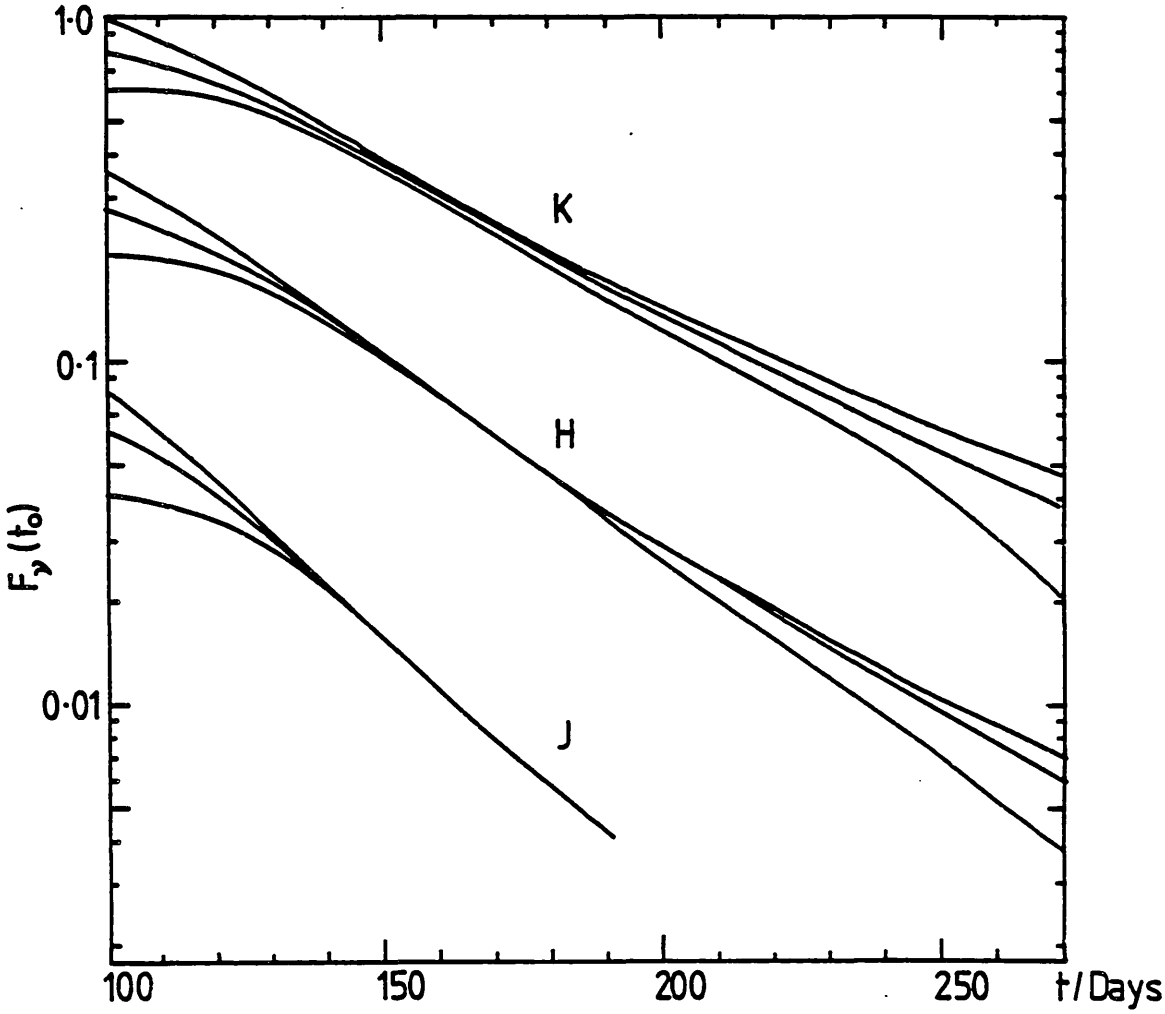

Figure 3.4

An illustration of the development of the IR echo (flux in arbitrary units) from a $1/r^2$ cloud with varying limits. The J,H, and K light curves for the following limits are shown. Top curve of the family R_{evap} = 90 l.d. (light days), R_2 = 230 l.d., middle curve R_{evap} = 100 l.d., R_2 = 190 l.d. and the bottom curve is R_{evap} = 110 l.d., R_2 = 150 l.d. All other parameters are as in Figure 3.3.

the dust density does indeed follow an inverse square law. Adjusting R_{evap} in the manner outlined above allows the model to fit the first two observational points, yet setting R_{evap} to its optimum value does not prejudice the quality of the fit at later times. Finally, reducing the outer cloud limit only worsens the fit to the last observations. On this basis a lower limit, $R_2 > 5.0\times10^{17}$cm(1σ), can be set on the outer cloud radius.

Thus it would seem that we have found a self-consistent scheme for determining the temperatures, and distribution of dust within the cloud. With this knowledge, we can adjust the optical depth of the model, and compare the observed and predicted fluxes, checking the assumption of low optical depth. With a knowledge of the absorption efficiency per unit mass we can express this optical depth in terms of a dust mass, and grain number density.

3.5.2 OPTICAL DEPTH OF THE CLOUD

The flux from the dust cloud described above was calculated and the optical depth required to reproduce the observed fluxes is $0.15<\tau^{*}<0.041$ corresponding to $50<H_0(km/s/Mpc)<100$. To check the accuracy of the optically thin approximation all the dust cloud parameters determined with the optically thin model were included in a calculation of the flux in which the attenuating effect of the dust was treated, and the Wien law was replaced by the Planck function. This accurate calculation produced almost identical IR light curves. This calculation and the IR data are compared in fig. 3.5. The only significant difference was that the flux generated at late times was a little lower than the flux predicted by the optically thin approximation, with the result that the fit to the last two observations was enhanced. There is little difference between the approximate and accurate model during the early stages when $t_o \sim 2R_{evap}/c$. At this time, which is when the first observations were made, the vertex distance is only slightly larger than the evaporation radius, so there can only be very little attenuation of the SN radiation in the short absorbing column of dust between the inner edge of the cavity and the radiating dust. The first few observations have the smallest error bars, and consequently they carry the greatest weight when determining τ^{*}, but these observations were made when the optically thin approximation was still very good, so the the total optical depth of the

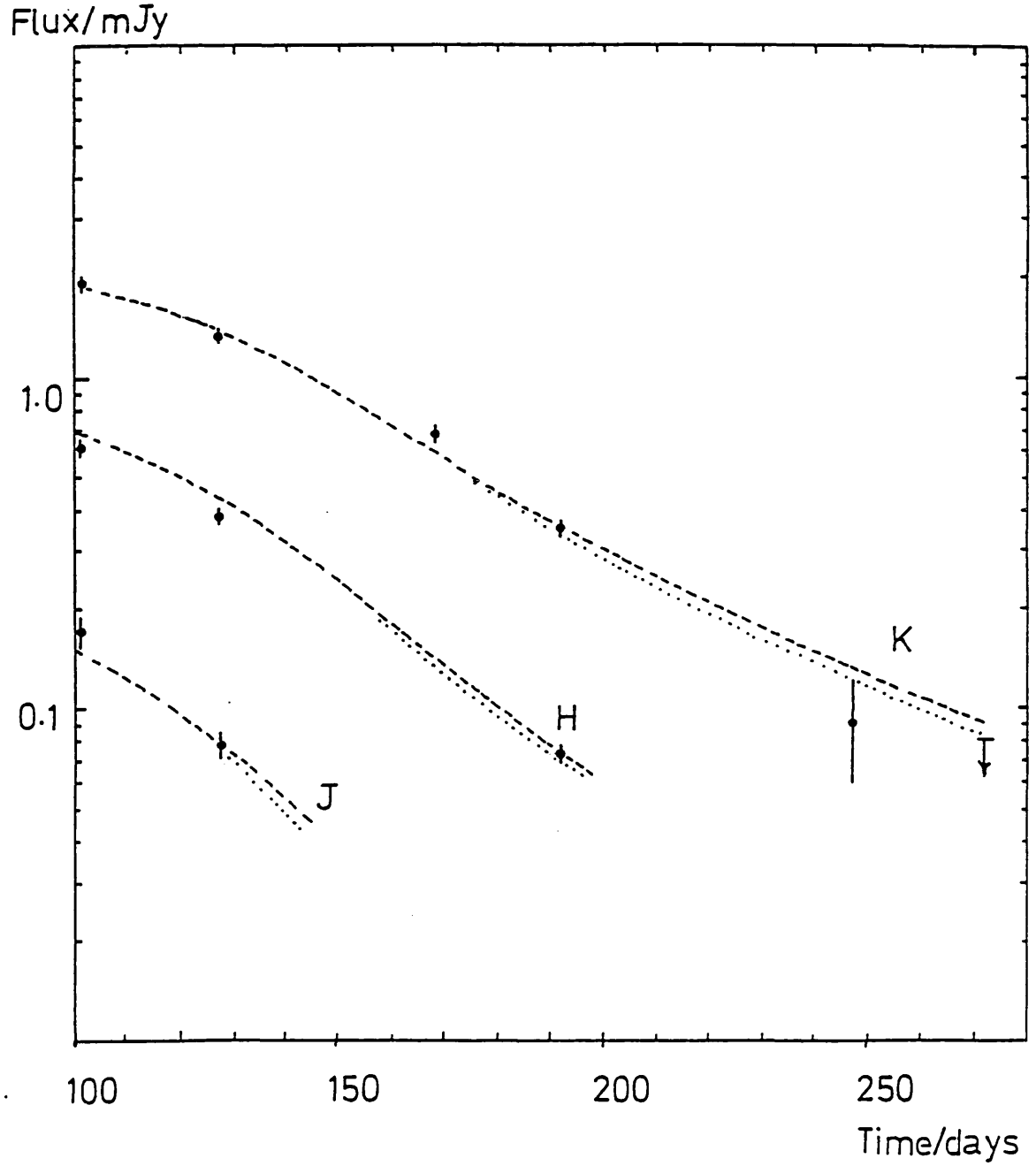

Figure 3.5

A comparison of the IR light curves of SN1982e with a dust cloud model with the final derived parameters; α =-1, β=-2, R_{evap}=1.3x10^{17}cm, R_2=5.0x10^{17}cm. The dashed line corresponds to the model for Ho=100 km/s/Mpc with τ*=0.04, and the dotted line is the model for Ho=50 km/s/Mpc, with τ*=0.15.

cloud calculated from the full model is the same as yielded by the approximation. The cloud optical depth has been calculated for several values of H_0, see table 3.1, and is approximately
$\tau^* \approx 0.08(H_0/75)^{-2}$

Table 3.1

Cloud optical depths

H_0(km/s/Mpc)	τ^*
50	0.15
75	0.068
100	0.041

3.5.3 DERIVED VERTEX TEMPERATURES

The vertex temperatures found by solving Equ. 3.14 for $L_0\nu_0^{\alpha}/Q_0$ using the dust cloud described above (i.e. $\alpha=-1$, $\beta=-2$, $R_{evap}=1.3\times10^{17}$cm, and $R_2=5.0\times10^{17}$cm) are shown in table 3.2. These temperatures can be used in the "speed of light" argument of Chapter 2 to identify an echo. According to equation 2.4, $T_v^{o\,-5/2}$ plotted against time should be a straight line intercepting the origin. Figure 3.6 shows this graph and demonstrates the high degree of linearity. An alternative way to think about this graph is to note that it will only be straight if $L_0\nu_0^{\alpha}/Q_0$ is constant. This quantity should of course remain fixed, so the linearity is an indication of the applicability of the echo model.

Table 3.2

Vertex temperatures

Day	T_v^o(K)
101	1320±30
127	1134±20
191	990±50

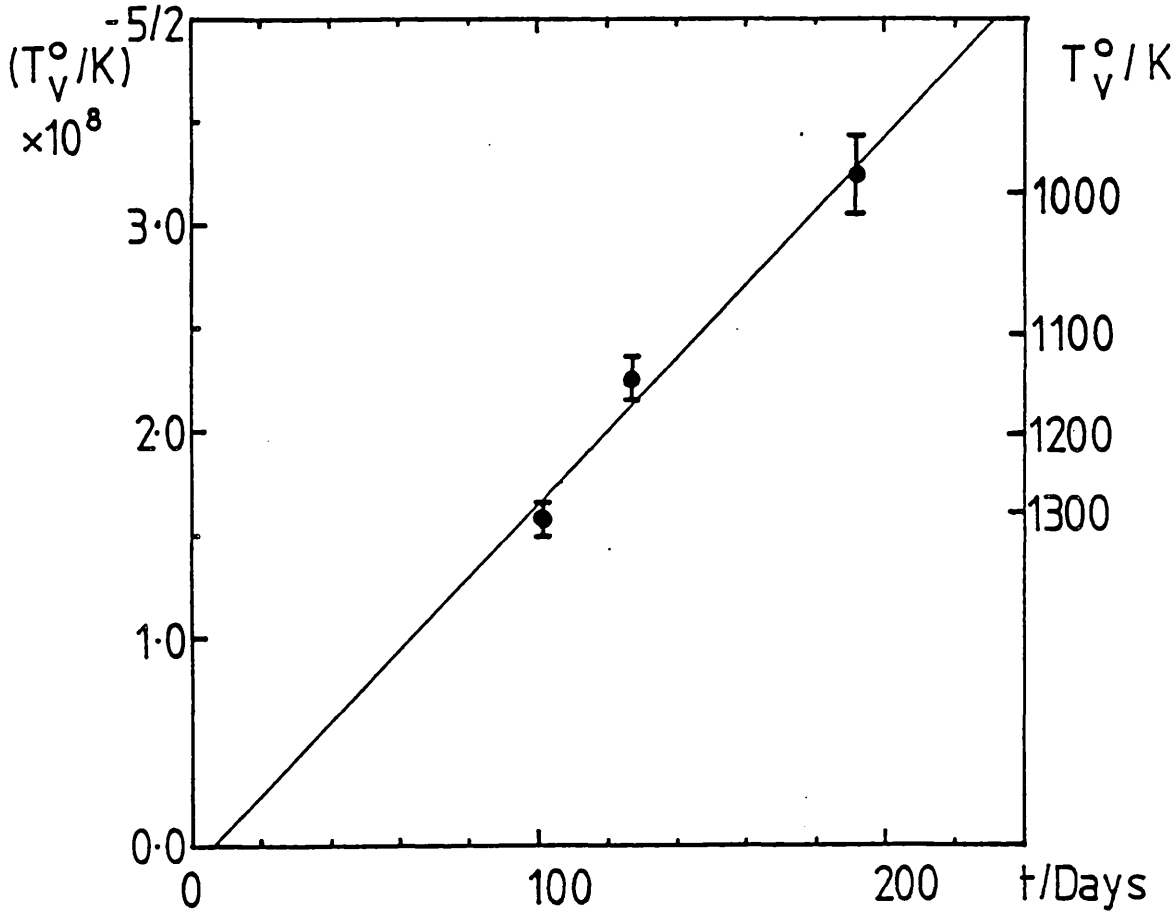

Figure 3.6

The vertex temperature of the outermost paraboloid, T_V^o, plotted against time. The solid line is the best fit straight line.

3.5.4 DERIVED DUST CLOUD PROPERTIES

During the process of fitting the IR observations our assumptions have been justified, and the values of several vital parameters have been determined. Although these quantities have particular relevance to the nature of the light echo, they can be used to provide key astrophysical insight to the SN dust cloud and its constituent grains. Of particular interest is the quantity $L_0\nu_0^{\alpha}/Q_0$. For carbon grains with $Q_a=2.5a/\lambda$ and $L_0=2.0\times10^{43}$ erg/s the grain radius $a=0.16\pm0.02\mu m$. A novel method of determing grain sizes which is in reasonable agreement with other workers. Another dust grain property, the evaporation temperature, can be found from the evaporation radius and $L_0\nu_0^{\alpha}/Q_0$. According to Equ. 3.12 the best fit value of R_{evap} corresponds to 1320 ± 30 K, a temperature which is more representative of oxygen rather than carbon rich refractory condensates, and is in fact the sublimation temperature of magnesium silicate (Salpeter 1974). This identification should be treated with some caution because, in novae, where the condensate is thought to be carbon derived sublimation temperatures vary between 1300-2000 K from nova to nova (Bode & Evans 1983). In addition to individual dust grain properties the extent and optical depth of the dust cloud has been found. Dust with the properties of amorphous carbon grains ($\rho=2.0$ gm/cm^3) is distributed according to an inverse square law, so that the cloud can be described by

$$\rho_{dust} = 4.7\times10^{-23}(r/10^{17}cm)^{-2}(H_0/75km/s/Mpc)^{-2}gm\ cm^{-3} \qquad (3.16$$

which when integrated between the cloud limits gives a total mass of dust

$$M_{dust} = 0.0015(H_0/75km/s/Mpc)^{-2}\ M_{\odot}\ . \qquad (3.17$$

It would seem extremely unlikely that the dust cloud is part of the local interstellar medium. Rather than being a uniform dust cloud, the dust distribution follows an inverse square law with the SN at its centre. The density of dust is also very high, presumably implying a

very high gas density. For a gas to dust ratio by mass of 100, n=2800 cm^{-3} at 10^{17}cm from the SN, which is more typical of a molecular cloud than the ISM expected in the halo of an early galaxy. The dust cloud was almost certainly produced by the pre-SN star during a phase of dusty mass loss.

3.5.5 ALTERNATIVE DUST DISTRIBUTIONS

We mentioned earlier that it is possible to reproduce the light curves by assuming a different dust distribution and adjusting the dimensions of the dust cloud to ensure that the model reproduces the observations. For the purpose of illustration we will use a 1/r density distribution of dust. Unlike an inverse square law cloud the infrared light curves predicted by a 1/r cloud fit no part of the light curves unless R_2 and R_{evap} are specially chosen. As before adjusting R_{evap} allows fitting of the early points. The resultant R_{evap} is not significantly different from that for the inverse square distribution. R_2 must be adjusted because the gradient of the infrared light curves is related directly to the steepness of the dust distribution, and imposing a sharp outer edge at an appropriate distance can cause the flux to fall very rapidly. The greater the degree of central condensation of the dust, the faster the echo decays. The echo from a 1/r distribution decays very slowly. For example, when t_0=250 days the predicted flux from a dust cloud with $R_2 >> ct_0/2$ at 2.2μm is 3 times greater than the observed flux. If the cloud is truncated by imposing an outer radius upon it, it is possible to reduce the flux at times $t_0 > 2R_2/c$. It is possible to modify R_2 until the latter part of the K light curve is reproduced by the model. However, justification of this drastic cut-off is difficult. The flux drops very rapidly after time $t_2=2R_2/c$ as the echo runs out of dust. Observations of a continued rapid decline after t_2 would be required to fully justify imposing this outer radius.

The 1/r model which reproduces the light curves best uses the following values (Ho=75km/s/Mpc).

Table 3.3

The 1/r dust cloud model

τ^*	$M_{dust}(M_\odot)$	R_{evap}(cm)	R_2(cm)
0.065	6.13×10^{-4}	1.23×10^{17}	3.0×10^{17}

Despite the fact that the dust distribution has been changed substantially the derived parameters have changed much less than the factor which any distance uncertainty would introduce.

3.6 THE SUPERNOVA PROGENITOR

Mass loss is observed during many phases of stellar evolution. It will therefore be difficult to unambiguously identify the SN progenitor solely from the presence of a circumstellar shell. During the post-main sequence evolution of nearly all stars, a considerable fraction of the initial stellar mass is returned to the ISM. Mass is returned during explosive events such as novae and supernovae, and on a scale of decreasing violence, as the ejection of planetary nebulae and steady mass loss as stellar winds. P-cygni profiles and chromospheric emission reveal directly material flowing away from the surfaces of stars (Cassinelli 1975). At sufficiently large distances from the stellar surface this material can cool and envelopes containing dust and various molecular species can form (Zuckerman 1980). Many, if not all, late-type giant star winds are both cool and dense enough to form dust, which shows up as an IR excess, and molecules which give rise to both thermal and maser emission.

It will be interesting to calculate the mass loss rate in steady state required to produce the observed dust distribution. For steady mass loss

$$\dot{M}=4\pi r^2\rho v, \qquad (3.18$$

where v is the wind velocity. Therefore knowing the density distribution from the echo the mass loss rate required is

$$\dot{M} = 0.93\times10^{-5}(\alpha/0.01)^{-1}(v/10km/s)\ (H_0/75km/s/Mpc)^{-2}\ M\odot/yr. \qquad (3.19$$

α is the dust-to-gas ratio. A value typical for the ISM has been inserted quite arbitrarily, however, Werner et al. (1980) found that α varies between 0.018 and 0.004 in a sample of circumstellar dust shells around OH/IR stars. Winds from late type stars are typically ~ 10km/s, and so a mass loss rate ~ $10^{-5}M\odot/yr$ is inferred. Mass loss rates of this order are observed from the most luminous K and M supergiants (Cassinelli 1975). The mass flows from sources with circumstellar molecular emission (e.g. OH or CO) involve some of the largest mass loss rates observed with $\dot{M}$ up to 10^{-4} M⊙/yr (Knapp et al. 1982).

3.6.1 LOW MASS STARS - EVOLUTION AND MASS LOSS

This SN arose from the old stellar population of an SO galaxy, and well away from the nucleus, far from any possible site of recent star formation. This would require that the progenitor star, or at least that star which produced the circumstellar shell was $\lesssim$ 1 M⊙. This evolutionary constraint allows us to discard the massive supergiant stars as possible progenitors. The Mira/Long Period Variables, as we will show, are excellent prospective candidates, with masses which satisfy the age criterion.

Cahn and Wyatt (1978) adopt the semi-empirical Reimers mass loss formula for a classical first overtone pulsator to describe the mass loss from Mira/Long Period variable type stars (asymptotic giant branch [AGB] stars on the Mira instability strip), and find that

$$\dot{M} = 7.9\times10^{-14}\ L^{1.69}\ M^{-1}\ M\odot/yr \qquad (3.20$$

where L amd M are luminosity and mass in solar units respectively. The luminosity of an AGB star is given by the Paczynski core-mass luminosity relation (Paczynski 1971), so the maximum luminosity of such a star is reached when $M_{core} = 1.4M\odot$, the AGB limit when $L = 5.3\times10^{4}$ L⊙ and so $\dot{M} < 7.6\times10^{-6}$ M⊙/yr. However, due to mass loss during the red giant phase only stars more massive than 2 M⊙ build up such massive cores. Studies of white dwarfs in open clusters suggest that the maximum initial mass which can leave a white

dwarf is somewhere between 3-7 M⊙ (van den Heuvel 1975; Romanishin and Angel 1980).

However, mass loss rates greatly in excess of this limit are observed from low mass AGB stars. Such stars are found in the infrared catalogues (e.g. the CRL and the AFGL surveys) as obscured stars buried in optically thick dust shells, and often associated with luminous molecular emission.

Pulsation masses of the most luminous AGB stars suggest that they lie in the range 3.5-8 M⊙. Knapp (1982) has observed molecular mass flows up to 10^{-4} M⊙/yr from AGB CO sources. Werner estimates $\dot{M}$ to be between 5×10^{-6} and 7×10^{-5} M⊙/yr for unclassified OH/IR sources, which are either Mira type stars or M supergiants. But of especial interest Jones et al. (1983) found that there is a class of low luminosity OH/IR sources with $L < 10^{4}$ L⊙, and very long periods. The luminosity of these sources is very much less than an extrapolation of the Mira period-luminosity relation would imply, so it is suggested that these sources are fundamental mode pulsators ~1M⊙ on the asymptotic giant branch. The following evolutionary picture has been proposed. A red giant ascends the AGB and becomes a classical first overtone pulsator when it enters the Mira instability strip. An IR excess and maser emission increase with the star's luminosity. The star switches to fundamental mode as the result of some unknown instability in the stellar atmosphere, and mass loss increases dramatically. The star develops a very massive circumstellar shell, consequently an extreme IR excess is produced, and it becomes a radio luminous OH/IR source.

3.6.2 PRE-SUPERNOVA EVOLUTION AND THE DUST SHELL

We adduce the following arguments in support of the supposition that the supernova dust cloud was produced by a low mass AGB star in the final stages of its evolution. The mass loss needed to produce the cloud requires that about 0.1M⊙ of gas must be ejected from the star. In fact, fundamental mode mass loss is so intense that the star will sustain a mass loss rate of $\sim10^{-5}$M⊙/yr until it completely ejects its envelope. From the number density of radio luminous OH/IR sources Jones et al. (1983) calculate that the lifetime

in the fundamental mode is ~10^4 years, leading to a mass estimate which is comparable to the supernova cloud.

We call upon two more important facts to substantiate this proposition. Firstly we note that the SN dust cloud has been greatly modified by the SN exposion. Dust is evaporated by the SN out to 1.2×10^{17} cm, but the outer cloud radius is > 5×10^{17} cm, therefore less than 20% of the cloud mass has been evaporated. However, dust close to the SN must have originally represented a significant opacity because of the inverse square density distribution. If we replace this evaporated dust we find that there was a very large optical depth, τ^*, through the pre-SN dust cloud.

$$\tau^*=0.11[R_0^{-1}-R_2^{-1}] \qquad (3.21$$

where R_0 is the original inner cloud radius, and both radii are in units of 10^{17}cm. Unless R_0 was atypically large , i.e. >> 5×10^{14} cm (Jones and Merril, 1976), then the pre-SN would have been completely obscured.

It seems paradoxical that the pre-SN was probably obscured by a few tens of magnitudes yet it was observed optically. This is not at variance with the postulate that SN1982e had a dust cloud. Under most circumstances when the pre-SN is obscured the SN will be visible. As mentioned above grains near the SN evaporate before they have time to radiate a substantial amount of energy. Grain destruction does not represent a significant energy sink either (Falk & Scalo 1975). So only when dust grains are at a safe distance from the SN and are not destroyed is the optical radiation attenuated. Therefore if the optical depth between the radius where grain destruction stops, and the outer edge of the cloud is small, i.e

$$\tau^*(Revap,R_2) << 1 \qquad (3.22$$

grains which survive the explosion will not significantly absorb or redden the primary SN radiation. This condition is satisfied by the dust cloud deduced in the previous section. In fact SN are so efficient at destroying dust that only an extremely massive star's dust cloud could present enough extinction to render it invisible. A dust cloud of similar structure to SN1982e's, but with a mass 100 times greater,

≈0.1M⊙, and presumably accompanied by ≈10M⊙ of circumstellar gas would provide about 10 magnitudes of extinction after the explosion.

Secondly, it is very tempting to point out that the fundamental mode pulsation lifetime is very short lived when compared to the timescales of most stages of stellar evolution, and that this phase immediately preceded the SN explosion. The possibility that the SN explosion and the switch to fundamental mode are causally conected must be investigated. The mass loss might be symptomatic of some instability which eventually disrupted the star. This would be a rather ad hoc postulate as possible mechanisms are unknown. The currently favoured models for type I supernovae, low mass supernova explosions, are based upon accreting white dwarfs (see section 1.6.2). If the pre-SN system consisted of a white dwarf and an evolved star in the process of ejecting its envelope, then the white dwarf might accrete enough matter from this flow to exceed the Chandrasekhar mass limit. A white dwarf above this limit will collapse violently to a neutron star releasing sufficient energy to power a SN outburst.

3.6.3 ACCRETION IN A BINARY SYSTEM

We can check whether or not a white dwarf could capture enough material from a stellar wind to drive it over the Chandrasehkar limit and thus trigger a supernova explosion . The mass accretion rate $\dot{m}_a$ onto a body moving at a velocity v relative to gas of density ρ by gravitational capture is

$$\dot{m}_a = \pi\left(\frac{Gm}{v^2}\right)^2 \rho v \qquad (3.23$$

(Hoyle and Lyttleton 1939), where G is the universal gravitational constant, and m is the mass of the accreting star. Captured gas will not fall directly onto the surface of the white dwarf, but will be maintained as a turbulent cloud. Because the gas has a high angular momentum accretion will not be spherically symmetric, and the gas will circulate in a disc. Viscosity will cause a loss of the gas' kinetic energy, and serve to transport angular momentum outward through the cloud so that mass can fall inward. If the density is given by eq 3.18 then the efficiency of mass loss capture for a system of two stars of equal mass m in circular orbits of radius r is

$$\dot{m}_a/\dot{M} \approx \frac{(Gm)^2}{16\, r^2 v^4} \qquad (3.24$$

Where a conservative approximation has been introduced by noting (ignoring gravity) that the maximum distance at which the white dwarf intercepts the stellar wind is equal to the diameter of the orbit. The relative velocity is simply the velocity of the wind relative to the companion star, and so the accretion efficiency for 1M⊙ stars is

$$\dot{m}_a/\dot{M} = 0.1\, r_{14}^{-2}\, v_6^{-4} \qquad (3.25$$

where r_{14} and v_6 are the orbital radius in units of 10^{14}cm and the wind velocity in units of 10km/s respectively. Therefore, it is not unreasonable to consider a binary system where the white dwarf could intercept a substantial fraction of the mass lost by its companion. Plausibly we might expect, given the mass loss rate derived at the beginning of this section, that the white dwarf will grow at a rate of 10^{-5} - 10^{-6} M⊙/year.

More efficient capture, and consequently a more rapid growth of the dwarf is not possible. If the luminosity of the white dwarf is given by the rate of liberation of gravitational potential energy, then the condition that the luminosity is less than the Eddington luminosity can be written in terms of the accretion rate

$$\dot{m}_a < \frac{4\pi R c}{\kappa} . \qquad (3.26$$

κ is the opacity of the matter, and R the radius of the white dwarf. If the opacity is due to Thomson scattering the radiation pressure and gravity are balanced when $\dot{m}_a < 1.5\times10^{-5}$M⊙/yr. And so the brief period (~10^4 years) of intense mass loss from the companion star must be thought of as only finally "tipping the scales". Under the circumstances where a white dwarf is just less than the critical mass the ejection of its companion's envelope at the end of its evolution on the asymptotic giant branch could trigger a supernova explosion within a dusty shell. One might predict, because rather special conditions would have to obtain to produce a dusty type I supernova, that dusty type I's should not be very common. It is certainly clear from present data that not all SNI have dust clouds as

massive as that around SN1982e. One might also suspect that dusty SN are those SN which almost don't make it to the critical mass, and consequently that they may be more prevalent in low mass stellar populations. Whereas, for example, if the donor star were much more massive, and consequently losing mass at a greater rate and for a longer period, a degenerate companion could accrete enough mass to explode before the giant had produced a substantial dusty envelope.

3.7 CONCLUSION

We have inferred, from the presence of a pre-existing dust cloud, revealed by IR observations of SN1982e, that the progenitor system experienced a period of intense mass loss before the SN explosion. Any hypothesis attempting to explain this which is consistent with the system being of low mass, requires that this mass loss phase must be due to the final stages of AGB star evolution. A white dwarf companion of such a star in a suitable orbit, close to the Chandrasekhar mass could accrete enough material from this wind to cause an explosion. Therefore the accreting white dwarf model for SN1982e fits well.

As a more general point it is very surprising that SNI, which appear so similar from event to event at optical wavelengths, should show such a profound variety of IR behaviour. SN1982e (probable type I) and SN1982r (confirmed type I) had strong IR excesses, but these SN were quite unlike the type I's 1980n, 81n, and 81d which showed no evidence for such a component. Does this mean that there are two types of SNI? This would seem difficult to accept give the optical homogeneity of SNI. It seems much more likely that all SNI are due to exploding white dwarfs, and the different IR behaviour is due to various types of donor star. A good way to test such a hypothesis would be to study the variation of IR emission from SNI with morphological class of parent galaxy, and hence with stellar population. It may be that both high and low mass donor stars could cause a companion white dwarf to explode, thus reconciling the current dispute regarding the origin of SNI.

CHAPTER IV

DUST IN SUPERNOVA REMNANTS

4.1 INTRODUCTION

It has been predicted for some time now that dust grains may be an important coolant in astrophysical plasmas because dust grains embedded in hot gas are heated by collisions with electrons and ions (Ostriker & Silk 1973). The energy deposited raises the grain temperature to between a few tens to a few hundreds of Kelvin, and so most of this energy is radiated at far-infrared wavelengths. Consequently, observational verification of grain cooling has proved difficult. Grain cooling is an important energy sink when gas temperatures exceed $\approx 7\times10^5$K. At temperatures characteristic of the X-ray emitting gas observed in supernova remnants (10^6-10^7K) the rate at which energy is lost to dust grains exceeds the normal cooling rate of a dust free plasma (Draine 1981, Dwek and Werner 1981). Therefore, a supernova remnant should constitute an ideal astrophysical laboratory where the consequences of grain cooling can be investigated. The following sections represent a theoretical attempt to investigate the effects of grain cooling upon supernova remnant evolution, and hence establish indirectly the importance of collisionally heated dust as a coolant of hot gas.

4.1.1 COOLING BEHIND SUPERNOVA SHOCKS

A theoretical investigation of the effects of radiative cooling behind a supernova remnant (SNR) shock is made in which the SNR is described by an adiabatic Sedov blast wave propagating into a uniform medium. Approximations are used to give the shock structure in Lagrangian form, and the effect of cooling upon an element of gas as it flows out of the shock is considered. The instability which radiative cooling triggers is described, and the modification of the subsequent expansion is considered. Dust cooling is predicted to be an order of magnitude more efficient than normal gas processes so departures from adiabaticity occur much earlier than previously suspected. The efficiency of grain cooling is dependant upon the details of grain dynamics and destruction, so these are studied. It is concluded that grains remain coupled to the gas and survive various destructive processes, so it

would seem that grains are important in determining early SNR evolution, and that SNR's should be luminous far-infrared sources. The x-ray data from the Large Magellanic Cloud (LMC) remnants are used as a sensitive test for the effects of grain cooling, and the observations indicate that, as predicted, the SNR's cannot be described by a simple adiabatic Sedov shock.

4.2 SUPERNOVA REMNANT DYNAMICS AND SHOCK STRUCTURE

The transition from supernova to supernova remnant could be defined to have occurred when the supernova ejecta has mixed with enough interstellar medium so that the supernova looses its identity. Once the supernova has swept up a few times its own mass of interstellar gas the SNR stage will have begun, and, if the expansion is adiabatic then the subsequent evolution can be described by the Sedov bast wave solution (Sedov 1959). The characteristics of the SNR shock can then be described in terms of the initial energy ε_0, the density of the interstellar medium ρ_0, and the time t since the explosion. For example, the position of the shock r_2 is given by

$$r_2=\xi(\varepsilon_0/\rho_0)^{1/5}t^{2/5} \qquad (4.1$$

Where ξ is a dimensionless constant of the motion, ~1, which can be determined from considering the conservation of energy once the detailed structure of the shock has been found. Sedov's exact solutions for the shock structure are complex, implicit relationships between the velocity similarity variable and the post-shock conditions. Taylor (1950), who independently found Sedov's results numerically, presents useful numerical approximations in terms of the dimensionless distance $\lambda=r/r_2$. The temperature, T, and density, ρ, structure described by Taylor's approximation to Sedov's solution is

$$T(\lambda,t) = T_2\lambda^{-9/2}[1+3/5(1-\lambda^5)]^{-1/6} \qquad (4.2$$

and

$$\rho(\lambda,t) = 4\rho_0\lambda^{9/2}[1+3/5(1-\lambda^5)]^{-5/2} \qquad (4.3$$

T_2 is the shock temperature. Just behind the shock $T \propto \lambda^{-9/2}$, so there is a very steep temperature gradient behind the

shock. Using the adiabatic invariant $T_2(t_0)\rho_2^{1-\gamma}$ to identify an element of gas within the shock which was shocked at time t_0 we find that its present position is now given by

$$\lambda = \left[\frac{5\tau^{4/5} + 3}{8}\right]^{-1/5} \qquad (4.4$$

where $\tau=t/t_0$, and $\gamma=5/3$. The temperature history of an element of gas just entering the shock is therefore, to a very good approximation

$$T=T_2\left[\frac{5\tau^{4/5} + 3}{8}\right]^{9/10} \qquad (4.5$$

In an adiabatic shock the shock temperature drops at a rate

$$dT_2/dt=-\tfrac{6}{5}(T_2/t) \qquad (4.6$$

which is faster than the rate at which freshly shocked material ($\tau \approx 1$) cools by adiabatic expansion

$$dT/dt=-\tfrac{3}{4}(T_2/t) \qquad (4.7$$

so maintaining the positive temperature gradient into the SNR. Cox (1972b) argues that if there is cooling in addition to adiabatic cooling then the temperature gradient will be flattened out and the post-shock temperature will eventually fall below the shock temperature. Radiative cooling triggers an instabiltiy which will eventually destroy the adiabatic shock structure. If material entering the shock cools below the shock temperature, then it will find itself sandwiched between older hot shocked gas, which has not cooled appreciably, and freshly shocked gas which has not had time to cool. Consequently, once the shock temperature has dropped sufficiently to allow cooling, shocked gas is compressed and swept up to form a dense cool shell.

Shell formation starts when the temperature gradient behind the shock becomes flat, i.e. when the rate of cooling due to the expansion and radiative cooling equals the rate at which the shock temperature drops. Cox (1972b), who first carried this type of analysis, approximated the adiabatic cooling rate by T_2/t, determined from Heiles' (1964)

graphs illustrating Sedov's exact solutions. But here, using the analytic result above, we find a slightly slower rate yielding a slightly longer (44%) time to reach temperature sag

$$t_{sg} = \frac{9}{8\mu}\frac{3kT_2}{20n_0\Lambda} \qquad (4.8$$

μ is the mean particle mass in a.m.u., and Λ is the cooling function for hot gas, defined so that the luminosity per unit volume = $n_e n_H \Lambda$, where n_e, and n_H are the electron and hydrogen ion number densities respectively. Once the thermal instability has been triggered at t_{sg} gas entering the shock cools and is compressed, and a dense shell will start to form after approximately a cooling time

$$t_{cool} = \frac{3kT_2}{8\mu n_0 \Lambda} \qquad (4.9$$

4.3 DYNAMICS OF A NON-ADIABATIC REMNANT

Once the SNR has suffered the temperature sag instability it can be thought of as consisting of a dense shell which is composed of all the mass, M_{shell}, which is swept up after the sag time and a hot interior which contains the mass, M_{int}, engulfed prior to the sag time. It is conventional to say that a remnant will have built up a well developed shell after it has radiated some arbitrary fraction of its initial energy, e.g. $(1/4)E_0$. A more physically reasonable, and more readily calculable requirement would be that

$$M_{shell} = M_{int} \qquad (4.10$$

and so

$$r_2 = 2^{1/3} r_{sg} \qquad (4.11$$

when a dense shell has been built. If Sedov expansion continues until this time

$$t_{shell} = 2^{5/6} t_{sg} \qquad (4.12$$

which turns out to be very similar to the result of Cox's original criterion for determining when the dynamics could no longer be described by an adiabatic treatment, which was when radiative and adiabatic cooling rates were equal. After t_{shell} the dynamics are governed by the conservation of momentum of the shell as it sweeps up more interstellar material, giving an expansion law $r_2 \propto t^{1/4}$. So-called snowplough expansion. If the pressure exerted on the shell by the hot gas is also included, then $r_2 \propto t^{2/7}$; pressure modified snow-plough expansion (PMS) (Oort 1951).

4.4 THE COOLING FUNCTION

4.4.1 ATOMIC COOLING

The radiative cooling of a collisionally ionized plasma can be calculated by considering all the atomic processes which give rise to emission e.g recombination line radiation. Bremsstrahlung losses from a collisionally ionised gas with cosmic abundances dominate line emission and recombination losses when $T > 4\times10^7$ K giving a gas cooling function (Raymond, Cox, & Smith 1976)

$$\Lambda = 7.6\times10^{-24}\ T_7^{1/2}\ \text{erg cm}^3\ \text{s}^{-1}\ . \qquad (4.13$$

T_7 is the temperature in units of 10^7K. In cooler gas, $10^5\text{K}<T<4\times10^7\text{K}$, in which line emission is important the cooling function is approximately

$$\Lambda = 4.0\times10^{-23}\ T_7^{-0.62}\ \text{erg cm}^3\ \text{s}^{-1}\ . \qquad (4.14$$

4.4.2 DUST COOLING

Gas grain impacts will deposit energy in dust grains contained within the plasma. This process heats the dust so that the plasma can cool by emission at IR wavelengths. If all the kinetic energy of an impinging particle of mass m is deposited in a grain of radius a, then the heating rate of the grain due to collisions will be

$$H = 4\pi a^2\ \frac{1}{4}\ n\ \bar{v}\ \frac{1}{2}\ m\ v_{rms}^2\ . \qquad (4.15$$

Where $\bar{v}$ and v_{rms} are the mean and root mean square velocities respectively. Thus if gas grain impacts deposited energy with constant efficiency the dust cooling function would be $\propto T^{3/2}$, but at temperatures in excess of 10^7K electrons begin to penetrate the dust grains and Λ_{dust} increases less rapidly than one might expect. The efficiency of collisional grain heating in hot gas has been investigated by Draine (1981), and Dwek & Werner (1981) using experimental energy loss rates for low energy (~10eV) electron and proton projectiles in intermediate Z targets which are characteristic of grain materials (e.g. C and Si). From these they have determined heating rates for interstellar grains for plasmas with temperatures from 10^5 to 10^9K. The functional form of the thermally averaged electron accommodation coefficient, the collisional energy deposition efficiency, suggests the following approximation to the dust cooling function obtained by detailed calculation for a gas to dust ratio (by mass) of 100

$$\Lambda = 10^{-20}(1+26a_{-5}^2 T_7^{-3})^{-1/2} \text{ erg cm}^3 \text{ s}^{-1} \qquad (4.16$$

a_{-5} is the grain radius in units of 0.1μm. This prescription reproduces Draine's (1981) and Dwek & Werner's (1981) calculations to about 20% over the temperature range 10^5-10^8K. In cool gas ($T<10^7$K) equation 4.15 is in fact quite accurate.

The atomic and dust cooling functions are compared in fig. 4.1. As dust cooling is very much greater than ordinary gas cooling, dust cooling will be extremely important in all young SNR shocks. Substituting Λ_{dust} in eq. 4.8, and taking the time evolution of T_2 from the Sedov solution yields

$$t_{sg}^{dust} = 2500\epsilon_{51}^{2/11} n_0^{-7/11} \text{ yr}, \qquad (4.17$$

and

$$t_{shell}^{dust} = 4500\epsilon_{51}^{2/11} n_0^{-7/11} \text{ yr}. \qquad (4.18$$

Where ϵ_{51} is the SN energy in units of 10^{51}erg, and n_0 is the gas number density in units of cm^{-3} The sag time of a

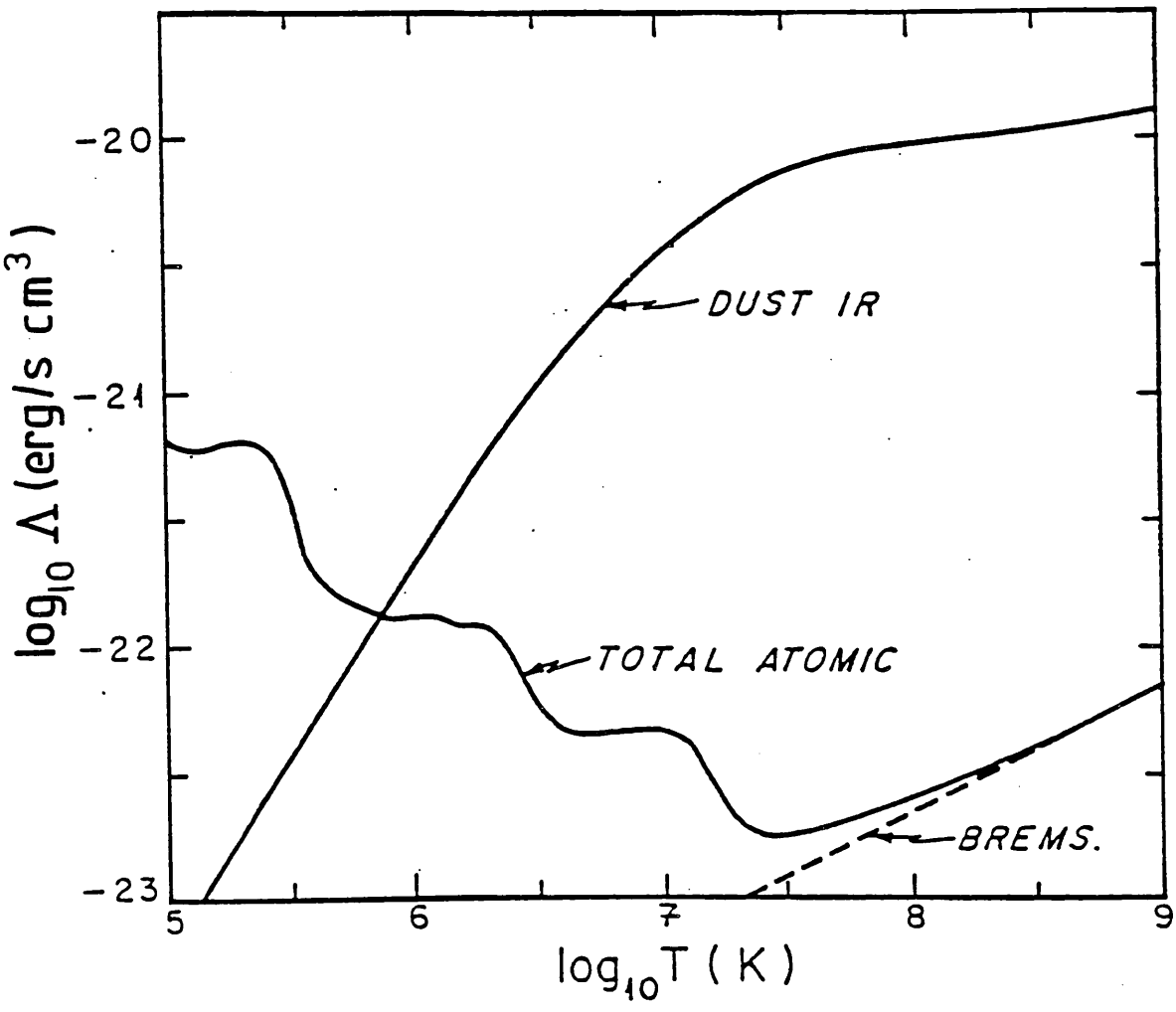

Figure 4.1

The dust cooling function compared with the atomic cooling function of Raymond et al. (1976).

shock is greatly advanced by dust, in terms of the gas-cooling sag time; the dusty sag time

$$t_{sg}^{dust} \cong 0.12 \; t_{sg}^{gas} \qquad (4.19$$

over a wide range of densities and supernova energies, or

$$t_{sg}^{dust} \cong 0.08 \; t_c \qquad (4.20$$

where t_c is the time calculated by Dwek (1981) for a Sedov remnant to radiate one half of its thermal energy if only atomic radiation processes are included.

Clearly dust cooling restricts the use of the adiabaticity assumption to a brief era. The remnant will have hardly had time to relax to Sedov expansion before radiative effects have profoundly modified the shock structure and altered the ensuing evolution.

Numerical calculations (Dwek 1981) confirm the above conclusions. For a supernova of energy 10^{51} erg in an ambient density of $1 cm^{-3}$ the temperature behind the shock had begun to fall faster than the shock temperature by the second time step at 4700 years. Denser models were run with a calculational grid which was too coarse to record the onset of temperature sag, but we can establish from these numerical simulations that

$$t_{sg}^{dust} \lesssim 5000 \varepsilon_{51}^{0.22} n_0^{-0.56} \; yr \qquad (4.21$$

It is important to note the significance of dust cooling in precipitating the temperature instability. Dwek's (1981) numerical calculations could not fully establish the evolutionary influence of dust because an adiabatic shock structure is enforced whereas the structure of a radiative shock is much more appropriate. For example, in his calculations, dust cooling, as one might expect, did not greatly accelerate the complete cooling of the remnant. The cooling time, when dust was included in his calculations, was found to be only 30% shorter. This is because grains cannot contribute significantly to the long term cooling of a shock with adiabatic structure because they suffer substantial destruction before they can radiate a significant fraction of the supernova energy. A self-consistent treatment of the

problem requires consideration of the effect on the dynamics of radiative cooling and subsequent compression behind the shock.

4.5 GRAIN DYNAMICS

The above investigation of how dust cooling modifies shock structure has assumed that the dust and gas are closely coupled together, and that dust grains do not suffer major destruction before they can radiate. These assumptions are now investigated.

On entering the shock, gas is decelerated (in the shock stationary frame) from V_2 to $\frac{1}{4}V_2$ within a distance of a few mean free paths, and so unless some drag force acts to slow dust grains down, they will be catapulted into the post shock gas at a relative velocity of $\frac{3}{4}V_2$. The relative cooling efficiency of the dust grains compared to gas cooling in unshocked gas will be reduced by a factor of 4 because there is no change of grain density behind the shock. Under these conditions gas and dust cooling make equal contributions at 3×10^6K, rather than at 7×10^5K. The effect of dust on the evolution of the SNR is reduced because under these conditions $t_{sg}^{dust} \sim t_{sg}^{gas}$. Therefore, as grain dynamics effect the efficiency of grain cooling we must consider how gas and grain motions are related.

Collisions with the gas atoms, of mass m, will slow down the grains relative to the gas when the grain has swept out a volume which contains a mass of gas equal to the grain mass, m_{gr}. It will do this in a distance

$$d_{slow} = \frac{m_{gr}}{m\ \sigma n} = \frac{1.3\ a_{-5}}{n_0}\ \text{pc} \qquad (4.22$$

Where σ is the geometric grain cross-section, a_{-5} is the grain radius in units of 0.1μm, and the grain material density has been assumed to be 2 g/cm³. This slowing down distance is large even compared to an aged remnant.

If however, the grain is charged this distance can be reduced. Electrostatic forces can be ignored since they are not likely to make an important contribution to the drag on grains with a velocity

significantly greater than the ion random velocity (Spitzer 1978). But magnetic forces can tie gas and dust together if the grain, carrying Z_{gr} electronic charges moving with velocity v_{gr}, finds itself in a sufficently strong magnetic field B. If the grain gyroradius a_B,

$$a_B = \frac{m_{gr}\, c\, v_{gr}}{Z_{gr}\, eB}, \qquad (4.23$$

which can be written as

$$a_B = 1.5\times10^{16}\,(Z_{gr}/100)^{-1}\, a_{-5}^{3}\, B_{-6}^{-1}\, v_7 \ \text{cm} \qquad (4.24$$

behind an adiabatic shock is small enough so that the magnetic field can be considered as being constant over the orbit, i.e.

$$a_B \ll \left(\frac{1}{B}\frac{dB}{dx} \right)^{-1}, \qquad (4.25$$

then the grain motion can be resolved into a drift velocity of the "guiding centre", and simple gyromotion (Spitzer 1978). v_7 is the velocity in units of 100km/s, and B_{-6} the magnetic field in μG. The drift velocity is the same for all charged particles, grains, electrons and ions alike, so the gas and grain motions are locked together. The electric charge on a stationary spherical grain resulting from the differential collision rate of electrons and ions is given by Spitzer (1978)

$$Z_{gr} = -2.51\, \frac{akT}{e^2}. \qquad (4.26$$

More detailed calculations by Draine & Salpeter (1979), (D+S) show that this simple relationship only holds below ~10^5K. In cool gas photoelectric emission is the only process which can reduce the above charge. At higher temperatures, grain penetration (as opposed to sticking) by ions and electrons, and the secondary particles knocked out of the grains must be considered. Furthermore, if the grain charge approaches Spitzer's value then the electric field at the surface of

the grain can cause emission of charged particles. In the temperature range of interest to the study of adiabatic shocks, $T=10^6-10^7$K, the D+S charging calculations yield complicated results. However, the number of electronic charges carried by a 0.1μm silicate grain is always > +550, whereas, a similar graphite grain carries a smaller charge which is > +100.

With a typical interstellar field ~ 3μG (Spitzer 1978) then the gyroradius for either grain type

$$a_B \lesssim 5\times10^{15}\ a_{-5}^3\ v_7 \quad \text{cm} \qquad (4.27$$

If we assume that the magnetic field scales with the density and use Taylor's approximations

$$\left(\frac{1}{B}\frac{dB}{dx}\right)^{-1} = \frac{1}{12}\ r_2 \qquad (4.28$$

at the shock. The "guiding centre" approximation will hold for young remnants as the condition that the gyroradius is very much smaller than the scale height of the magnetic field is satisfied if $t \gg 80a_{-5}$ yrs.

Shull (1978) has calculated the grain charge within radiative shocks, and finds that gas and grain motions are coupled so long as the shock propagates into ionised gas of density < 10cm^{-3}. This first condition is always guaranteed for young remnants because a fast shock ($V_2>110\text{kms}^{-1}$) produces a radiative precursor which completely ionises the gas entering the shock (Shull and McKee 1979).

Gyromotion about magnetic field lines serves to couple gas and dust motions behind a SNR shock, and therefore dust grains will be present in the hot post-shock gas. It now remains to show that dust grains can survive under such hostile conditions.

4.6 DUST SURVIVAL

4.6.1 THERMAL SPUTTERING BEHIND ADIABATIC SHOCKS

Impinging ions with energy above some critical threshold level can knock atoms out of the grain lattice. With typical site binding energies of a few eV (Shull 1977) grains will suffer sputtering when gas temperatures exceed a few thousand Kelvin. To investigate the effects of sputtering we will use the calculations of D+S which are based upon a study of the physical processes responsible for sputtering. At temperatures above 10^6K the thermal sputtering rate is approximately constant, and dependant only upon gas density. In cooler gas, grain erosion is $\propto T^3$. The results of D+S can be summarised as

$$\frac{da}{dt} = 9\times10^{-7}(1 + 0.002\ T_7^{-3})^{-1}\ n\ \mu m/year\ , \qquad (4.29$$

where T_7 is the temperature in units of 10^7K. The grain lifetime $t_g=a/(\frac{da}{dt})$ behind an adiabatic shock is

$$t_g = 3\times10^4\ a_{-5}(1+0.002T_7^{-3})/n_o \qquad \text{years.} \qquad (4.30$$

The survival prospects for a dust grain entering an adiabatic shock will be good if the gas behind the shock expands and cools on a timescale shorter than t_g. As the adiabatic cooling time is of the order of the age of the remnant then grains survive in young remnants ($t<<3\times10^4$years). To illustrate this point the grain size profiles behind an adiabatic shock have been calculated assuming instantaneous grain deceleration behind the shock. The temperature and density of an element of gas is followed as it flows out of the shock, $\dot{a}$ is found according to Equ. 4.29, $\int\dot{a}dt$ and hence a(t) is calculated numerically using the Taylor approximations for an adiabatic shock expressed in Lagrangian form. The grain size profile behind the shock is shown for several epochs in figure 4.2. The grain size is plotted against the dimensionless radius λ. Profiles are shown for t = 0.48,1.0,and 2.0 x 10^4 years. Tick marks show when the particular grain identified entered the shock, and for how long that grain has been behind the shock. The profiles pass through a minimum indicating that grains which are swept up soon after the explosion survive. This

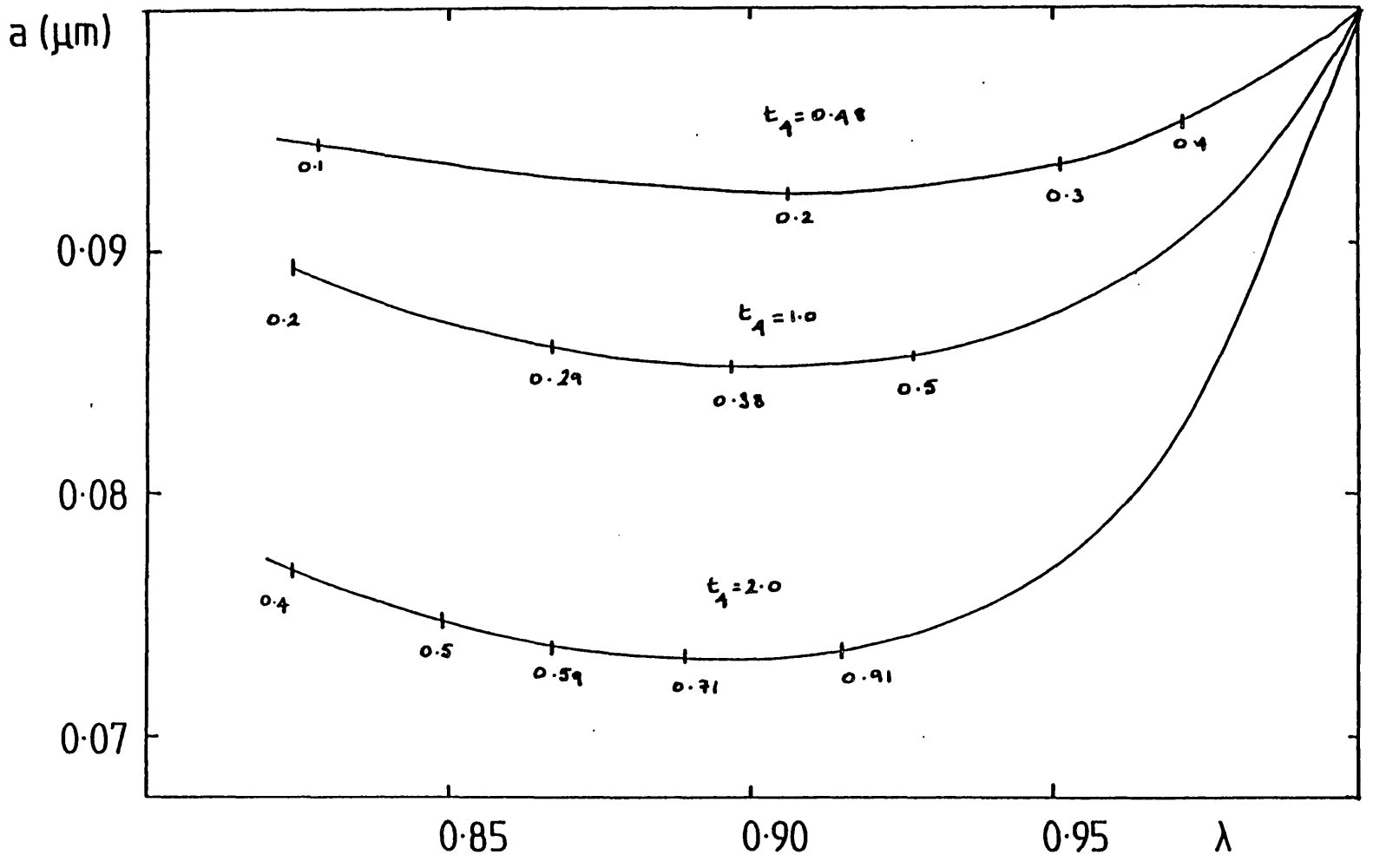

Figure 4.2

Grain size profiles behind an adiabatic shock. Grain size is plotted against the dimensionless radius λ. Profiles are shown for three epochs, and tick marks indicate when grains at that location entered the shock. All times are in units of 10^4 years.

minimum occurs because grains which have just entered the shock at the edge of the remnant have not been in the hot gas long enough to suffer severe erosion, whereas grains which were engulfed less recently have now been subjected to sputtering for some time. The grains which entered the remnant early in its evolution are in fact larger than more recent acquisitions because they have passed into the low density interior where they no longer suffer much destruction.

Dust is not significantly sputtered on a timescale comparable to the time required for dust to modify the dynamics of a SNR. Therefore thermal sputtering should not inhibit the effects of dust cooling.

4.6.2 DUST SURVIVAL BEHIND RADIATIVE SHOCKS

As pointed out many years ago by Oort and van de Hulst (1946) collisions of two grains can provide the energy needed for complete evaporation of the grains. For refractory grains composed of the compounds of Si, Mg, and Fe rough estimates require a velocity of ~10km/s as the relative velocity giving sufficient energy for complete evaporation (Spitzer 1976). The chief difficulty associated with this mechanism is the much longer mean free path for collisions between grains than for slowing down by collisions with gas atoms. If λ_{dg} is the distance over which the mass of the gas intercepted equals the mass of the grain, and λ_{dd}, the corresponding distance for collisions with another grain, then

$$\frac{\lambda_{dg}}{\lambda_{dd}} \approx 4\alpha \qquad (4.31$$

Where α is the dust to gas ratio by mass ($\alpha \approx 0.01$). If the gas is compressed by the shock, but the dust grains are not, then the dust to gas ratio becomes even smaller and destructive collisions less likely. To make collisions possible a magnetic field and a grain charge must be assumed. In the shock stationary frame a grain enters the shock with velocity v_2. Unless the grain is slowed down by viscous forces the dust grain will execute gyromotion about the magnetic field with a velocity equal to the relative velocity between the out flowing dust and gas, $\frac{3}{4}v_2$. If the gas cools, and is compressed, and if the magnetic field scales with density, then the grains will spin up about the field

lines as the density increases, so the slowing down effects of collisions with gas atoms are counteracted. The immediate consequence of this situation is that grains at different phases in their gyration circles will collide with each other at velocities up to $2v_{gr}$. Numerical hydrodynamic calculations which follow the motion of grain behind a shock by Shull (1978) show that at velocities ~100km/s approximately half of refractory grains entering the shock may be destroyed by such collisions. Despite the fact that some of his assumptions only just hold, e.g. the use of the guiding centre approximation in the dense post-shock gas, grain-grain collisions are the most destructive process yet considered. It is interesting to note that this destruction mechanism might check shell formation by dust cooling. If dust cooling triggers compression behind the shock grains will be accelerated and spun up about magnetic field lines and destroyed in grain-grain collisions. If the process is sufficiently quick this destruction will halt further cooling, i.e. if the cooling time is slower than the grain-grain collision time . Inspection of Shull's (1977) calculations shows that significant grain destruction does not occur until cooling is almost complete, and the density has reached the limit set by the magnetic field. Thus grain destruction occurs too late to halt shell formation.

4.7 OBSERVATIONAL CONSEQUENCES

The approximate results presented above, and Dwek's numerical calculations, show that dust triggered shell formation should start very early in the remnant's evolution. To this extent the numerical calculations reveal the importance of dust cooling, even if the subsequent enforcement of an adiabatic structure is artificial. Consider the effect of grain cooling in the absence of any dust destruction. Once shell formation has begun then the thermal energy deposited in the gas at the shock is radiated away, so the SNR loses energy at a rate

$$\dot{E} = \frac{9}{32} \rho_0 v_2^3 4\pi r_2^2. \qquad (4.32$$

If the dynamics can be described by the PMS solution then $r_2 \propto t^{2/7}$ and so

$$\dot{E} = \frac{4\varepsilon_0}{7\, t_{sg}}(t/t_{sg})^{-11/7}. \qquad (4.33$$

Inserting numerical values, and using equation 4.17 we find

$$\dot{E} = 1.8\times10^{6}\ \varepsilon_{51}^{9/11}\ n_0^{7/11}\ (t/t_{sg})^{-11/7}\ L\odot. \qquad (4.34$$

A fraction, $\Lambda dust/(\Lambda gas+\Lambda dust)$, of this is radiated by dust grains, so we can see that a SNR which has just entered the shell building phase will be a luminous infared source. Balancing energy deposition with radiative losses for a single grain we find that the grain temperature, T_g, is given by,

$$T_g^{\,4} = \frac{n_e\ \Lambda_{dust} m_g}{\alpha\ m\ 4\pi\ a^2\ \overline{Q}_o}, \qquad (4.35$$

or with the Planck average emissivity $\overline{Q}$ appropriate for Carbon grains (see section 3.4.1)

$$T_g = 70\ n_e^{1/5}\ (1 + 26a_{-5}^{2}\ T_7^{-3})^{-1/10}\quad K \qquad (4.36$$

so the bulk of this energy emerges at far-infrared wavelengths. In the absence of observations at these wavelengths let us turn to radio, optical, and x-ray data.

Shell formation should not affect the radio emission from a SNR unless particle acceleration is a continuing process at the shock front. It is however thought that the SNR's supply of relativistic particles are generated soon after the SN explosion (Gull 1973a) when the mass of swept up interstellar medium exceeds the mass of ejected material. Rayleigh-Taylor instabilities in the decelerating ejecta transform about 1% of the explosion energy into small-scale turbulent motions and magnetic field amplification. The generation of relativistic electrons proceeds until equipartition of turbulent, magnetic, and particle

energies is achieved.

Optical emission lines from a SNR arise from the cooling region behind the shock, where the temperature has fallen to ~10^4K. It is therefore not easy to see how optical spectra can tell us whether the gas cools from post-shock temperatures ~10^6K by traditional gas processes, or by dust cooling. In contrast to radio and optical observations, x-ray observations relate directly to the hot gas contained within the SNR. Accordingly, it should be possible to use x-ray observations to infer the effects of dust cooling.

4.7.1 X-RAY OBSERVATIONS AND SHELL FORMATION

The x-ray luminosity of a SNR will be severely modified when shell formation sets in. Instead of the mass of x-ray emitting gas increasing with radius, it remains constant at $\frac{4}{3}\pi r_{sg}^3 \rho$ because the freshly shocked gas cools and joins the dense shell. X-ray emission from a Sedov blast wave will arise from the thin $\Delta r/r_2 \approx 1/12$ region $n_0 \approx 4n_0$ behind the shock, so that the x-ray luminosity of a Sedov remnant before shell formation is

$$L_x \approx (4/3)\pi r_2^3[1-(11/12)^3]16n_0^2\Lambda_x \ . \qquad (4.37$$

If the mass of the hot bubble stops increasing at r_{sg} then the density of the x-ray emitting gas is reduced by the expansion by a factor of $(r_2/r_{sg})^{-3}$. Therefore, if r_{sg} is very much smaller than typical remnant radii, then the x-ray luminosity will be a sensitive test for the early onset of shell formation.

Although there are many observations of Galactic SNR's their study is complicated by distance uncertainties. The large scatter in the radio surface-brightness diameter relation has been revealed by the detailed study of the Large Magellanic Cloud (LMC) remnants (Mathewson et al. 1983). The LMC remnants form a unique sample. Although they are extra-galactic and therefore at a known distance, they are bright enough to study with the tools of radio, optical, and x-ray astronomy.

Assuming an emission measure, Λ, of 3×10^{-23}erg cm^3/s in the Einstein energy range (0.14-4.5keV), which is consistent with the results obtained with the Einstein Solid State Spectrometer which

indicate that most remnants have 0.14-4.5keV spectra dominated by lines characteristic of a gas with a temperature $\approx 6\times10^6$K (Clarke et al. 1982), and taking the LMC x-ray data (Long et al. 1981) we can calculate $n_o^{1/3}r_{sg}$ (Table 4.1). The mean sag radius for the 25 known LMC remnants (see figure 4.3) is $7.3n_o^{-1/3}$pc with an r.m.s. scatter of $1.9n_o^{-1/3}$pc. Using equation 4.1 this sag radius corresponds to a sag time of 3500 $n_o^{-2/9}\varepsilon_{51}^{-1/3}$ years.

Inspection of figure 4.3 shows, as predicted, that the mass of x-ray emitting gas increases until $r=r_{sg}$ then remains more or less constant. A least squares fit to the data for those remnants with $r>r_{sg}$ shows that there is a small but significant (3σ) trend for the mass of x-ray emitting gas to increase as the remnant radius increases. The adiabatic model would of course predict that the mass of hot gas increases much faster - as radius cubed, a straight line of gradient 1 on figure 4.3. This is clearly not happening, so this simple model describes x-ray data better than Sedov theory, and yields a sag time remarkably close to the prediction of dust cooling.

4.8 CONCLUSION

Without direct evidence for the efficiency of dust grain cooling in a hot plasma from infrared observations, it is difficult to exclude the possibility that gas-grain collisions do radiate away a substantial fraction of the SNR energy into the IR and trigger shell formation. In particular a simple model of x-ray emission from a SNR which has suffered shell formation describes the LMC remnant data much better than the Sedov picture. It is this last piece of evidence which suggests that the IR observations presented in the next Chapter will reveal dust cooling of SNR's.

TABLE 4.1

The sag radius of the LMC SNR's

SNR	Lx(10^{35}erg/s)	Rx(pc)	Rsg(pc)
N11L	2	7.5	4.3
N86	7.5	23	7.5
N186D	1.4	13	5.3
DEM71	62	9.5	8.7
N23	46	6	>6
N103B	12.5	2.8	>2.8
0509-67.5	24	3	>3
N120	0.7	11.5	4.6
0519-69.0	76	3.3	>3.3
N49B	62	15	10.7
N132D	580	11	>11
N49	135	7.5	>7.5
DEM204	14	25	7.4
N206	5	19	7.9
0534-69.9	18.3	7.1	6.7
DEM238	2.1	19	6.9
N63A	383	7.7	>7.7
DEM249	2.1	17	6.3
N157B	21	1.7	>1.7
0540-69.3	81	1.3	>1.3
DEM299	7.7	29	10.5
0520-69.4	4.2	13	6.4
N135	5.6	23	8.9
0548-70.4	6.3	10.5	6.1

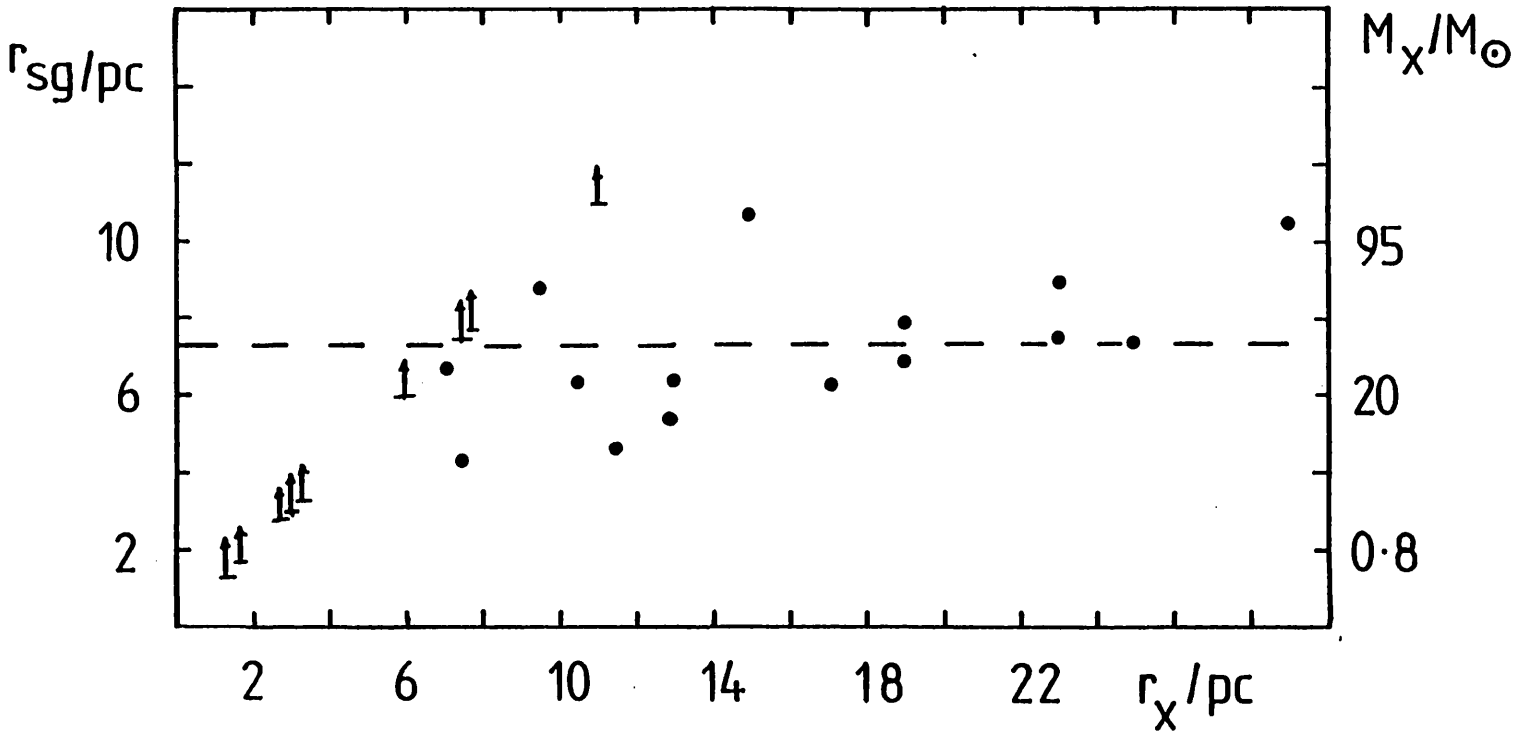

Figure 4.3

The sag radius for the LMC SNR's. The dashed line shows the mean value of the sag radius. The right hand ordinate shows the implied mass of x-ray emitting gas for a density of $1cm^{-3}$.

CHAPTER V

IRAS OBSERVATIONS OF SUPERNOVA REMNANTS

5.1 INTRODUCTION

The preceding chapter attempted to assess the extent to which dust will determine the evolution of supernova remnants, and hence determine, by indirect means the effeciency of dust cooling in an astrophysical plasma. This chapter reports observations designed to detect radiation from collisionally heated grains, and determine experimentally the efficiency of grain cooling. As we expect that dust will reach a temperature ~30K in x-ray emitting gas then any energy radiated by supernova remnants will emerge at far-infrared wavelengths, peaking at 100μm. Observation of this radiation would provide direct evidence for collisionally heated dust. However, the opacity of the atmosphere at these long wavelengths, even at high altitude reduces the detection sensitivity to very poor levels, therefore until the availability of the IRAS satellite observatory, the infrared study of supernova remnants was very difficult. Wright et al. (1980) have obtained far-infared (λ~100μm) upper limits for Cas A, Tycho and Kepler. Unfortunately, these young remnants (~300years) cannot have swept up much dust so the limits are not very severe. Dinerstein et al.(1982) claimed to have detected dust in the fast moving knots of Cas A, however, it seems that at least some of the flux is in fact due to emission lines of [NeII] (Dinerstein, private communication 1983). To date the only detection of luminous far-IR emission from a SNR is Cambell et al.'s (1981) detection of DR4. The remnant is associated with a complex of luminous HII regions, and an unambiguous interpretation in terms of collisionally heated dust is difficult. The only other IR data are the 10μm observations of N63A and N49 in the Large Magellanic Cloud (LMC) (D'Odorico & Moorwood 1982). These place only very poor limits on the mass of cool dust.

5.2 OBSERVATION STATEGY

Large Magellanic Cloud supernova remnants were chosen as good targets to observe. It was decided to observe LMC remnants in preference to Galactic remnants for several reasons. The pre-flight estimates of the

IRAS confusion limit in the Galactic plane (Joseph & Robertson 1982) suggested that sensitive limits could only be achieved for a few high Galactic lattitude SNR's. It was also not expected that the observatory would be able to observe large extended objects. Not only do the LMC remnants form an extremely well studied sample at x-ray, optical, and radio wavelengths, but they satisfy the observational constraints of typically having sizes of the order of the IRAS apertures, and they should be less confused than the galactic remnants because the Cloud is not seen edge on. The LMC remnants also have the unique property that they are at a known distance (46kpc, de Vaucouleurs, 1978). Unlike the Galactic remnants, for which the distances are uncertain, intrinsic properties such as size and luminosity can be derived.

5.3 THE IRAS SATELLITE

5.3.1 THE TELESCOPE

The IRAS satellite consists of a spacecraft which accommodates a liquid helium cooled cryostat containing a cooled telescope. The telescope is a f/9.6 Ritchey-Chrétien design with a 0.57m aperture. The optics are made of beryllium and cooled to <10K. The focal plane assembly is located at the Cassegrain focus of the telescope, and cooled to <3K, is shown in fig. 5.1, its characteristics are summarised in table 5.1. Sources are scanned, by a combination of orbital motion and rotation of the satellite, across the focal plane so that a source is seen consecutively by at least two detectors in any wavelength band, thus providing confirmation of a source on a timescale of seconds. (A detailed description of the mission can be found in Neugebauer et al., 1984)

5.3.2 POSITIONAL RECONSTRUCTION

For some 2000 SAO stars detected in bands I and II the reconstructed positional uncertainty is 45" x 9" 3σ (cross-scan x in-scan). For sources detected only at 60μm the uncertainty is 45" x 15", while for sources detected only at 100μm the corresponding uncertainty is 45" x 20".

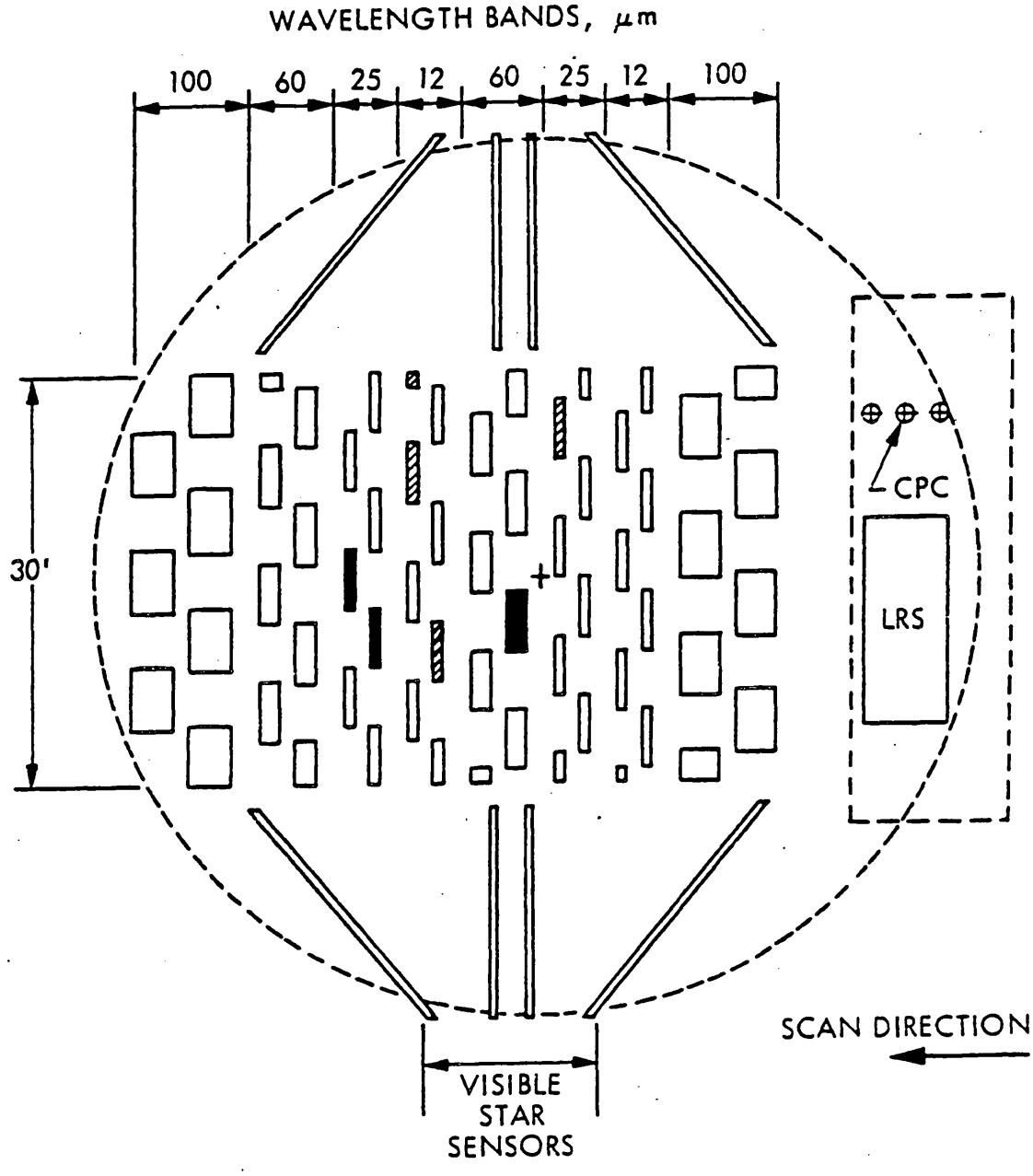

Figure 5.1

The IRAS focal plane. The rectangles in the central portion each represent a detector, filter, and field lens combination of the survey array. The scanning direction is indicated. The shaded detectors were inoperative.

Table 5.1

Characteristics of the focal plane assembly

Band	Centre Wavelength (μm)	Wavelength interval (μm)	Field of view (')
I	12	8.5-15	0.75x4.5
II	24	19-30	0.75x4.6
III	60	40-80	1.5 x4.7
IV	100	83-120	3.0 x5.0

5.3.3 FLUX CALIBRATION

The IRAS source calibration at 12μm is based on the ground based 10μm absolute calibration by observations of α Tauri. The relative responsivity of the other IRAS bands is determined with respect to the 12μm band by modelling the emission of observed asteroids.

5.4 ADDITIONAL OBSERVATION DATA

While the prime objective of the IRAS mission was to produce an all sky survey, part of the observing time was set aside so that IRAS could study particular objects in greater depth - so called additional observations (AO's). The IRAS AO is produced from a combination of the pointing history of the satellite, and the calibrated detector data. The data are reduced by filtering and coadding them in a spatial grid. Two sets of spatially smoothed grids are produced, one having no filtering, and one having a point source filter applied. Processing includes a threshold source extraction program, and displaying the data as contour maps in RA and DEC coordinates. Calibration was incomplete when the LMC AO's used here were obtained, and the photometry is not accurate to better than 30% - although this figure is undoubtedly pessimistic (Gregorich et al. 1983). This figure is soon to be improved. After launch it became apparent that uncertainty in the baselines of the individual detectors introduced intensity stripes into the data which had not been through the point source filter. In addition, smooth intensity gradients were observed across many fields and are presumed to be due to variations in the zodiacal background. Stripe removal and flat-fielding is done in the post processing. The difference between each pair of adjacent cross-scan intensities was found. This difference was averaged in the in-scan direction so generating a destriping function across the focal plane which could be subtracted from every point in the grid. The grids were flat fielded in the in-scan direction by fitting and subtracting a linear function.

5.4.1 RESULTS

For the nine LMC remnants for which IRAS AO data has been made available, there are four which are unambiguously associated with IR

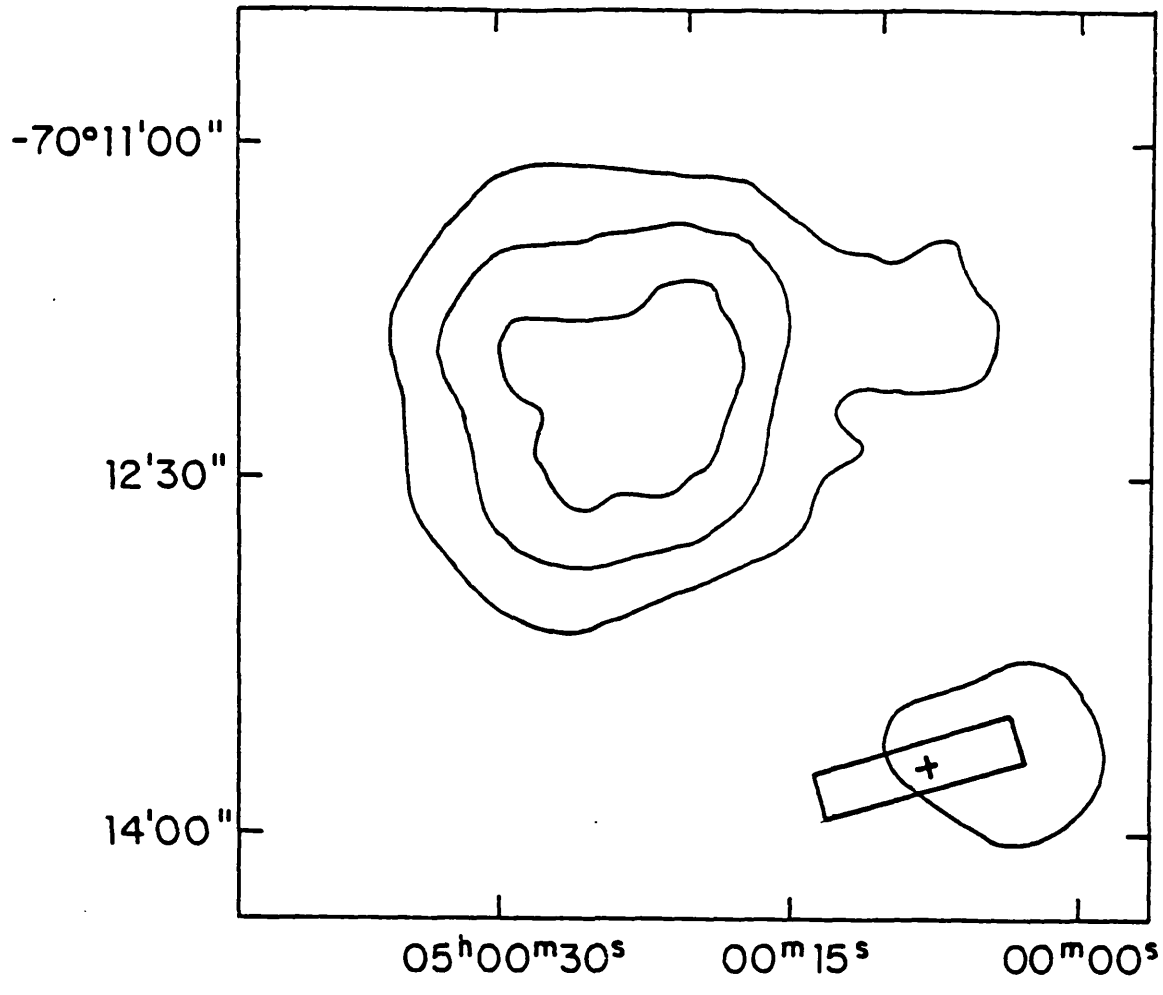

Figure 5.2

SNR N186d. X-ray contours of the SNR are shown along with the mean IR position indicated by a cross. The positional uncertainty (1σ) is represented by the rectangle.

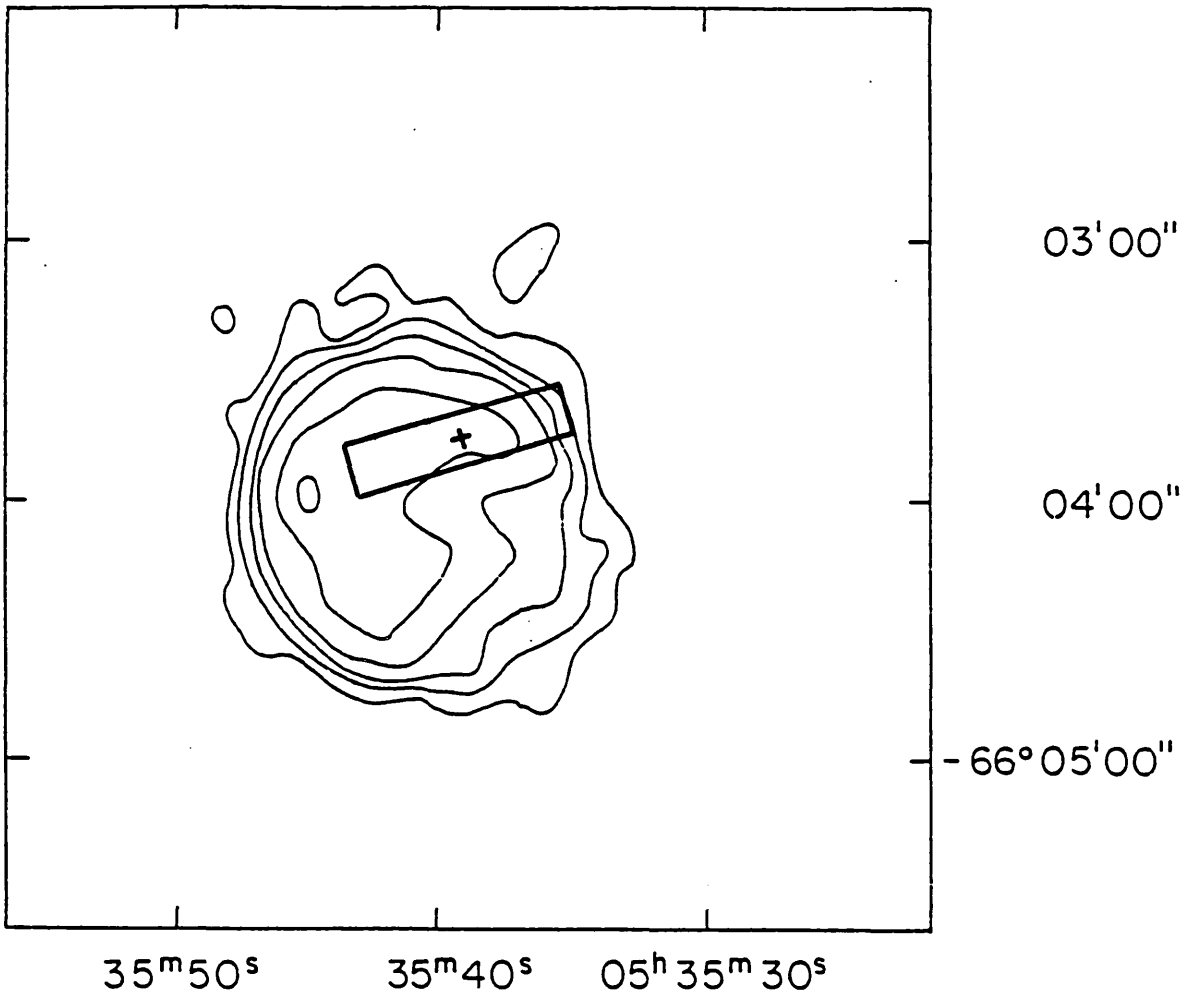

Figure 5.3

SNR N63a. X-ray contours of the SNR are shown along with the mean IR position indicated by a cross. The positional uncertainty (1σ) is represented by the rectangle.

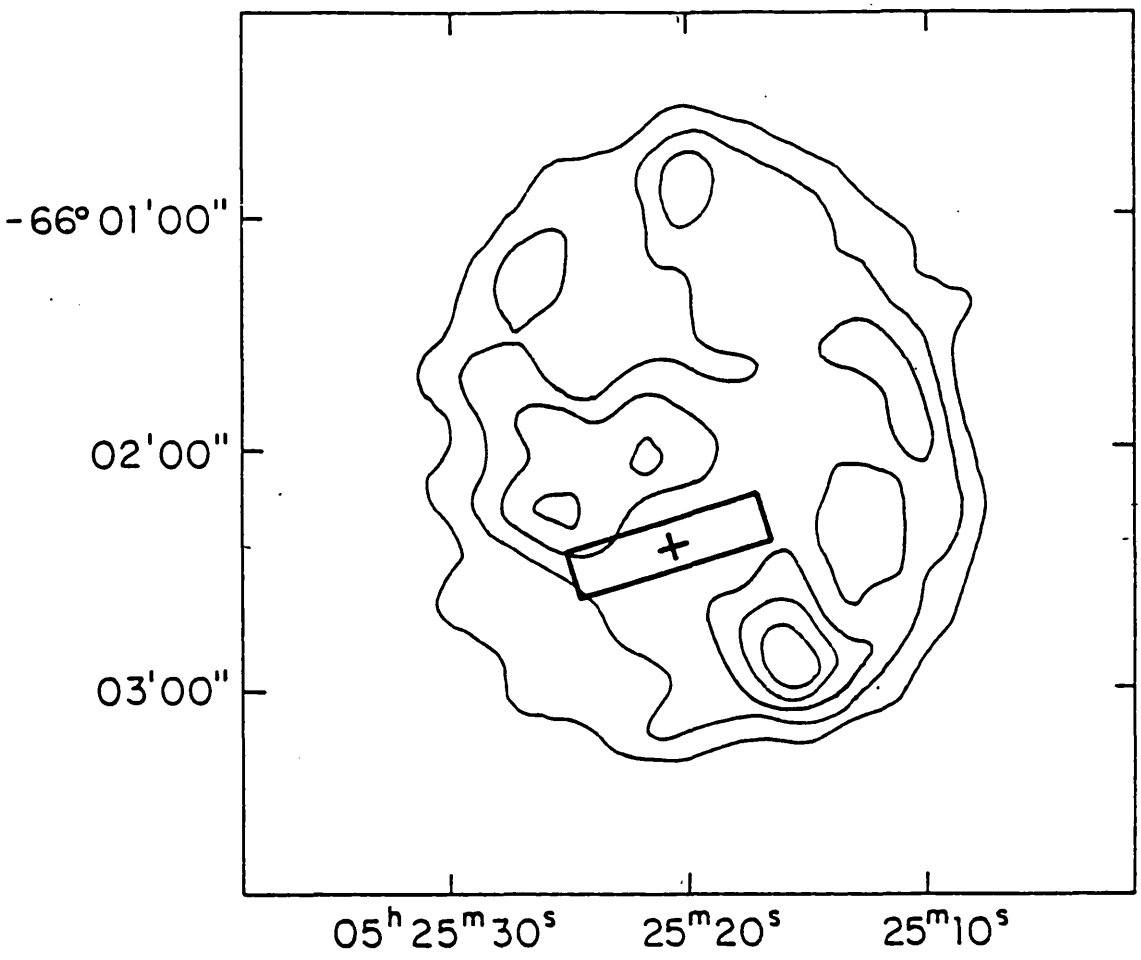

Figure 5.4

SNR N49b, X-ray contours of the SNR are shown along with the mean IR position indicated by a cross. The positional uncertainty (1σ) is represented by the rectangle.

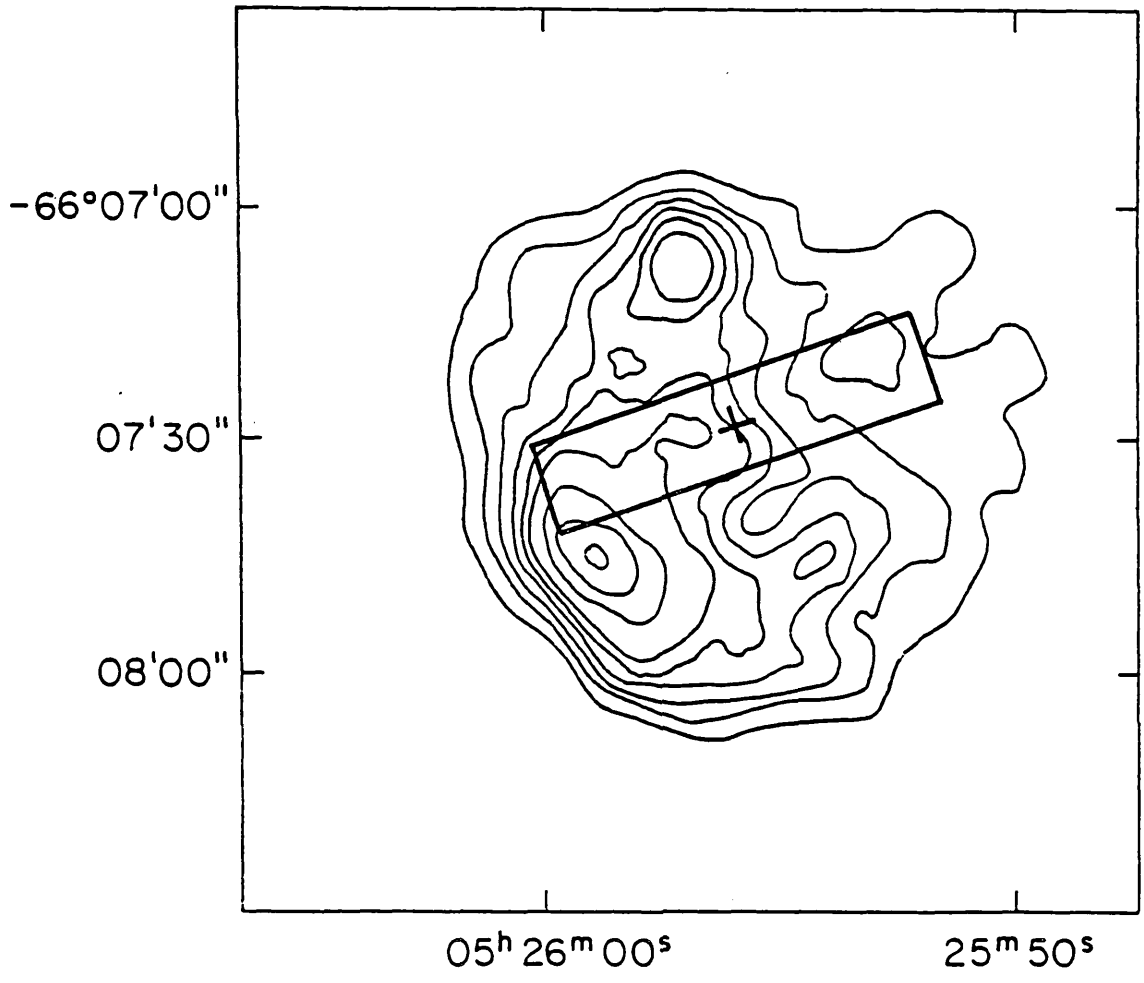

Figure 5.5

SNR N49. X-ray contours of the SNR are shown along with the mean IR position indicated by a cross. The positional uncertainty (1σ) is represented by the rectangle.

Table 5.2

Positional Information

SNR	Band	Position (Epoch 1950.0) α H M S	δ ° ' "	IR size(') (FWHM)	X-Ray size (')
N63A	I	05 35 42	-66 03 54	1.8x5.3	1.2
	II	05 35 39	-66 03 47	1.3x5.3	
	III	05 35 35	-66 03 39	2.9x7.1	
	IV	05 35 30	-66 03 45	5.7x6.4	
Mean IR		05 35 39	-66 03 46		
X-Ray		05 35 41	-66 04 03		
N49	I	05 25 58	-66 07 30	-	1.1
	II	05 25 57	-66 07 34	1.1x3.5	
	III	05 25 56	-66 07 34	3 x6	
	IV	05 25 41	-66 07 17	-	
Mean IR		05 25 56	-66 07 28		
X-Ray		05 25 56	-66 07 31		
N49B	I	- - -	- - -	-	2.3
	II	- - -	- - -	-	
	III	05 25 20	-66 02 13	-	
	IV	05 25 06	-66 02 34	-	
Mean IR		05 25 21	-66 02 24		
X-Ray		05 25 19	-66 01 54		
N186D #1	I	05 00 20	-70 12 27	1.5x5.6	
	II	- - -	- - -	-	
	III	- - -	- - -	-	
	IV	- - -	- - -	-	
N186D #2	I	05 00 12	-70 13 42	4.1x5.7	2
	II	05 00 03	-70 13 43	1.2x5.6	
	III	05 00 03	-70 13 43	4.6x5.3	
	IV	04 59 53	-70 13 45	5.2x5.4	
Mean IR		05 00 08	-70 13 42		
X-Ray		05 00 20	-70 12 13		

Table 5.3

IRAS In Band Fluxes ($W/m^2 x 10^{-13}$)

SNR	I	II	III	IV
N63A	0.736	1.58	6.23	6.38
N49	0.61(9)	0.91	4.53	2.29
N49B	<0.102	<0.041	0.23(11)	0.60(8)
N186D #2	0.47(8)	0.344	2.08	3.30
N103B	-	-	<0.148	<0.53
N135	-	-	<2.4	<0.705
N206	-	-	<0.75	<4.87

All limits are 3σ. The statistical uncertainty, as a percentage, is shown in brackets following the flux entry. Where no figure is quoted the accuracy is better than 5%.

sources, i.e. the remnant falls within the IRAS positional uncertainty error box. The position of the peak IR emission is shown on the x-ray maps of the remnants in figures 5.2 to 5.5. For a further three remnants there are upper limits, and the remaining two were too close to bright sources to obtain useful limits. The positional data is summarised in table 5.2. The flux presented in table 5.3 is the peak flux at the position of maximum emission. No attempt has been made to integrate the flux over the source, because the format of the early AO releases was only designed for the extraction of point source fluxes. These fluxes should be regarded as lower limits, but in all cases the Band III and IV apertures encompass the remnant being observed.

The fluxes derived from AO observations have been cross-checked with the IRAS survey Point Source Catalogue. This can only be done for the brightest remnants because an AO, which consists of between 4 and 8 co-added survey-like scans, has a much more sensitive detection level than the survey. The correspondence in flux for N63A and N186D is to within a few percent. N49B is too faint to have been recorded, and in the case of N49 the value for the Band IV flux is very much higher than that derived from the AO. This discrepancy is almost certainly due to a nearby bright source which confuses the automatic source identification routine.

The total luminosity of each supernova remnant has been calculated from the 60 and 100 μm in-band fluxes assuming that the spectrum is Planckian. If F_ν is the flux density in Band IV, B_ν the Planck function , and T the grain temperature derived from the ratio of Bands III to IV then the total flux is

$$F = \frac{F_\nu \sigma T^4}{B_\nu \pi} \qquad (5.1$$

The luminosities are calculated for a distance of 46kpc and presented in Table 5.4

Table 5.4

Far-infrared luminosities of LMC SNR's

SNR	T(K)	L($10^5 L_\odot$)
N63A	40	1.55
N49	60	0.80
N49B	28	0.170
N186D	33	0.811
N103B	35*	<1.2
N206	35*	<0.87
N135	35*	<1.3

* Assumed dust temperature. All limits 3σ

5.5 INTERPRETATION

The positional coincidence between the IR and x-ray sources constitute prima facie evidence that the IR emission originates from the SNR. In some 2×10^4 □' (square minutes of arc) of the LMC scanned, the density of sources detected at a level of significance >10σ is 0.002/□' in band IV. Therefore, the probability of detecting an unassociated source at 100μm falling within a LMC SNR (d~1') is ~ 0.002. This probability is sufficiently small so that it is worth investigating whether or not the observed fluxes can be accounted for by collisionally heated dust.

5.5.1 COLLISIONAL HEATING OF DUST

The respective masses of infrared (M_d) and x-ray (M_x) emitting material can be calculated. If the x-ray emitting gas heats the dust, then the ratio of these masses in the absence of grain destruction should just be the gas to dust ratio in front of the shock. If this ratio has a value similar to its Galactic value then we expect $M_d/M_x \sim 0.01$, although it is noted that the dust to gas ratio shows evidence for variability over the LMC (Koornneef 1984). The x-ray emitting gas detected by the Einstein Observatory is at a temperature of 5.2×10^6K in N49 and, 6.2×10^6K in N63A (Clarke et al. 1982). If we take a temperature of 6×10^6K to typify all the LMC remnants (c.f. section 4.7.1) the corresponding

emissivity in the Einstein energy band is $\Lambda_x=3\times10^{-23}$erg cm^3/s (Raymond, Cox and Smith 1976). The Sedov model described in section 4.7.1 is used to give the mass of hot gas

$$M_x = \left[\frac{\pi Lx\ r^3}{3\Lambda_x}\right]^{1/2} m \qquad (5.2$$

Where m is the mean atomic mass, and Lx is the x-ray luminosity from Long et al. (1981). From the ratio of the IR in-band fluxes a dust temperature is derived. If the mass absorption coefficient is known, then the dust mass can be found. taking the mass absorption coefficient, κ

$$\kappa = \frac{4\pi a^3 \rho}{3Q_a \pi a^2} \qquad (5.3$$

at 100μm to be 250 gm/cm^2 (Campbell et al. 1981) where Q_a is the absorption efficiency, a the grain radius, and ρ the density of the solid material, then the flux, F_ν, at the Earth resulting from an optically thin assembleage of N_g dust grains is

$$F_\nu = N_g Q_a \pi (a/d)^2 B_\nu(T_g) \qquad (5.4$$

and so the flux is related to the dust mass by

$$M_d = \frac{d^2 F_\nu}{\kappa B_\nu(T_g)} \qquad (5.5$$

The hot gas to dust ratio is shown in table 5.5 . The ratios for N49, N63A, N49B, and the limits, are close, (within a factor of 2), to 0.01 and consequently in good agreement with the hypothesis that this hot dust is embedded in the x-ray emitting gas. N186D is clearly different as there must be a large fraction of the remnant's luminosity due to dust in cool gas ($T<<10^6$K) which is unobservable by Einstein.

Table 5.5

Hot gas to hot dust ratios in the LMC SNR's

SNR	$M_x(M\odot)$	$M_d(M\odot)$	M_d/M_x
N48B	128	0.98	0.007
N49	60	0.28	0.005
N63A	104	2.2	0.02
N186D	15	2.43	0.16
N103B	13	<3.5	<0.27
N135	65	<4.4	<0.07
N206	47	<3.2	<0.068

5.5.2 ENERGETICS

Given that it is reasonable to propose that the hot dust and x-ray emitting gas are mixed together, we now investigate whether or not it is energetically feasible that collisional heating is responsible for maintaining the observed IR sources. The observed dust temperatures are consistent with the collisional heating hypothesis if pre-shock densities are ~ 0.3-1/cm^3. The contribution which dust in this hot X-ray gas should make towards the IR luminosity if collisional heating is invoked is $\frac{\Lambda dust}{\Lambda x}Lx$, so the ratio Lir/Lx=$\Lambda$dust/$\Lambda$x.
At 6×10^6K this ratio should be 32 if there is no grain destruction. The infrared to x-ray luminosity is presented in table 5.6. When compared with the x-ray luminosity, the IR radiation is at a level close to our expectations. The upper limits do not constrain collisional heating very well, but dust heating by collisions is only 1/2-2/3 as efficient as predicted. Once again N186D is peculiar, with a very large "infrared excess". An additional source of heating must be important in the energy balance if the very high hot dust to hot gas ratio and the unusually large IR luminosity are to be explained.

Table 5.6

IR to X-Ray Luminosities for the LMC SNR's

SNR	L_{ir}/L_x
N63A	16.2
N49	23.7
N49B	10.9
N186D	2320
N206	<696
N135	<929
N103B	<38.3

We conclude that the IR sources are associated with the SNR's. The dust in the hot x-ray emitting plasma is heated to temperatures of 30-60K, so that the gas cools at a rate an order of magnitude greater than it would by free-free emission, and in N186D an additional energy source must be invoked to power the IR emission.

5.5.3 ADDITIONAL ENERGY SOURCES

Galactic and extra-galactic far-infrared sources are usually interpreted as being due to dust grains re-radiating the light of luminous young stars. It would therefore be reasonable to look to radiative heating as the additional energy source in N186D. If we can trace this to a luminous star, then it will be possible to discover whether or not the other SNR's also contain such stars. If these are not found then the collisional heating hypothesis will be further strengthened for these SNR's.

Most of the LMC remnants have been classified as type II supernova remnants, and therefore are extreme population I objects (Tuohy et al. 1982). N49,N49B, and N63A lie to the North of the LMC in a region rich in bright blue stars and neutral hydrogen. N63A is a member of an association of massive young stars, whereas N49 and N49B which lie 1 degree to the West of N63A are not members of any association in the same obvious way. The nebula N49 is one of the most extensively studied SNR in the Magellanic Clouds, partly due to its high x-ray,radio, and optical surface brightness, and partly because of its

position free from confusion away from the Bar and 30 Doradus. N186D is found in a local peak in the HI distribution (McGee & Milton 1966) to the SW of the bar, only 4' away from the supergiant star R67 which is thought to be similar to η Carina.

5.5.4 STELLAR CANDIDATES FROM CATALOGUES

Objective prism surveys of the LMC have been used to compile catalogues of emission line regions and early stars. There is a high probability that any star in these lists which is classified as O or B which is fainter than $m_{pg}=10$ will be a cloud member (Sanduleak, 1970). As the deepest survey's limits (Sanduleak, 1970) are ~13.5 most cloud members earlier than O9 ($L>4\times10^4 L_\odot$) should be included.

Mezger (1984) estimates that the dust absorption cross-section per H atom in the UV is $\approx10^{-21}cm^2$, which gives an optical depth through a SNR shell of $\tau\approx0.001nr$, where r is the remnant radius in parsecs. Taking typical densities, $n\sim1/cm^3$ (McGee & Milton 1966), we see that the efficiency of re-radiating starlight will be at most a few percent, and therefore, a star more luminous than O9 (Osterbrock 1978) would be required to account for the observed IR luminosity in all the remnants under consideration. Accordingly, if the energy source in any of these remnants is an early star, then it will have been catalogued.

The surveys of Henize (1956), Fehrenbach & Duflot (1970), and Sanduleak (1970) have been searched for early stars within or around (~5') the SNR's which were detected. Only N186D contains an early star; S152=Sand -77 30a ($m_{pg}=12.4$, Spectral type= "OB" α=05h00m 19.65s,$\delta=-70°12'27.2"$:1950) There is exact positional correspondence between this star and a source which is seen at 12μm (N186D#1). The source is "hot"; the temperature given by the ratio of 12 to 25 μm flux is 350K. This source is swamped at 60 and 100μm by the far brighter IR emission which peaks at the centre of the radio shell of N186D. There are two more notable stars within the vicinity of the SNR, although neither of these correspond to IRAS sources. The luminous supergiant R67 lies 4' to the SE of N186D, and DM-70 5006, spectral type BOI (Ardeberg et al. 1972) is a similar distance to the SW. R67 and DM-70 5006 are proven cloud members on the basis of radial velocity measurements (Ardeberg et al. 1972), but S152's association with the LMC is only based upon its faintness and

spectral type.

N63A contains no catalogued hot stars, but the remnant is embedded in the NE corner of an almost circular diffuse HII region some 4.3' in diameter. The HII region's exciting star can probably be identified with Sand -66 163 (m_{pg}=12.0, Spectral type "OB", α=05 35 37.1 δ=-66 04 21.3:1950) which is only 1.3' SW of N63A. Any IR emission from the HII region must be very diffuse as emission peaks at the centre of N63A and is of comparable extent to the SNR. Baseline uncertainties make it difficult to determine whether or not there is any low surface brightness emission associated with the HII region. In any case the HII contribution to the flux can be no more than a few percent.

N49 and N49B are found in a much less densely populated region of the LMC and no early stars are found either in or around them.

5.5.5 LYMAN ALPHA RADIATION

A possible alternative heating mechanism to absorption of starlight is that dust absorbs resonantly trapped Lyα. Short wavelength ionising photons originating either from a stellar surface, or from recombination behind the shock are degraded by multiple absorption and subsequent recombination until they are converted into Lyα photons plus Balmer and higher series lines. These Ly α photons are scattered many times, until they either reach the edge of the nebula, or the absorbing H atom decays by 2 photon emission. The multiple scattering process increases the path length which photons must travel, and so in the presence of dust the effective cross-section for absorption is very high. The Lyα luminosity of the remnant can be inferred from the Hα luminosity (Dopita, 1979) and hydrogen recombination theory. At high densities ($n_e >> 2\times10^3 cm^{-3}$) every effective recombination (all recombinations except those to the ground state) leads to the production of a Lyα photon, i.e. $\alpha^{eff}_{Ly\alpha}/\alpha_B$=1 (Mezger et al.1974). The spectra of the remnants show that the line emission arises from collisional excitation rather than photoionisation by a star, so shock conditions should be most appropriate. Shock models indicate that recombination is complete before $n=10^3 cm^{-3}$ (Raymond 1979), so the low density limit $\alpha^{eff}_{Ly\alpha}/\alpha_B$=0.64 (Mezger et al. 1974). Taking numerical values for

the recombination coefficients from Osterbrock (1978) allows the Lyα flux to be related to the Hα flux, giving

$$F_{H\alpha}/F_{Ly\alpha}=0.0875 \qquad (5.6$$

Dopita's (1979) measurements of the total Hα flux have been used to calculate the Lyα luminosities. The infrared to Lyα luminosity ratio $L_{IR}/L_{Ly\alpha}$ is shown in table 5.7.

TABLE 5.7

The infrared to Lyman α luminosity ratio.

SNR	$L_{IR}/L_{Ly\alpha}$
N49	1.9
N186D	15.8
N63A	11.3
N206	<5.4
N135	<1.5

No measurements are available for N49B or N103B

The remnants N49, N186D, and N63A all have an infrared luminosity in excess of that which could be provided by Lyα radiation. This demonstrates that absorption of radiation from the shock could not power the IR source. None of the limits are low enough to show that Lyα heating makes no contribution to the IR, but at most it contributes ~10%.

A stellar energy source can be ruled out for N49, N49B, and N63A because the stellar luminosity required to account for the IR corresponds to stars which are brighter than the limiting magnitudes of the catalogues. The radiation from the shock itself has also been excluded. In the absence of accurate spectroscopic classification of the star in N186D it is not possible to accurately estimate its luminosity and thus it is difficult to evaluate the contribution which

it could make to the measured luminosity. Based on its magnitude, the star in N186D could be as early as O4. An O4 star is sufficiently luminous ($1.3\times10^6 L_\odot$, Osterbrock, 1978) to provide the power required, yet remain consistent with the dust temperature and the low expected optical depth, but many of the ionising photons would have to escape to be compatible with the measured Hα luminosty. It is possible that S-152 is the brightest member of a cluster of B0 or O9.5 stars, whose integrated luminosity could produce the observed IR source.

Finally, the success of this technique in identifying luminous stars in and around N186D suggests that it would have been equally successful if a similar situation had obtained in the other remnants studied. Consequently we assert that the case for collisional heating of dust grains has been strengthened by this search.

5.6 DISCUSSION

These are the first infrared observations which have been sensitive enough to detect collisionally heated dust in a hot plasma. Grain cooling is less efficient than predicted by a factor of between 1/3 and 2/3 if there were total grain survival behind the shock. Nevertheless, grain cooling is an order of magnitude larger than traditional atomic gas processes. The analysis of section 4.6 demonstrates that grains are partially sputtered behind a shock. Accordingly, the grain cooling function will be reduced. For example, in a 10^4 year old remnant, there can be up to 15% (by radius) erosion of grains. As the grain cooling function is approximately proportional to grain surface area this sputtering would lead to a 30% drop in grain cooling. According to a Sedov analysis of the x-ray observations of the LMC SNR's, N63A is the youngest remnant (4700yrs), followed by N49 (6400yrs), and N49B (10,000yrs). The lower gas to dust ratio in the two older remnants could probably be attributed to grain sputtering. The grain cooling function is $\propto a^2$, and the dust to gas ratio, α, is $\propto a^3$.
Therefore on the assumption of a constant x-ray cooling function in all three remnants let us define a grain erosion parameter

$$\alpha^{-2/3} \frac{L_{IR}}{L_X} \propto a^{-2} \Lambda_{dust} \qquad (5.7$$

which should be a constant. This product is tabulated in Table 5.8

Table 5.8

Grain Erosion parameter

SNR	$\alpha^{-2/3} L_{IR} / L_X$
N63A	220
N49	340
N49B	300

Although α varies by a factor of 4, and L_{IR}/L_X by 2, the grain erosion parameter shown in table 5.8 varies by a significantly smaller amount, suggesting that the variation in the grain cooling efficiency relative to x-ray cooling is, at least in some part, due to grain erosion.

5.6.1 GRAIN EROSION RATE

We have measurements of the gas to dust ratio in three remnants of different ages. Therefore it should be possible to estimate the grain lifetime. Admittedly though, conditions (e.g. initial gas to dust ratio, density) in these three remnants are not the same - as witnessed by the fact that N49B, although older than N49 has apparently suffered less sputtering. If α_1 and α_2 are the dust to gas ratios in remnants 1 and 2 of ages t_1 and t_2 respectively then

$$\frac{\alpha_2}{\alpha_1} = \left(\frac{1-t_2/\tau}{1-t_1/\tau}\right)^3 \qquad (5.8$$

where τ is the grain lifetime $a/\dot{a}$. If remnant 1 is N63A, and N49 is remnant 2, then τ =13,000 years. Similarly if remnant 1 is N63A and N49B is remnant 2, then τ = 23,000 years. The

mean grain lifetime is 18,000 years. This is remarkably close to the grain lifetime estimated for $n_o=1/cm^3$ in Chapter 4, and indicates that the treatment used there is reasonable.

5.7 CONCLUSIONS

Both direct (IR) and indirect (x-ray) observations confirm that dust in a hot plasma makes a substantial contribution towards the cooling of that plasma. The original contention of Chapter 4 that this additional cooling accelerates the evolution of supernova remnants can be upheld. Even if the dust cooling function is not extrapolated to the higher temperatures expected in younger remnants, and the value of the function determined in the relatively cool x-ray emitting gas observed by Einstein is used, then the sag time is

$$t_{sg} \sim 5000\epsilon_{51}^{2/11} \quad n_o^{-7/11} \quad yr \qquad (5.9$$

approximately 1/4 of the gas cooling only sag time. Thus we reach the inescapable conclusion that dust cooling dominates over gas cooling in determining when temperature sag occurs and hence when the adiabatic approximation must be relinquished.

This deduction has many far reaching astrophysical implications. As described in section 1.8.1 it is generally supposed that the hot gas in the interior of a SNR takes a very long time to cool, and so eventually becomes the hot component of the interstellar medium (McKee & Ostriker 1977). If so then the inclusion of dust cooling will modify, for example, the predicted mass balance between hot and cold components of the interstellar medium because the early onset of shell formation reduces the mass of hot gas supplied by the SNR by $\sim 1-(R_{sg}^{dust}/R_{sg}^{gas})^3$, i.e a dusty SNR supplies only ~ 20% of the hot gas which a dust free SNR would. Theories in which the structure of the ISM is determined by SNR's clearly need to be re-evaluated in the light of these results.

Whenever we encounter hot gas the effect of cooling by dust must be considered. One fascinating possibility is that the x-ray emitting gas observed in clusters of galaxies is not primordial, but blown out of cluster members. In this case the gas may well carry with it a component of dust which will aid the cooling of the gas. One might expect that the x-ray haloes composed of primordial and non-primordial

gas should exhibit quite different structure.

The scope for theoretical work is clearly very broad. Firstly though, it would be most desirable to confirm these findings by inspecting the IRAS data for Galactic remnants. This, unfortunately, will have to be delayed until the problem of source confusion in the Galactic plane is well understood, and it becomes as straightforward to obtain data about extended sources, as it presently is for point-like sources.

CHAPTER VI

CONCLUDING REMARKS

The infrared study of supernovae and supernova remnants is still in its infancy. However, a systematic survey of the infrared properties of supernovae is now underway. Chapters 2 and 3 represent the first fruit of this work. For the first time light curves of an infrared excess supernova have been obtained with sufficient photometric accuracy and temporal coverage so that it has been possible to discriminate between grain condensation and pre-existing dust cloud models. An analysis of these light curves in terms of an infrared echo from a pre-existing dust cloud yields detailed information regarding the structure of this cloud. This information has been used to construct a self-consistent picture of the evolution of a low mass supernova progenitor.

IRAS observations of the supernova remnants in the Large Magellanic Cloud provided the first evidence for dust heated collisionally by hot gas. The infrared luminosity of these remnants is an order of magnitude greater than the x-ray luminosity, indicating that dust is more important in the energy balance of hot (10^6K) gas than processes such as bremsstrahlung and recombination. This excess cooling accelerates the evolution of supernova remnants and restricts the use of the adiabatic approximation to a comparitively short time span.

At the begining of Chapter 2 several research programmes of infrared supernova photometry were suggested. The work on supernovae has proceeded along just one of these many possible avenues. Our knowledge of the infrared development of supernovae is still based on just a few examples. More high quality photometry with good temporal coverage is needed, with special emphasis upon obtaining complete light curves.

The discovery of the infrared [FeII] line in SN1983n (see appendix) was possible with current technology only because this was an unusually bright supernova. However, this study points to the future, when the potential of space observatories and improved ground based sensitivities become available.

Far-infrared observations of supernova remnants have far-reaching

astrophysical consequences. Extending the results obtained for the supernova remnants in the Magellanic Clouds to Galactic remnants, where the emission would be resolved, is very important. The full implications for the evolution of supernova remnants and the structure of the interstellar medium are yet to be deduced. However, these two topics represent only a small number of the possible situations where the importance of dust cooling should be explored.

There is much work to be done as the infrared study of supernovae and their remnants develops. The exciting results presented in this thesis indicate the promise which future observations hold.

REFERENCES

Aannestad P.A., (1975), Ap. J., 200, 30.

Ardeberg A., Brunet J.-P., Maurice E., and Prevot L., (1972), A. A. Suppl., 6, 249.

Arnett W.D. (1975), Ap. J., 195, 727.

Arnett W.D., (1980), Ann N.Y. Acad. Sci., 366, 366.

Assousa G.F., and Erkes J.W. (1973), Astron J., 78, 885.

Axelrod T.S., (1980), Ph. D. Thesis, University of California, UCRL52994.

Barbon R., Ciatti F., and Rosino L., (1973), Astron. Astrophys., 25, 241.

Barbon R., Ciatti F., and Rosino L., (1979), Astron. Astrophys., 72, 287.

Bath G.T., and Shaviv G., (1976), M.N.R.A.S., 175, 305.

Bode M.F. and Evans A., (1979), Astron. Astrophys., 73, 113.

Bode M.F. and Evans A., (1980), Astron. Astrophys., 89, 158.

Bode M.F. and Evans A., (1983), M.N.R.A.S., 203, 285.

Borst L.B., (1950), Phys. Rev., 78, 807.

Blackwell D.E., and Shallis M.J., (1977), MNRAS, 180, 177.

Blackwell D.E., Shallis M.J., Selby M.J., (1979), MNRAS, 188, 847.

Branch D., Falk S.W., McCall M.L., Rybaski P., Uomoto A.K., and Wills B.J., (1981), Ap. J. 244, 780.

Branch D. (1982), In Supernovae: A survey of current research. Eds. Rees M.J., and Stoneham R.J., p267, D. Reidel, Dordrecht.

Branch D., Lacy C.H., McCall M.L., Sutherland P.G., Uomoto A., Wheeler J.C., and Wills B.J. (1983), Ap. J., 270, 123.

Burbidge G.R., Burbidge E.M., Fowler W.A., and Hoyle, F. (1957), Rev. Mod. Phys., 29, 547.

Cahn J.H. and Wyatt S.P., (1978), Ap.J.,211, 163.

Cambell M.F., Hoffmann W.F., and Thronson H.A., (1981), Ap. J., 247, 530.

Cassinelli J.P., (1975), Ann. Rev. Astron. Astrophys., 17, 275.

Chevalier R.A., (1981), Ap.J.,251,259.

Clark D.H. and Caswell J.L., (1976), M.N.R.A.S., 174, 111

Clarke D.A., Tuohy I.R., Szymkowiak A.E., Dopita M.A., Mathewson D.S., and Culhane J.L., (1982), Ap. J., 255, 440.

Clayton D.D.,(1979), Astron. & Space Sci., 65,179.

Clayton D.D., (1982), In Supernovae: A survey of current research. Eds. Rees M.J., and Stoneham R.J., p535, D. Reidel, Dordrecht.

Colgate S.A. and McKee C., (1969), Ap. J., 157, 623.

Colgate S.A., (1979), Ap. J., 232, 404.

Cox D.P. (1972a), Ap. J., 178, 143.

Cox D.P., (1972b), Ap. J., 178, 159.

Cox D.P., (1976), Paper presented at IAU General Assembly., Grenoble.

Cox D.P. and Smith B.W., (1974), Ap. J. Lett., 189, L105.

de Vaucouleurs G., (1978), Ap. J., 233, 730.

de Vaucouleurs G., de Vaucouleurs A., and Corwin H.G., (1976), Second Reference Catalogue of Bright Galaxies, University of Texas Press, Austin.

Dinerstein H.L., Werner M.W., Dwek E., and Capps R.C., (1982), Ap. J., 255, 552.

D'Odorico S. and Moorwood A.F.M., (1982), E.S.O. Messenger, 28, 29.

Dopita M. A. (1979), Ap. J. Suppl. Ser., 40, 455.

Donn B., Hecht J., Khana R. Nunth J., Strang D. and Anderson A.B., (1981), Surf. Sci., 106, 576.

Draine B.T., (1981), Ap.J., 245, 880.

Draine B.T. and Salpeter E.E., (1979), Ap. J., 231, 77.

Duin R.M., and van der Lann H., (1975), Astr Astrophys., 40, 111.

Dwek E., and Werner M.W., (1981), Ap. J., 248, 138.

Dwek E., and Scalo J.M., (1980), Ap.J.,239,193.

Dwek E., A'Hearn M.F., Becklin E.E, Hamilton Brown R., Capps R., Dinnerstein H.L., Gatley I., Morrison D., Telesco C.M., Tokunaga A.T., Werner M.W., and Wynn-Williams C-G., (1983), Ap. J., 274, 168.

Dwek E. (1983), Ap. J., 274, 175.

Elias J.H., Frogel J.A., Hackwell J.A., and Persson S.E., (1981), Ap. J. Lett., 251, L13.

Fabian A.S., Willingdale R., Pye J.P., Murray S.S., and Fabbiano G., (1980), M.N.R.A.S., 193, 175.

Falk J.F. and Arnett D.A., (1977), Ap. J. Suppl. Ser., 33, 515.

Falk S.W. and Scalo J.M., (1975), Ap. J., 202, 690.

Fehrenbach C. and Duflot M., (1970), Astron. Astrophys. Special Suppl. Ser., 1.

Frish P.C. and York D.G., (1983), Ap. J. Lett., 271, L59.

Fujimoto M.Y., (1980), In Type I supernovae, ed. T.C. Wheeler, p155. University of Texas Press, Austin.

Gregorivh D., Kopan E., Miley G., Oken C., and Young E., (1983), The IRAS AO Interpreter, JPL unpublished circular, Pasadena .

Gull S.F., (1973a), M.N.R.A.S., 161, 47.

Gull S.F., (1973b), M.N.R.A.S., 162, 135.

Hainebach K.L., Norman E.B., and Schramm D.N., (1976), Ap. J., 203, 245.

Heiles C., (1964), Ap. J., 140, 470.

Heiles C., (1976), Ap. J. Lett., 208, L137.

Henize K.G., (1956), Ap. J., Suppl Ser., 2, 315.

Hoyle F. and Lyttleton R.A., (1939), Proc. Camb. Phil. Soc., 35, 592.

Iben I. Jr. and Tutukov A.V., (1984), Ap. J. Suppl. Ser., 54, 335.

Inoue H., Koyama K.,Matsouka M., Ohashi T., Tanaka Y., and Tsnunemi H., (1980), Ap. J., 238, 886.

Jenkins E.B. and Meloy D.A., (1974), Ap. J. Lett., 193, L121.

Jones T.J., Hyland A.R., Wood, P.R., and Gatley I., (1983), Ap. J., 273, 669.

Jones T.W. and Merrill K.M., (1976), Ap. J., 209, 509.

Joseph R.D. and Robertson N.A., (1982), Proc. E.S.O. 2nd IR Workshop, Garching.

Kamper K.M. and van den Berg S., (1978), Ap. J., 224, 851.

Kare J.T., Pennypacker C.R., Muller R.A., Mast T.S., Crawford, F.S., and Burns M.S., (1982) In Supernovae: A survey of current research. Eds. Rees M.J., and Stoneham R.J., p325, D. Reidel, Dordrecht.

Karzas W.J. and Latter R., (1961), Ap. J. Suppl. Ser., 6, 167.

Kirshner R.P., Willner S.P., Becklin E.E., Neugebauer G., and Oke J.B., (1973), Ap. J. Lett., 180, L97.

Kirshner R.P. and Oke J.B., (1975), Ap. J., 200, 574.

Kirshner R.P. and Kwan J. (1975), Ap. J., 197, 415.

Kirshner R.P. and Chevalier R.A., (1977), Ap. J., 218, 142.

Koorneef J., (1984), I.A.U. Symp. 108, Structure and Evolution of the Magellanic Clouds, p333, D. Reidel, Dordrech.

Klein R.I. and Chevalier R.A., (1978), Ap. J., 219, 994.

Knapp G.R., Phillips T.G., Leighton R.B., Lo K.Y., Wammier P.G., Wootten H.A., and Huggins P.J., (1982), Ap. J., 252, 616.

Koike C., Hasegawa H., and Manabe A., (1980), Astrophys. Space Sci., 67, 495.

Kowal C.T., (1984), The Palomar Supernova Search Master List, Caltech.

Ku W. H. -M., Long K., Pisarski R., and Vartanian M., (1983), In Supernovae Remnants and their x-ray emission. IAU Symp. 101. Eds J. Danziger and P. Gorenstein, p253. Reidel, Dordrecht.

Kulsrud R.M. and Zweibel E., (1975), Munich Cosmic Ray Conf., Pap. OG9, 1-12.

Lee T.A., Wamsteker W., Wisniewski W.Z., and Wdowiak T.J., (1972), Ap. J. Lett., 177, L59.

Long K.S., Helfand D.J., and Grabelsky D.A., (1981), Ap. J., 248, 925.

Lingenfelter R.E., (1973) Astrophys. Space Sci., 24, 83.

Mathewson D.S., Ford V.L., Dopita M.A., Tuohy I.R., Long K.S., and Helfand D.J., (1983), Ap. J. Suppl. Ser., 51, 345.

Maza J., (1982), IAU Circular #3684

Maza J. and van den Berg S., (1976), Ap. J., 204, 519.

McDonald J., (1983), Ap. J., 267, 732.

McGee R.X. and Milton J.A., (1966), Aust. J. Phys., 19, 343

McKee C.F. and Ostriker J.P., (1977), Ap. J., 218, 148.

Merrill K.M., (1980), IAU Circular #3444.

Mezger P.G., (1983), XVI ESLAB Symp.: Galactic & Extragalactic IR Spectroscopy, Eds Kessler M.F. and Phillips J.P., p419, E.S.A., Paris.

Mezger P.G., Smith L.F., and Churchwell E., (1974), Astron. Astrophys., 32, 269.

Mills B.Y. (1983), In Supernovae Remnants and their x-ray emission. IAU Symp. 101. Eds J. Danziger and P. Gorenstein, p551. Reidel, Dordrecht.

Morrison P., and Sartori L., (1969), Ap.J.,158,541.

Neugebauer G., & 27 others, (1984), Ap. J. Lett., 278, L1

Ney E.P. and Hatfield B.F., (1978), Ap. J. Lett., 219, L111.

Oemler A. Jr. and Tinsley B. M., (1979), Astron. J., 84, 985.

Oort J.H., (1951), Problems of Cosmical Aerodynamics, p118, Dayton, Ohio.

Oort J.H. and van de Hulst H.C., (1946), B.A.N., 10, 187, #376.

Osterbrock D.E., (1978), Astrophysics of Gaseous Nebulae, W.H. Freeman, San Francisco.

Ostriker J.P. and Silk J., (1973), Ap. J. Lett., 184, L113.

Paczynski B., (1971), Acta. Astr., 21, 417.

Panagia N. et al. (26 others), (1980), M.N.R.A.S., 192, 861.

Raymond J.C., (1979), Ap. J. Suppl. Ser., 39, 1.

Raymond J.C., Cox D.P., and Smith B.W., (1976), Ap. J., 204, 290.

Romanishin W. and Angel J.R.P., (1980), Ap.J., 235, 992.

Rowan-Robinson M., (1980), Ap J. Suppl. Ser., 44, 403.

Rowan-Robinson M., (1984), Talk given at the University College London IRAS discussion meeting.

Salpeter E.E., (1974), Ap. J. 193, 579.

Sanders W.T., Kraushaar W.L., Nousek J.A., Fried P.M., (1977), Ap. J. Lett., 217, L87.

Sanders W.T., Burrows D.N., McCammon D., and Kraushaar W.L., (1984), In Supernova Remnants and their x-ray emission. IAU Symp. 101, Eds J. Danziger and P. Gorenstein, p361. Reidel, Dordrecht.

Sanduleak N., (1970), Contributions of Cerro Tololo Inter-American Observatory #89.

Schnopper H.W., and 8 others, (1982), Ap. J., 253, 131.

Sedov L., (1959), Similarity and dimensional methods in mechanics, Academic Press, New York.

Sersic J. L., Carranza G., and Pastoriza M., (1972), Astrophys. Space Sci., 19, 469.

Shapiro P.R. and Field G.B., (1976), Ap. J., 205, 762.

Shull J.M., (1977), Ap. J., 215, 805.

Shull J.M., (1978), Ap. J,, 226, 858.

Shull J.M. and McKee C.F., (1979), 227, 131.

Smith B.W., (1977), Ap. J., 211, 404.

Spitzer Jr. L., (1978), Physical processes in the interstellar medium, John Wiley, New York.

Tammann G., (1978), Mem. Soc. Astron. Ital., 49, 315.

Tammann G. (1982), In Supernovae: A survey of current research. Eds. Rees M.J., and Stoneham R.J., p371, D. Reidel, Dordrecht.

Taylor G., (1950), Proc. Roy. Soc. A, 201, 159.

Telesco C.M., Becklin E.E., Koehler R., and Gatley I., (1981), IAU Circular #3613.

Tinsley B.M., (1980), In Type I supernovae. Ed. J.C. Wheeler, p196. University of Texas Press, Austin Press.

Tubbs D.L., Weaver T.A., Bowers R.L., Wilson J.R., and Schramm D.N., (1980), Ap. J., 239, 271.

Tuohy I.R., Dopita M.A., Mathewson D.S., Long K.S., and Helfand D.J., (1982), Ap. J., 261, 473.

Trimble V.,(1982), Rev. Mod. Phys., 54,1183.

van den Heuvel E.P.J., (1975), Ap. J., 196, L121

van der Laan H., (1962), M.N.R.A.S., 124, 175.

Weaver T.A. and Woosley S.E., (1980), Ann. New York Acad. Sci., 336, 335.

Weiler K.W., Sramek R.A., van der Hulst J.M., and Panagia N., (1982) In Supernovae: A survey of current research. Eds. Rees M.J., and Stoneham R.J., p281, D. Reidel, Dordrecht.

Werner M.W., Beckwith S., Gatley I., Sellgren K., Berriman G., and Whiting D.L., (1980), 239, 540.

Wheeler J.C., (1978), Ap. J., 225, 212.

Wheeler J.C., (1981), Rep. Prog. Phys., 44,85.

Wild P., (1980), IAU Circular #3532

Woosley S.E. Arnett W.D., and Clayton D.D., (973), Ap.J., Suppl. Ser., 26, 231.

Woosley S.E., Axelrod T.S., and Weaver T.A., (1984), Proc Erice Conf. on Nucleosynthesis. D. Reidel, Dordrecht.

Wright E.L., Harper D.A., Loenstein R.F., Keene J., and Whitcomb S.E., (1980), Ap. J. Lett., 240, L157.

Zuckerman B., (1980), Ann. Rev. Astron. Astrophys., 18, 263.

APPENDIX

PULBLICATIONS AND PREPRINTS

The following research papers, to which I have contributed, are enclosed:

1) Discovery of an IR echo from a supernova dust cloud.
   J.R. Graham, W.P.S. Meikle, M.J. Selby, D.A. Allen,
   A. Evans, G.Pearce, M.F. Bode, A.J. Longmore, & P.M. Williams.
   Nature, 304, 709-710, (1983).

2) NGC 3256: an emerging elliptical galaxy.
   J.R. Graham, G.S. Wright, W.P.S. Meikle, R.D. Joseph, & M.F. Bode.
   Nature, 310, 213-214, (1984)

3) Discovery of a large mass of iron in a type I supernova
   J.R. Graham, W.P.S. Meikle, D.A. Allen, A.J. Longmore, & P.M.
   Williams.
   Unpublished manuscript.

Reprinted from Nature, Vol. 304, No. 5928, pp. 709-710, 25 August 1983

Discovery of an IR echo from a supernova dust cloud

J. R. Graham*, W. P. S. Meikle*, M. J. Selby*, D. A. Allen†, A. Evans‡, G. Pearce‡, M. F. Bode§, A. J. Longmore‖ & P. M. Williams‖

* Astronomy Group, Physics Department, Imperial College of Science and Technology, Prince Consort Road, London SW7 2BZ, UK
† Anglo-Australian Observatory, PO Box 296, Epping, New South Wales 2121, Australia
‡ Department of Physics, University of Keele, Keele, Staffordshire ST5 5BG, UK
§ Los Alamos National Laboratory, Los Alamos, New Mexico 87545, USA
‖ United Kingdom Infrared Telescope, 900 Leilani Street, Hilo, Hawaii 96720, USA

Supernova (SN) 1982g in NGC1332 was discovered by Maza on 28 March 1982 at $m_{pg}=14.0$ (ref. 1) some 30 kpc ($H_0=50$ km s^{-1} Mpc^{-1}) from the nucleus of the parent galaxy (distance, 30 Mpc; type, SO)[2]. No other optical data have been reported so the SN type is uncertain, although no Type II SN has ever been identified in a galaxy earlier than SA[3]. We have obtained IR light curves for SN 1982g covering 100–250 days after its discovery. We show here that the IR radiation is due to heated dust. No evidence has been found for grain condensation in the SN ejecta. In fact, the light curves reveal that the IR emission originates from a pre-existing circumstellar dust cloud and is produced by an 'echo' of the UV and visible pulse of the SN.

IR observations of the SN were carried out at the 3.9-m Anglo-Australian Telescope and the 3.8-m United Kingdom Infrared Telescope (Hawaii) in the J(1.25 μm), H(1.65 μm) and K(2.2 μm) bands (plus a single upper limit at L(3.4 μm)) (see Fig. 1). If we use the typical optical colours of a SN to specify the temperature of a black body spectrum which we then extrapolate into the IR, a much lower IR flux is deduced than that which we observed. For example, at 100 days the SN is at least 3 mag brighter at K than such an extrapolation would predict. The IR colours J–H and H–K indicate that this excess is due to a continuum with a colour temperature of 1,170 K at 100 days which cools gradually to 920 K at 200 days. SN 1979c and 1980k, both Type IIs are also known to have developed IR excesses[4,5]. For SN 1982g galactic interstellar reddening is negligible at $JHKL$ because it is of high galactic latitude ($b=-50°$). The large distance from the nucleus of the parent galaxy ensures that the reddening, as well as any stellar contribution to the IR flux, due to NGC1332, is also unimportant. In any case, dust in any location could not redden the SN to produce the observed IR colours without rendering it optically undetectable.

We have considered three possible mechanisms for the IR emission. These are free–free emission from SN shock-heated circumstellar gas[6], thermal emission from grains formed in the SN ejecta[7,8], and thermal emission from pre-existing circumstellar grains[9]. Only the last of these provides a convincing interpretation of the data. It is possible that the SN progenitor was surrounded by an optically-thin gas shell formed by the progenitor wind. This gas would be shock-heated by the SN, producing a free-free contribution to the IR flux. However, it is implausible that a significant fraction of the observed IR radiation arises from this mechanism as it would be accompanied by a radio flux ~×50 stronger than that which seems to be typical for SN[10]. If the gas were optically thick ($\tau_{IR}\geq 1$) then unlikely mass loss rates of $\dot{M}>10^{-2}M_\odot$ yr^{-1} from the progenitor would be needed to produce the necessary gas densities. Emission from dust formed in the ejecta can also be dismissed. A thermal source must be at least as large as a black body of the same luminosity and temperature. At 100 days the appropriate black body radius is 1.9×10^{16} cm, implying an ejection velocity of $23{,}000(H_0/50)^{-1}$ km s^{-1} for the emitting material. However, Doppler widths of lines indicate that the outermost layers of SN reach velocities of up to only 10,000 km s^{-1} (ref. 11). Furthermore, conditions favourable for rapid grain growth only exist much deeper in the SN in the slower moving mantle[8].

The large SN to grain distances required to account for the observed IR flux suggests that dust formation must pre-date the SN explosion. If the progenitor were surrounded by an extensive dust cloud similar to that around Betelgeuse[12] (radius, $R=0.1$ pc; $\tau_{UV\text{-}VIS}=0.15$) a substantial amount of the UV-visible pulse of the SN will be converted into IR radiation. Given the extended nature of the dust cloud, light travel times across it must be considered and so one might expect the geometry of the emission to be similar to that of the UV-fluorescence models of Morrison and Sartori[13]. This provides a natural explanation for the IR light curves. Bode and Evans[9] have adapted this 'echo' model to describe the general case of a variable light source within a dust cloud. The SN flash of UV and visible radiation propagates outwards into the cloud. Since the bolometric light curve is sharply peaked[14,15] we can approximate the time dependence of the luminosity to a top hat function,

$$L_{SN}=\begin{cases}10^{43}\text{ erg s}^{-1} & 0<t<10\text{ days}\\ 0\text{ erg s}^{-1} & t>10\text{ days}\end{cases}$$

where t is the time after the outburst, which is assumed to have occurred within a few days of discovery. As a consequence of this narrow pulse only the thin shell of dust (10 light days thick) coincident with this pulse of energy is hot at any given instant.

The temperature of the dust can be used to determine the SN to hot grain distance by means of the radiation balance for

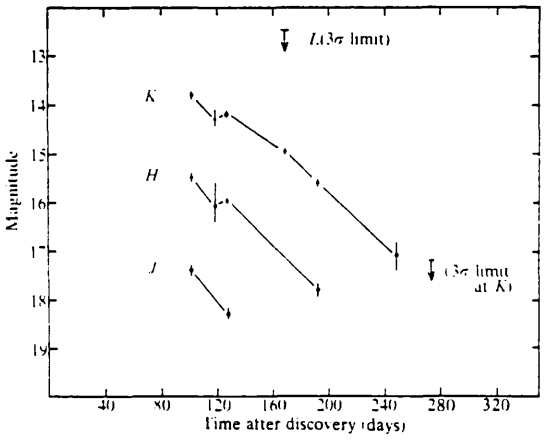

Fig. 1 IR light curves of SN 1982g.

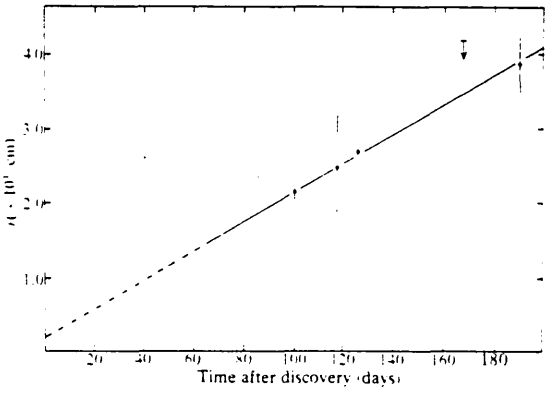

Fig. 2 Distance, r, of heated grains from SN as a function of time.

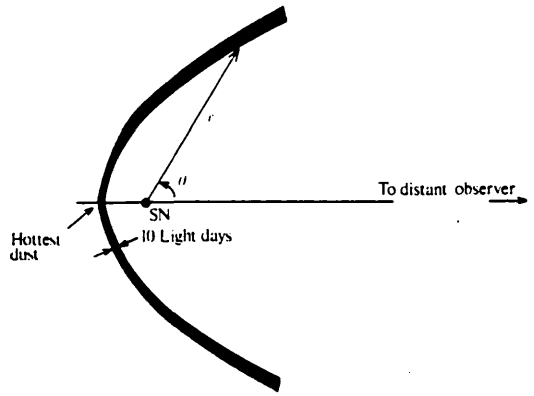

Fig. 3 The paraboloidal shell $r = ct/(1-\cos\theta)$ of hot dust from which a distant observer receives IR radiation.

the grains,

$$\frac{L_{SN}}{4\pi r^2}\bar{Q}(a, T_{SN})\pi a^2 = 4\pi a^2 \bar{Q}(a, T_g)\sigma T_g^4 \qquad (1)$$

where r is the SN-hot grain distance, $\bar{Q}(a, T)$ the Planck average emissivity, a the grain radius, T_{SN} the colour temperature of the SN photosphere, T_g the grain temperature, derived from the IR colours assuming a λ^{-1} emissivity law, and σ Stefan's constant. We have assumed that the optical properties of the grains are described by $\bar{Q}/a \propto T_g$. For illustration we have used the values for $\bar{Q}$ quoted by Draine[16] for carbon. (Use of a dielectric grain material such as silicate[16] does not affect our conclusions.) Rearranging equation (1) and substituting typical numerical values, we obtain

$$r = 7.2\times10^{24}\, T_g^{-5/2}\left(\frac{a}{0.1\ \mu\text{m}}\right)^{-1/2}\left(\frac{L_{SN}}{10^{43}\ \text{erg s}^{-1}}\right)^{1/2}\ \text{cm} \qquad (2)$$

The observed change in grain temperature is interpreted as being due to the increasing distance, r, at which the heated grains lie. The distances inferred by this method are presented in Fig. 2, plotted against time. A straight line fits these points well, and gives as the gradient a constant velocity

$$v = (2.2\pm0.2)\times10^5\left(\frac{a}{0.1\ \mu\text{m}}\right)^{-1/2}\left(\frac{L_{SN}}{10^{43}\ \text{erg s}^{-1}}\right)^{1/2}\ \text{km s}^{-1} \qquad (3)$$

For typical values of a (ref. 17) and L_{SN} (ref.14) this velocity is comparable to the speed of light. The echo model predicts this result. In general when a source 'switches on' in a dust cloud, light travel-time arguments show[9] that the grains from which a distant observer receives IR emission lie within a paraboloid of revolution $r = ct(1-\cos\theta)^{-1}$ (Fig. 3). For a pulse-like light curve this heated dust is confined within the shell as shown in Fig. 3. For a given paraboloid the temperature distribution is such that the hottest dust is situated at the vertex ($r = ct/2$, $\theta = \pi$), the point closest to the SN. Integrating the flux from the paraboloidal shell, one can show that nearly all the flux comes from this hot region around the vertex providing that the observations are made on the Wien slope of the thermal emission; for example, if the dust at the vertex has a temperature of 1,000 K and observations are made at 2.2 μm, 90% of the flux comes from within 30° of the vertex. Cooler grains further from the SN do not contribute significantly to our measurements. The expected recession velocity of the vertex

$$\frac{\partial}{\partial t}\left(\frac{ct}{1-\cos\theta}\right)\Big|_{\pi} = \frac{c}{2}$$

consistent with the determined velocity v. In addition, extrapolation of the graph back to $t = 0$ gives $r = 0$ within the errors. The linearity, gradient and (0, 0) intercept of the r versus t graph are all strong evidence for the echo model. Detailed numerical modelling (J.R.G. *et al.*, in preparation) of a SN embedded in a Betelgeuse-type dust cloud of $\tau_{UV\text{-}VIS}\sim0.1$, mass $\sim10^{-2}M_\odot$ and radius $\sim10^{18}$ cm shows that the observed IR light curves are reproduced.

We conclude that the IR emission from SN 1982g was due to a pre-existing circumstellar dust shell heated by the SN pulse. This is the first clear evidence for the occurrence of an IR echo in any source.

We thank Dr Bob Joseph and Dr Norna Robertson for valuable comments and suggestions, and Mr David King for efficient measuring of star positions. We are also grateful for the support provided by the staffs of the AAO, RGO and UKIRT. J.R.G. thanks the Department of Education for Northern Ireland for a research studentship and travel funds. G.P. thanks the University of Keele for a research studentship and the SERC for travel funds. M.F.B. is supported by the US Department of Energy.

Note added in proof; Dwek[18] has recently interpreted the IR light curves of both SN 1979c and SN 1980k as being due to an echo of the UV-visual output of the SN.

Received 25 May; accepted 6 July 1983.

1. Maza, J. *IAU Circ.* No. 3684 (1982).
2. de Vaucouleurs, G. & de Vaucouleurs, A. *Second Reference Catalogue of Bright Galaxies* (University of Texas Press, 1976).
3. Cowal, C. T. *The Palomar Supernova Search Master List* (Caltech, 1982).
4. Merrill, K. *IAU Circ.* No. 3444 (1980).
5. Dwek, E. *et al. Bull. Am. astr. Soc.* **13**, 795 (1981).
6. Chevalier, R. A. *Astrophys. J.* **251**, 259–265 (1981).
7. Cernuschi, E., Marsicano, F. & Codina, S. *Ann. Astrophys.* **30**, 1039–1051 (1967).
8. Hoyle, F. & Wickramasinghe, N. C. *Nature* **226**, 62–63 (1970).
9. Bode, M. F. & Evans, A. *Astr. Astrophys.* **73**, 113–120 (1979).
10. Weiler, K. W., Sramek, R. A., van der Hulst, J. M. & Panagia, N. in *Supernovae: A Survey of Current Research*, 281–291 (Reidel, Dordrecht, 1982).
11. Branch, D. *et al. Astrophys. J.* **244**, 780–804 (1981).
12. McMillan, R. S. & Tapia, S. *Astrophys. J. Lett.* **226**, L87–L89 (1978).
13. Morrison, P. & Sartori, L. Astrophys. J. **158**, 541–570 (1969).
14. Colgate, S. A., Petschek, A. K. & Kriese, J. T. *Astrophys. J. Lett.* **237**, L81–L85 (1980).
15. Panagia, N. *et al. Mon. Not. R. astr. Soc.* **192**, 861–879 (1980).
16. Draine, B. T. *Astrophys. J.* **245**, 880–890 (1981).
17. Rowan-Robinson, M. & Harris, S. *Mon. Not. R. astr. Soc.* **200**, 197–215 (1982).
18. Dwek, E. *Astrophys. J.* (in the press).

Printed in Great Britain by Macmillan Production Ltd., Basingstoke, Hampshire

Reprinted from Nature, Vol. 310, No. 5974, pp. 213-214, 19 July 1984

NGC3256: an emerging elliptical galaxy

J. R. Graham, G. S. Wright, W. P. S. Meikle & R. D. Joseph

Astronomy Group, Physics Department, Imperial College of Science and Technology, Prince Consort Road, London SW7 2BZ, UK

M. F. Bode*

Los Alamos National Laboratory, Los Alamos, New Mexico 87545, USA

NGC3256 is a spectacular peculiar galaxy, with a highly chaotic nuclear region consisting of several bright knots. Two diffuse tidal tails are visible evidence of violent past history. The galaxy has been classified on the basis of this tidal damage as the remnant of two colliding galaxies in the final throes of merging[1]. The galaxy is highly luminous, with $M_B = -22.6$, as well as being a bright, narrow emission-line galaxy[2]. At radio wavelengths, NGC3256 is one of the brightest in Wright's survey[3] of interacting galaxies. We have discovered bright and exceptionally extended 10-μm emission that is evidence for an extremely luminous starburst extending over several kiloparsecs, which will leave the system severely gas-depleted. This depletion, in combination with the violent stellar relaxation which accompanies galaxy mergers, suggests that NGC3256 will become an elliptical galaxy.

NGC3256 was observed in February 1984 as part of our programme to investigate the IR properties of interacting galaxies[4]. Merging galaxies such as NGC3256 are an interesting subgroup of these, not only because the interactions are expected to be particularly violent, but also because of the suggestion[1] that a significant fraction of elliptical galaxies could be the endpoint of mergers. The 1.5-m telescope at the Cerro Tololo Inter-American Observatory was used to make measurements at *JHKL* (1.25, 1.65, 2.2, 3.5 μm) and 10 μm in a 15 arc s aperture centred on the optical nucleus. 3×3 maps using the same beam, with pixel centres displaced one half beamwidth, were also made at these wavelengths. In addition, *JHKL* measurements were made in a 30 arc s aperture on the nucleus. At 10 μm, the flux density measured on the nucleus was 1.7 ± 0.15 Jy. Emission was also detected in the pixels to the east and south-east at 1.2 ± 0.2 Jy and 1.3 ± 0.3 Jy respectively. The integrated flux of about 3 Jy makes this object one of the brightest extragalactic 10-μm sources. At the distance of 53 Mpc inferred from its redshift[5] (H_0 = 50 km s^{-1} Mpc^{-1}) the nuclear 10-μm luminosity of NGC3256 is $\simeq 1.8 \times 10^{10}\ L_\odot$. This surpasses the 10-μm luminosity of all recognized 'starburst' galaxies by an order of magnitude, and rivals that of the powerful Seyfert galaxies. Extrapolating this spectrum into the far IR suggests a total IR luminosity of order $3 \times 10^{11}\ L_\odot$ (ref. 6). The mass contained within the central 15 arc s (4kpc) determined from the mean rotation curve[5] is $6 \times 10^9\ M_\odot$. Thus the mass/luminosity ratio in solar units is $\simeq 0.02(H_0/50)$. Clearly this ratio cannot be sustained by normal star formation over the lifetime of the galaxy.

The 10-μm source must be extended on a scale of several arcseconds. This follows directly from consideration of the 10-μm fluxes observed at three positions together with the measured beam profile. In fact, the 10-μm emission is almost certainly more extended than these measurements suggest. A remarkably red $K - L$ colour $\simeq 1.0$, indicating a large excess at L, extends over most of the central 30 arc s (typical galaxy colours are $\simeq 0.3$). Furthermore, one third of the total luminosity at L measured in the 30 arc s beam falls beyond the central 15 arc s. The most plausible interpretation of these results is that a mammoth burst of star formation has been triggered by the violent gravitational tides and collisional shocks produced by the interaction. The steeply-rising IR spectrum looks very much like that typical of known starburst galaxies such as M82 (ref. 6). The very small mass/luminosity ratio, and the evidence for spatially extended 10-μm emission are features characteristic of starbursts. In a starburst, the luminosity at 10 μm and at L is due to massive early-type stars. The dust cocoon surrounding these stars at birth absorbs their light and reradiates it in the IR. The considerable variations we find in the *JHK* colours measured at different positions in our maps suggest that we have within the same aperture both the unreddened light from knots of less massive blue stars and emission from hot dust.

Apart from the intrinsic interest of an unusually luminous starburst, this discovery has one interesting further implication. There are both theoretical and observational arguments which support the suggestion that merging galaxies can evolve into ellipticals. Numerical simulations[2,7] show that the violent relaxation following a collision produces a stellar velocity distribution similar to that in ellipticals. Observations of galaxies like NGC7257 and NGC5128 show this effect in the stellar velocity distribution, as well as an $r^{1/4}$ luminosity profile[8]. However, as White[7] and others have pointed out, the ultimate fate of the gas which the two merging galaxies originally contain is an outstanding difficulty. If mergers generally result in powerful starbursts similar to that in NGC3256, this lacuna in the merger–elliptical evolution scenario is resolved. The massive early-type stars responsible for the high IR luminosity eventually become supernovae, and the mechanical energy in the supernovae ejecta is sufficient to drive a galactic wind which will leave the galaxy severely gas-depleted.

Galactic winds driven by supernovae have been discussed elsewhere[9] but we can argue that, on simple energetic grounds, the supernovae resulting from the starburst in NGC3256 will be able to sweep the galaxy free of gas. The IR luminosity L_{IR} is powered by early-type stars of average luminosity l_*, so the total mechanical energy supplied by the supernovae produced when these stars explode is $(L_{IR}/l_*)E_{SN}$, where $E_{SN} \simeq 10^{51}$ erg is the energy liberated by each supernova. The condition that this ejected gas, and any remaining interstellar gas, escape from the galaxy is

$$\frac{GM^2}{r} < \frac{L_{IR}}{l_*} E_{SN} \qquad (1)$$

where we have made the conservative assumption that all the mass, M, inside a radius, r, is gas. In fact, a considerable fraction may be locked up in remant objects and low-mass main sequence stars. If the duration of the starburst, τ_b, exceeds the lifetime of a typical early-type star, τ_*, then additional generations of supernovae will contribute to the kinetic energy, increasing it by a factor τ_b/τ_*. We may therefore re-express the condition for gas ejection in terms of the mass/luminosity ratio:

$$\frac{M}{L_{IR}} < 1 \times \left(\frac{\tau_b}{2 \times 10^7\ \mathrm{yr}}\right)\left(\frac{m_*}{10\ M_\odot}\right)^{-1} \frac{M_\odot}{L_\odot} \qquad (2)$$

where m_* is the mass of a star characterizing the starburst. If we take a 10 $M_\odot$ star to typify the early-type stars in the burst[10], and we assume, conservatively, that there is only one generation of stars, (that which we are presently observing), then the condition for escape of all the gas is that $M/L_{IR} < 1$. As the observed M/L_{IR} for NGC3256 is 0.02, this condition is easily satisfied. Thus, there is more than enough mechanical energy to drive a galactic wind which will carry the gas out of the galaxy.

NGC3256 is, therefore, one of the most luminous examples of a starburst yet discovered. It also demonstrates that merger-induced star formation is sufficiently vigorous to produce a remnant as gas depleted as any elliptical galaxy. The discovery of the super-starburst in NGC3256 supports the idea that at least some of present-day elliptical galaxies could have been formed by mergers.

We thank the staff of the Cerro Tololo Inter-American Observatory, especially Jay Frogel, Brook Gregory and Oscar

* Present address: Department of Astronomy, The University, Manchester M13 9PL, UK.

Rivera, for support. We also thank Norna Robertson for helpful discussions. J.R.G. is a Department of Education for Northern Ireland supported research student. G.S.W. is an SERC supported research student. M.F.B. was supported by the Association of Universities for Research in Astronomy and by the US Department of Energy. J.R.G., W.P.S.M. and M.F.B. are visiting astronomers at Cerro Tololo Inter-American Observatory, which is operated by the Association of Universities for Research in Astronomy, Inc., under contract with the NSF.

Received 6 April; accepted 25 May 1984.

1. Toomre, A. in *Evolution of Galaxies and Stellar Populations* (eds Tinsley, B. M. & Larson, R. B.) 401–426 (Yale University Observatory, 1977).
2. de Vaucouleurs, G. & de Vaucouleurs, A. *Mem. R. astr. Soc.* **68**, 69–87 (1961).
3. Wright, A. E. *Mon. Not. R. astr. Soc.* **167**, 251–272 (1974).
4. Joseph, R. D. Meikle, W. P. S., Robertson, N. A. & Wright, G. S. *Mon. Not. R. astr. Soc.* (in the press).
5. Feast, M. W. & Robertson, B. S. C. *Mon. Not. R. astr. Soc.* **185**, 31–46 (1978).
6. Telesco, C. M. & Harper, D. A. *Astrophys. J.* **235**, 392–404 (1980).
7. White, S. D. M. *Mon. Not. R. astr. Soc.* **184**, 185–203 (1978).
8. Schweizer, F. in *Internal Kinematics and Dynamics of Galaxies, IAU Symp.* No. 100, 319–329 (1983).
9. Mathews, W. G. & Baker, J. C. *Astrophys. J.* **170**, 241–259 (1971).
10. Rieke, G. H., Lebofsky, M. J., Thompson, R. I., Low, F. J. & Tokunaga, A. T. *Astrophys. J.* **238**, 24–40 (1980).

Printed in Great Britain by Macmillan Production Ltd., Basingstoke, Hampshire

DISCOVERY OF A LARGE MASS OF IRON IN A TYPE I SUPERNOVA

J. R. Graham and W. P. S. Meikle
Astrophysics Group
Physics Department
Imperial College
LONDON

D. A. Allen
Anglo-Australian Observatory
P.O. Box 296
Epping
New South Wales 2121
Australia

A. J. Longmore and P. M. Williams
United Kingdom Infrared Telescope
900 Leilani Street
Hilo
HAWAII

ABSTRACT

We have discovered 0.3 M⊙ of iron in the Type I Supernova (SNI) 1983n in M83 about one year after explosion. This is the first time that a massive quantity of iron has been directly and unambiguously detected in a SNI. It was accomplished by the observation of strong FeII forbidden line emission in the infrared at 1.644μm from the optically thin ejecta. This result was predicted by the ^{56}Ni-^{56}Co-^{56}Fe radioactive decay scenario for SNI, and provides strong support for its credibility.

1. INTRODUCTION

One of the most astonishing features of type I supernovae is the exponential decline of the light curve which, in some cases, has been followed for over ten half-lives. It has long been realised that such behaviour cannot be accounted for simply by the release of thermal energy from the exploded, low mass progenitor. Adiabatic cooling during the expansion is much too rapid. Consequently a strongly favoured hypothesis is that the light curve is powered by the decay of radionuclides synthesised in the explosion. The production of about a solar mass of radioactive ^{56}Ni is expected under the conditions of high temperature and density which occur (Woosley et. al., 1973). Colgate and McKee (1969) suggested that SN-I luminosity would be powered by the decay of ^{56}Ni. In the expanding ejecta the ^{56}Ni ($\tau^1/_2$ = 6.1d) decays via electron capture to an excited state of ^{56}Co which undergoes a γ-transition to the ground state. The ^{56}Co ($\tau^1/_2$ = 77d) decays by electron capture or positron emission to an excited state of ^{56}Fe which reaches its stable ground state also by γ-ray emission. The light curve peak and initial decline is accounted for by the deposition in the ejecta of γ-rays from the decaying ^{56}Ni. As the expansion continues, the fall in density increases the probability that γ-rays from both the ^{56}Ni and ^{56}Co decay will escape. However, about 4% of the total decay energy of the ^{56}Co is released in the form of energetic positrons (mean energy = 0.66MeV) which suffer severe ionisation losses, their kinetic energy heating the electron gas via secondary electrons. Colgate and McKee (1969) suggested that this process might dominate the late time luminosity. Arnett (1979) and Colgate et. al. (1980) accounted for the discrepancy between the light curve decay time and that of ^{56}Co as being due to the increasing effect of positron escape from the nebula on the kinetic energy deposited. However, Meyerott (1980) and Axelrod (1980a,b) have argued that the positrons would be completely trapped and that the shorter half-life of the optical light curve relative to that of ^{56}Co could be the result of efficient cooling of the nebula by far-infrared fine structure lines of iron. Indeed, Axelrod (1980) has shown that to determine the energy balance in the ejecta and hence its temperature, both the optical and IR spectra must be included.

Regardless of the positron escape controversy, a hundred days or so after the explosion, the supernova should consist of an exotic plasma composed principally of iron, heated and ionised mainly by γ-rays at first, but ultimately by positrons from the ^{56}Co decay. Despite the success of this radioactive decay model in accounting for the light curve, the dramatic prediction that a huge mass of iron must be present in the ejecta has proved difficult to test.

The presence of iron in SN-I at early times (< 100 days after maximum light) has been inferred from the optical spectra of both SN1972e (Branch, 1980) and SN1981b (Branch et al, 1983). However, the matching of synthetic spectra to those observed yields only tentative evidence for freshly synthesised ^{56}Ni. Direct determination of the iron mass from these observations seems to be impractical owing to the huge optical depths of the permitted Fe lines; most of the iron remains hidden. X-ray studies of iron in young galactic supernova remnants (SNR's) are severely penalised by the lack of detailed non-equilibrium ionization models (Itoh, 1984), as well as by uncertainties in the iron distribution (Arnett, 1980) and whether or not reverse shock heating has occurred. X-ray spectra therefore do not yet provide a useful measure of the synthesised iron mass. Wu et al (1983) have inferred the presence of a large mass of iron in SN1006 from UV absorption lines present in the spectrum of a star on the far side of the SNR. However, as well as being subject to the above uncertainties affecting X-ray studies , this result also requires extrapolation from the observed line of sight to the entire volume of the probably inhomogeneous SNR.

An encouraging development in the search for vindication of the ^{56}Ni model has come with the realisation that once the ejecta has become thin to optical radiation (>100 days after maximum) then the radioactive energy input is balanced by forbidden radiative transitions following collisional excitation (Axelrod, 1980a; Meyerott, 1980). The optical depth of forbidden lines (A < 1/s) becomes less than unity after ~10days and so they will suffer only negligible self-absorption. Numerical calculations which follow the atomic processes at work in the SN nebula in detail predict the temperature and ionization conditions and consequently that the emergent spectrum (100 < t < 600 days) will consist almost entirely of forbidden

transitions of FeII and FeIII excited by thermal electrons with temperature ~ 6000K. Despite the complexity of optical SN-I spectra, due to large line widths and severe line blending, synthetic spectra show remarkable similarity to observations (Axelrod, 1980a, 1980b). With only a minimum of free parameters, viz. ^{56}Ni mass and ejection velocity, both the shape of individual spectra and their subsequent evolution can be reproduced. An important success of this work has been to demonstrate that CoIII is responsible for "filling in" part of the spectrum around 6000Å which if Co were absent would represent a serious discrepancy. The amount of Co needed to account for the strength of the feature decreases exactly as the radioactive decay law requires. Despite these successes, there are still some unresolved difficulties which arise when considering optical spectra. Axelrod's models suffer from a lack of precise wavelength registration for several bright "features", and the same region discussed above at 6000Å is, according to Branch (1980), associated with Na.

In marked contrast to the confusing situation in the optical region, the IR spectrum should be simple and uncluttered, with individual lines clearly identifiable (Axelrod, 1981). The observational difficulties encountered at the wavelengths of the bright, fine structure lines which are found $\geq$ 20μm constrained us to consider the near-IR (1 - 5μm). Axelrod's original calculations did not suggest any near-IR lines which were accessible to existing ground-based instrumentation. However, identification of the 1.644μm line of [FeII] in the nucleus of the galaxy M82 (Rieke et al, 1980), combined with newly available Einstein A values for FeII (Nussbaumer and Storey, 1980) drew our attention to the possibility of observing the components of the a^4F-a^4D multiplet, which fall neatly in the H-band atmospheric window. A prediction made on the basis of the physical conditions calculated by Axelrod led to the conclusion that the 2J=9-7 a^4F-a^4D 1.6440 μm line of Fe should be detectable in a nearby supernova containing a few tenths of a solar mass of iron.

2. OBSERVATIONS

The discovery of the SN-I 1983n in M83 (NGC5236) by R. Evans (Thomson, 1983) afforded an exceptional opportunity for the observation of the late time infrared spectrum. The proximity of M83 meant that SN1983n was the brightest SNI since SN1972e, bringing the predicted infrared

line intensities well within the range of state-of-the-art IR spectrometers.

We observed SN1983n on May 15 and July 11, 1984 at the Anglo-Australian Telescope (AAT), and at the United Kingdom Infrared Telescope (UKIRT) on July 18, 1984. Details of the observation parameters are given in Table 1. The dates of observation correspond to days 321, 378, and 385 after the estimated explosion date of June 29, 1983 (Sramek et al, 1984). At these dates, the optical emission from the supernova had faded to a level comparable to that from the adjacent OB/HII complex in M83. The supernova was located accurately by offsetting from a star a few arcminutes away, the offsets having been obtained in July 1983 when the supernova was near optical maximun ($m_v \approx 11.5$, Wamsteker, W. et. al., 1983). Spectra in the H-window (λ=1.65μm) were obtained on the above dates using circular variable filter (CVF) spectrometers of resolution ~ 100. Fig. 1 shows the two spectra obtained at the AAT. The anticipated position of the 1.644μm FeII line redshifted by 518 km/s (de Vaucouleurs et al., 1976) is indicated. Casual inspection reveals, in both spectra ,the presence of a bright, broad, feature within half a resolution element of this wavelength. (Following the May AAT run, it was found that a loose coupling in the dewar was resulting in a calibration uncertainty of about one channel ($\Delta\lambda \approx 0.006$μm). This was probably responsible for the one channel displacement in the May spectrum, of the line peak from the expected position.) The UKIRT spectrum was obtained under very difficult conditions (high air mass with the setting of the source restricting the available integration time) and is consequently of lower signal to noise. Nevertheless, it provides independent confirmation of the presence of strong emission at 1.644μm. The shape of the AAT spectra seems to reproduce from May to July suggesting that the 1.600μm line which also arises from the same multiplet as the 1.644μm line is also present.The estimated continuum levels are shown in Table 1. Determination of the continuum level is difficult because of the paucity of off-line points in the spectra. For the AAT spectra the continuum values were determined from points lying between the positions of the 1.600 and the 1.644 μm line, and at the extreme long wavelength side of the spectrum. They were then checked against H-band photometry ($\delta\lambda$ = 0.29 μm) measurements at the AAT in a 7" aperture carried out both in May and July, and against a July 3.5" resolution H-band map of the region

around the supernova. Within the observational errors, the continua derived from broad-band photometry agree with those obtained from off-line spectral points and are therefore representative of the continuum throughout the H-window. The difference in the continuum levels between these two dates is due to the combination of aperture difference (which was reduced from 5" (May) to 3.5" (July) to improve spectral resolution), and supernova decline. The continuum at UKIRT was assessed purely on the basis of points obtained several resolution elements away on either side of the 1.644 μm line. Table 1 gives the integrated line intensities obtained from our three spectra, where the errors include the contribution due to the uncertain values of the continua. These have been corrected for galactic extinction using the AB given by Burstein & Heiles (1984) and the Van de Hulst curve 15 (Johnson 1968). At H this amounts to 2%. The problem of what internal extinction should be adopted within M83 is discussed next.

3. EXTINCTION WITHIN M83

Several different observations suggest that M83 may be an exceptionally dusty galaxy. Balmer line ratios for about thirty HII regions (Dufour, 1980, Brand et al. 1981, Webster and Smith, 1983) exhibit a spread of Av of between 0.1 and 3, with a mean of about Av=1.5. Webster and Smith remark that the reddening in M83 is "somewhat higher" than the reddening in other galaxies which they studied. Of greater importance, however, is the demonstration by Brand et al. that a large part of the extinction in M83 must be external to the source of emission lines. Jensen et al (1981) modelled young star clusters in M83 using a Salpeter IMF. Comparison of observed U-B,B-V colours with the predicted evolutionary track suggested a high extinction (A_B=0.5 to 2 to mid-plane) in M83. From these observations, we infer an extinction to the mid-plane of Av=1.0 ± 0.3 in the supernova vicinity.

We note that other apparently more direct measures of the extinction to SN1983n are probably unreliable. Combining the Jenkins et al (1984) measurement of the NaI column density to the SN with Hobb's (1974) relation between NaI column density and reddening yields an Av of only 0.35 to the SN. However, if the SN is either in or behind the OB/HII complex (RK220/234 Rumstay & Kaufman, 1983), then any additional

extinction within this region will not be revealed by the NaI column density. Due to its the low ionization potential, the NaI will be effectively completely destroyed by ionizing photons over a considerably larger volume than the HII region itself. Early time IUE spectra of the SN (Panagia 1984) reveal no evidence for a 2200Å absorption feature, suggesting that Av < 0.5, on the basis of the relationship established in the Galaxy. However, the reliability of this feature as an indicator of extinction in other galaxies has been barely tested. The few galaxies which have been examined all exhibit a weaker feature than our own galaxy. In particular, Rosa (1980) finds little evidence of the feature in the late-type spiral M101, in spite of radio measurements indicating $A_{H\beta}$ of 1 to 1.5. We have therefore not used the 2200Å feature an an indicator of the extinction. Finally, if we use the 21cm HI column density within M83 (Rogstad et al 1974) and assume the Galactic relation between extinction and NHI, then a mid-plane Av of only 0.37 is found. However this measurement was made with a 2' beam and covers a large region compared with the OB/HII complex. In addition, the heavy element abundance in M83 is considerable higher than in the Galaxy, being ~4.5 times greater in the vicinity of the SN (Talbot 1980). The impact of this higher abundance upon the gas/dust ratio would have to be understood before inferring the extinction from HI measurements.

The depth of the supernova into the plane of M83 is not known. We therefore assume an extinction of Av=1.3± 0.8 to the SN, including the 0.1 magnitudes for extinction within our own galaxy. The large errors reflect mainly our uncertainty in the depth of the SN into the plane. Assuming Van de Hulst's curve 15 (Johnson 1968) we find an extinction at H of 0.19± 0.11 magnitudes.

4. DISTANCE TO M83

The derived iron mass is clearly sensitive to the supernova distance adopted. We believe that the most reliable estimate of the distance to M83 is that of de Vaucouleurs (1979). The main "secondary indicator" which he used was the largest "ring-type" HII region, the diameter of which increases very slowly with galaxy luminosity. This indicator has the advantage of being insensitive to large internal extinction, and is therefore well suited for M83, yielding a value of 3.7 Mpc. Allowing for the extinction correction already present in de Vaucouleurs'

estimate, we have examined the effect of a total extinction of Av = 1.6 on the distance determination. The extinction causes a reduction of the apparent blue magnitude of the galaxy resulting in a distance underestimate of ~15%. In view of the uncertaintywhich we would attach to this correction, we think that a reasonable figure for the M83 distance is 5 ± 1 Mpc.

5. LINE IDENTIFICATION AND PRELIMINARY INTERPRETATION

We are confident that the emission observed around 1.644 μm is in fact due to the predicted [FeII] line because of the exact wavelength correspondence. Emission at 1.644 μm from astronomical sources has been reported by both Rieke et. al. (1980) and Seward et. al. (1983). Rieke et. al. identified the line as due to FeII on the basis of a thorough search of line lists. The line is resolved by the CVF, and has an intrinsic width of ~2,500 km/s. It must therefore be of supernova origin as it is much broader than expected for any systematic motions within, for example, the OB/HII complex. A check was also made at UKIRT for contamination by Brackett theta (λ = 1.641μm, n=12-4), by measuring the strength of Brackett gamma in the K-window and using standard recombination theory (Brocklehurst 1971; Giles 1977). We find that the theta line strength was < 3% of the measured Fe line.

The flux at the Earth is related to a Fe mass, M_{Fe} by

$$F_{1.644} = \frac{A_{a^4F_{9/2}-a^4D_{7/2}}}{4\pi d^2} h\nu \frac{n_{a^4D_{7/2}}}{n_{FeII}} \frac{n_{FeII}}{n_{Fe}} \frac{M_{Fe}}{m_{Fe}} e^{-\tau_H}$$

where A is the Einstein spontaneous decay probability, d is the distance to M83 and hν is the energy of the transition. The lower case n's are the number densities of the species indicated by the subscript. m_{Fe} is the mass of an iron atom, and τ_H is the optical depth at 1.644μm due to dust along the line of sight. The forbidden lines are excited by thermal electrons with T ≈ 6500K, so under conditions of LTE $n_{a^4D_{7/2}}/n_{FeII}$ = 0.028. Axelrod (1980a) and Meyerott (1980) calculate that the ionization fraction

n_{FeII}/n_{Fe} =0.1 between days 300 and 400. Therefore, our measurement of a line flux of ~3×10^{-14}erg/s/cm/cm implies ~0.3M⊙ of Fe in the M83 SN. Thus we present, for the first time, unambiguous evidence that the ejecta of a supernova explosion contains a significant fraction of a solar mass of iron.

6. COMPARISON OF OBSERVATIONS WITH SYNTHETIC SPECTRA

We originally predicted the infrared line intensities using the above simple prescription which assumes local thermodynamic equilibrium, with the temperature and ionization fraction taken from Axelrod's calculations. Adequate as this was for the purposes of evaluating the feasibility of observations, a more realistic calculation capable of producing synthetic spectra should maximise the information extracted from the data. The first step towards accommodating this was to abandon the assumption of LTE. After ~200 days, electron densities are typically < 10^6 cm^{-3} (t>200) and so spontaneous radiative decays start to become important in determining level populations. The FeII ion was assumed to be a 16 level system consisting of the 4 lowest terms; a6D, a4F, a4D, and a4P, whose relative populations were determined by spontaneous radiative decay, and excitation and de-excitation by collisions with thermal electrons. The collision strengths of Nussbaumer & Storey (1980) and new A values calculated by Nussbaumer (Allen, private communication) were used.

Next, line profiles were generated by supposing that FeII was distributed uniformly throughout an homologously expanding sphere, thus the emergent lines have a characteristic parabolic shape. Homologous expansion is a reasonable approximation to the resultant dynamic state following shock acceleration under a variety of initial conditions, and models of the ionization state within a SN with a realistic density structure predict a near uniform FeII density (Woosley, Axelrod, and Weaver, 1983).

Finally, to allow direct comparison with the SN spectra the emergent lines were convolved with the instrumental profile which was determined from observations of the 1.530μm line from a Hg discharge lamp.

Synthetic spectra were calculated for an array of iron masses and expansion velocities (expansion velocity is defined with respect to the centre of mass) and compared with the observations using the chi-squared statistic. Chi-squared contours were found to be approximately rectangular in the iron mass - expansion velocity plane, and so the 1σ confidence area of parameter space for the May and July AAT spectra can be described by the values given in Table 2. An iron mass was also derived from the poorer quality UKIRT observation by using the integrated line flux. The population of the a^4D level, the ionization (from Axelrod 1980a) and the line emissivity used to calculate the mass from each of the spectra are also shown in Table 2. A distance of 5Mpc and an extinction at H of 0.19 magnitudes was assumed. The best fit model spectrum for the July AAT data is shown in Figure 2. This comparison demonstrates the exactness of the wavelength correspondence of the 1.644μm line and even suggests that the 1.600μm line has been recorded as well. The observed line ratio suggests, not unexpectedly, that the electron density >> $10^6/cm^3$. On inclusion of the uncertainties in the distance and extinction, the weighted mean of the masses derived from all three spectra is $0.3\pm0.1M_\odot$, where the largest contribution to the error quoted arises from the distance uncertainty.

The most significant departure of the July AAT spectrum from the calculation is in the strength of the blend of the 1.664+1.677 μm lines. Here one may suspect the accuracy of the atomic data as being the cause of the excess predicted flux. The 1.600, 1.664, and 1.677 μm lines show similar variation in strength with density, relative to 1.644 μm, and so the discrepancy cannot be attributed to the adoption of inappropriate conditions. When previously these lines have been observed in conditions of high density in MSH 15-52 (Seward et al, 1983) the 1.600, 1.644, and 1.664+1.677 μm blend are clearly seen but the peak flux at 1.600 μm is almost twice that due to 1.664+1.677 μm. A similar discrepancy would account for the observed SN spectrum. Calculating the expected line ratios for MSH 15-52, and then comparing with the observed spectrum suggests that if the ratio of the transition probabilities of the 1.664μm and the 1.677μm lines is assumed correct, then their A values must be reduced by a factor of about two to 0.34 and 0.18 respectively of the A value for the 1.644μm transition.

7. DISCUSSION

The low expansion velocity derived from the IR lines is a surprising aspect of this measurement, because this is apparently in conflict with optical measurements made around or just after maximum light, which yield 10^4km/s . Some of the discrepancy can be resolved by recognising that observation of a low ionization stage of Fe allows us to see deep into the stellar ejecta. If density rises towards the centre of the expansion, then there will be a correspondingly higher recombination rate in the slower moving material. When a realistic density profile is included in the calculations of ionization structure FeII is indeed found to be confined to the centre of the expansion (Axelrod, 1984). Even so the expected velocities are ~4000km/s, which seems to be in some conflict with our observations.

The hypothesis that the luminosity of a SN-I is derived from the radioactive decay of ^{56}Ni is supported by our IR spectroscopic observations of SN 1983n in M83. The detection of the 1.644μm line of FeII has been used to infer that the SN ejecta contain ~0.3 M⊙ of iron. If this iron has resulted from the decay of ^{56}Ni created in the high temperature and density conditions of the initial explosion, then the decay of 0.3 M⊙ of ^{56}Ni to ^{56}Fe would yield ~10^{50} ergs. This is easily sufficient energy to power the SN luminosity. This measurement of the iron mass ejected by a SN-I is consistent with Axelrod's (1980a) study of the optical spectra of SN 1972e. It is also compatible with the observed iron abundance in the solar neighbourhood, given an SN-I rate of ~100/yr in the Galaxy (Sutherland and Wheeler, 1984).

If we accept that M83 lies at a distance of between 4 Mpc and 6 Mpc then the inferred iron mass is between 0.2M⊙ and 0.4M⊙.
However it is difficult to assess the accuracy of the atomic physics used in this estimate. We note with concern that the A-value for the 1.644μm line increased by x3 between the calculations of Nussbaumer and Storey (1980) and the more recent calculations of Nussbaumer (Allen, private communication). If we therefore allow the A-value to lie in the range x0.5 to x2 of the actual value used in our mass estimate, then we can only conclude that the iron mass is somewhere in the range 0.1 M⊙ to 0.8 M⊙. Essentially all of the SN-I

models involving ^{56}Ni as the energy storage mechanism for the light curve, have little difficulty in producing ^{56}Ni masses in this range. However with such a large uncertainty in the mass we are unable to distinguish between these models.

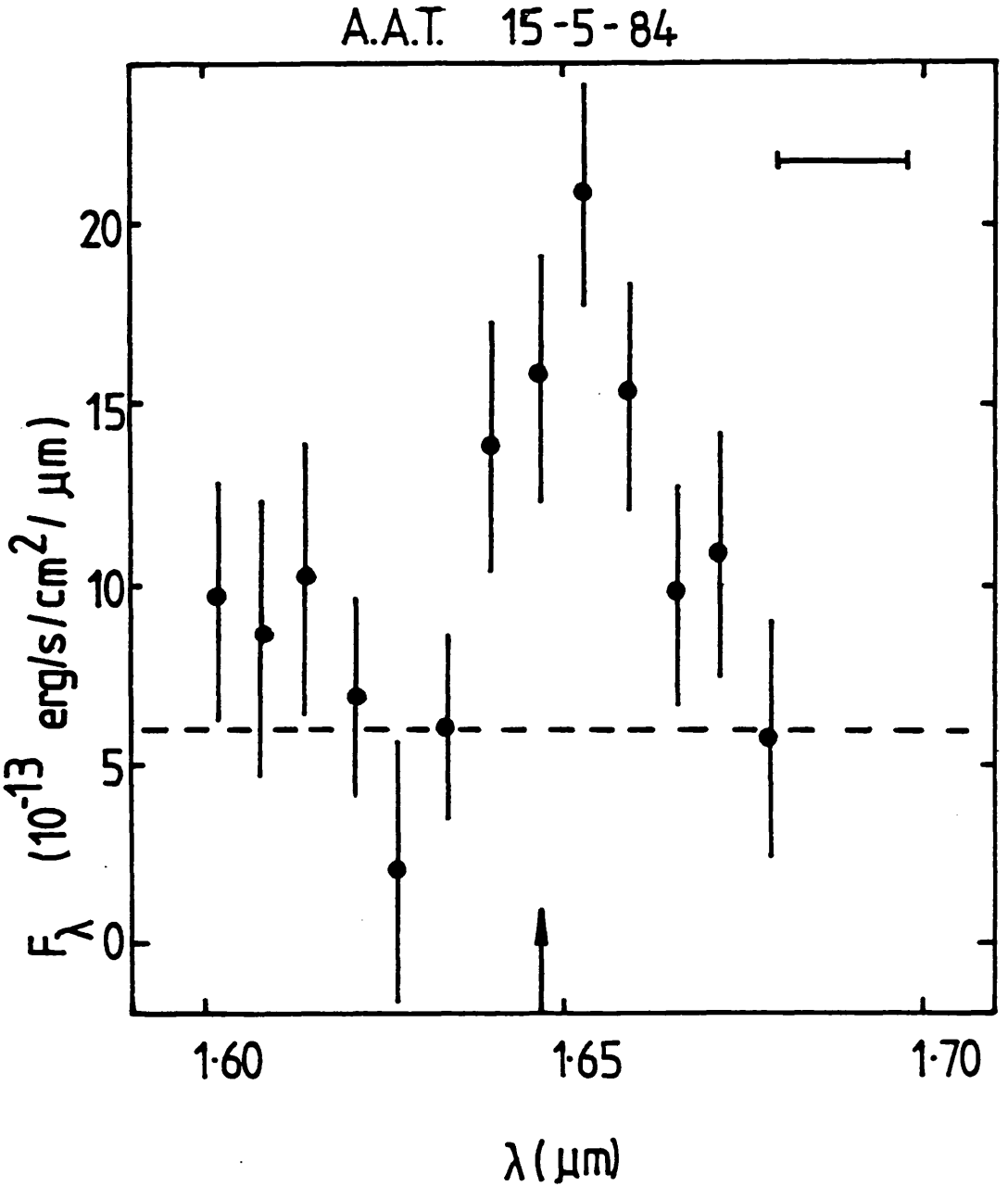

Figure 1a

The May A.A.T. spectrum. The dotted line represents the continuum, and the horizontal bar indicates the resolution.

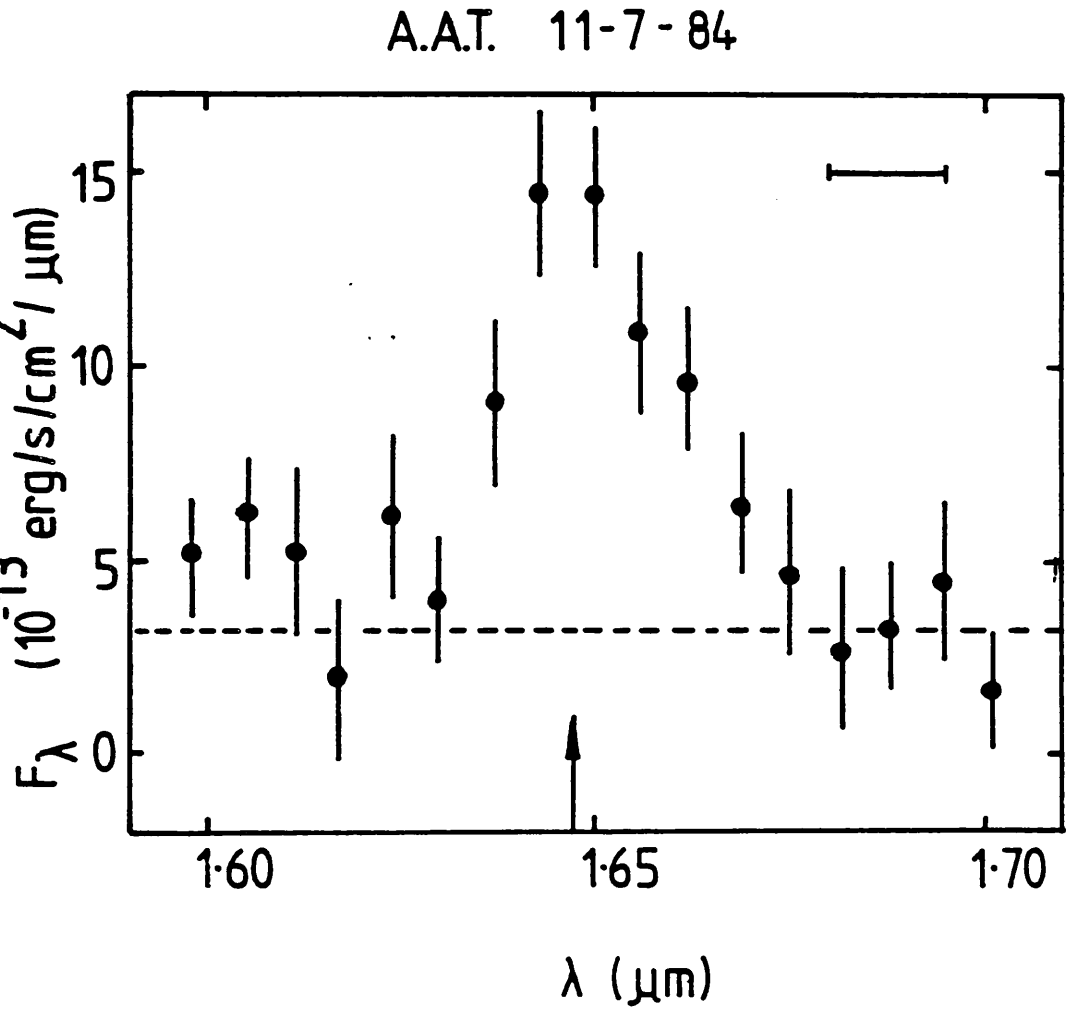

Figure 1b

The July A.A.T. spectrum. The dotted line represents the continuum, and the horizontal bar indicates the resolution.

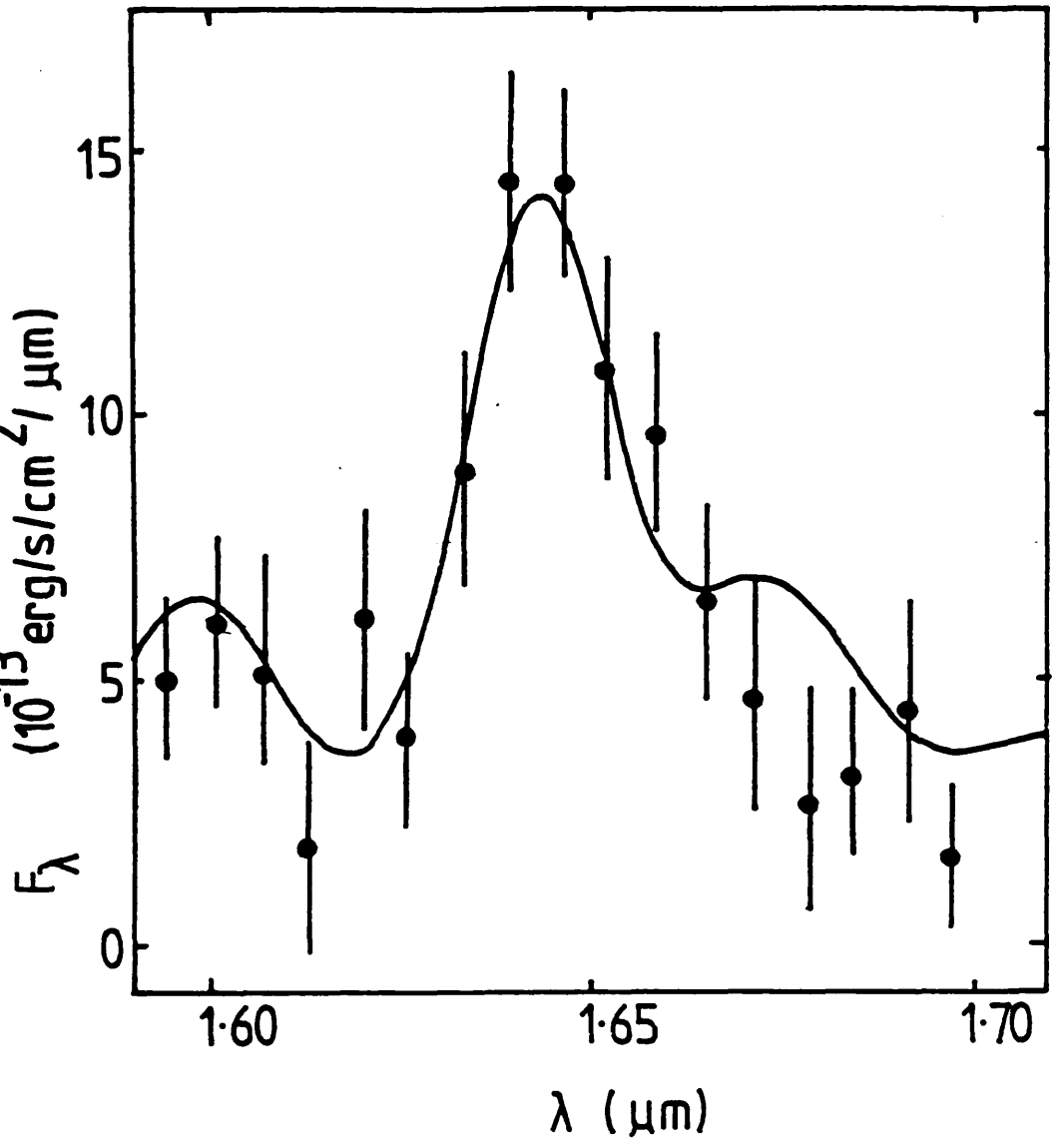

Figure 2

The best fit model spectrum and the July data compared.
For details of the model parameters see Table 2.

Table 1

Telescope	Date	Aperture	Chop Throw	Resolution	Continuum ($\times 10^{-13}$erg cm^{-2} s^{-1} μm^{-1})	Line Intensity ($\times 10^{-14}$erg cm^{-2} s^{-1})
AAT (3.9m)	15/5/84	5"	12" N-S	100	6 ± 2.5	3.38 ± 0.83
AAT	11/7/84	3.5"	12" N-S	100	3.2 ± 0.6	2.82 ± 0.50
UKIRT (3.8m)	18/7/84	8"	15" E-W	140	12 ± 4	4.0 ± 1.5

Table 2

Date	$\frac{n_{a^4D_{7/2}}}{n_{FeII}}$	$\frac{n_{FeII}}{n_{Fe}}$	Emissivity ($\times 10^{-16}$erg s^{-1} atom^{-1})	$\frac{M_{Fe}}{(M_\odot)}$	Expansion Velocity (km s^{-1})
15/5/84	0.033	0.072	2.31	0.32 ± 0.08	2,300 ± 1,600
11/7/84	0.032	0.079	2.11	0.27 ± 0.05	2,500 ± 1,000
18/7/84	0.032	0.079	2.11	0.38 ± 0.14	—

REFERENCES

Arnett, W. D. Astrophys. J. Lett., 230, L37-L40, (1979)

Axelrod, T. S. Ph. D. Thesis, UCRL52994, University of California, (1980a)

Axelrod, T. S. Proceedings of the Texas Workshop on Type I Supernovae (ed. J.C. Wheeler), 85-90, University of Texas, (1980b)

Axelrod, T. S. private communication (1981)

Axelrod, T. S. private communication (1984)

Branch, D. Proceedings of the Texas Workshop on Type I Supernovae (ed. J.C. Wheeler), 66-71, University of Texas, (1980)

Branch, D., Lacy, C. H., McCall, M. L., Sutherland, P. G., Uomoto, A., Wheeler, J.C. and Wills, B. J. Astrophys. J., 123-139, (1983)

Brand, P. W. J. L., Coulson, I. M., and Zealey, W. J. Mon. Not. R. astr. Soc., 195, 353-360, (1981)

Brocklehurst, M. Mon. Not. R. astr. Soc. 153, 471-490, (1971)

Burstein, D., and Heiles, C. Astrophys. J. Suppl., 54, 33-79, (1984)

Colgate S.A., and McKee C., Ap. J. 157, 623, (1969)

Colgate, S. A., Petschek, A. G., and Kriese, J. J. Astrophys. J. Lett., 237, L81-L86, (1980)

de Vaucouleurs, G., de Vaucouleurs, A., and Corwin, H. G. Second Reference Catalogue of Bright Galaxies, (University of Texas Press, 1976)

de Vaucouleurs, G. Astron. J., 84, 1270-1280, (1979)

Dufour, R. J., Talbot, R. J., Jensen, E. B., and Shields, G. A. Astrophys. J., 236, 119-134, (1980)

Giles, K. Mon. Not. R. astr. Soc., 180, 57p-59p, (1977)

Hobbs, L. M. Astrophys. J., 191, 381-393, (1974)

Itoh, H. Physica Scripta, T7, 19-24, (1984)

Jenkins, E. B., Rodgers, A. W., Harding, P., Morton, D. C., and York, D. G. Astrophys. J., 281, 585-592, (1984)

Jensen, E. B., Talbot, R. J., and Dufour, R. J. Astrophys. J., 243, 716-735, (1981)

Johnson, H. L., "Nebulae and Interstellar Matter" (eds. Middlehurst, B. M. and Aller, L. H.) 167-220 (University of Chicago Press, 1968)

Meyerott, R. E. Astrophys. J., 239, 257-270, (1980)

Nussbaumer, H. and Storey, P. J. Astron. Astrophys. 89, 308-313, (1980)

Panagia, N. private communication (1984)

Rieke, G. H., Lebofsky, M. J., Thompson, R. J., Low, F. J., and Tokunaga, A. T. Astrophys. J., 238, 24-40, (1980)

Rogstad, D. H., Lockhart, I. A., and Wright, M. C. H. Astrophys. J., 193, 309-319, (1974)

Rosa, M. Astr. Astrophys., 85, L21-L24, (1980)

Rumstay, K. S. and Kaufman, M. Astrophys. J. 274, 611-631, (1983)

Seward, F. D., Harnden, F. R., Murdin, P., and Clarke, D. H. Astrophys. J. 267, 698-710, (1983)

Sramek, R. A., Panagia, N., and Weiler, K. W. Astrophys. J. (in the press)

Sutherland P.G. and Wheeler J.C., Astrophys. J., 280, 282, (1984)

Talbot, R. J. Astrophys. J., 235, 821-832, (1980)

Thomson, G. D. IAU Circular, 3835, (1983)

Wamsteker, W. et al. IAU Circular 3842, (1983)

Webster, B. L. and Smith, M. G. Mon. Not. R. astr. Soc., 204, 743-763, (1983)

Woosley, S. E., Arnett, W. D., and Clayton, D. D. Astrophys. J. Suppl., 26, 231-312, (1973)

Woosley, S. E., Axelrod, T. S., and Weaver, T. A. preprint (1983)

Wu, C., Leventhal, M., Sarazin, C. L. and Gull, T.R. Astrophys. J. Lett. 269, L5-L9, (1983)